EXPERIMENTAL MEASUREMENT AND ANALYSIS OF WALL PRESSURE DISTRIBUTION FOR A 50% ECCENTRIC WHIRLING ANNULAR SEAL

A Thesis

by

ARUN SURYANARAYANAN

Submitted to the Office of Graduate Studies of
Texas A&M University
in partial fulfillment of the requirements for the degree of

MASTER OF SCIENCE

August 2003

Major Subject: Mechanical Engineering

EXPERIMENTAL MEASUREMENT AND ANALYSIS OF WALL PRESSURE DISTRIBUTION FOR A 50% ECCENTRIC WHIRLING ANNULAR SEAL

A Thesis

by

ARUN SURYANARAYANAN

Submitted to Texas A&M University
in partial fulfillment of the requirements
for the degree of

MASTER OF SCIENCE

Approved as to style and content by:

Gerald L. Morrison (Chair of Committee)	David L. Rhode (Member)
Kenneth R. Hall (Member)	Dennis O' Neal (Head of Department)

August 2003

Major Subject: Mechanical Engineering

ABSTRACT

Experimental Measurement and Analysis of Wall Pressure Distribution for a 50% Eccentric Whirling Annular Seal. (August 2003)

Arun Suryanarayanan,

B.E., University Visvesvarya College of Engineering, Bangalore, India

Chair of Advisory Committee: Dr. Gerald Morrison

In any rotating machinery, the geometry of the seal influences the extent of systemleakage. The path taken by the flow in the clearance volume is dependent on the seal and rotor profile. The clearance between a new “seal-rotor” combination is uniform except for small variations during manufacturing and assembly. With time this annular cross section undergoes further physical changes causing non-uniform flow in the annular volume. This azimuthally varying leakage through the seal-rotor annulus creates unbalanced forces on the rotor causing it to whirl. It is essential to identify the reasons for these unwanted forces. Velocity profiling of the clearance volume flow was performed by Morrison et al. (1992) using 3-D LDA measurements on annular and labyrinth seals operating with 50% dynamic eccentricities and a whirl ratio of one. However, this alone does not provide a complete matrix of data for the conditions prevailing in the clearance zone. Additional information of mean and instantaneous wall pressure distributions for 0%, 10%, 25% and 50% rotor dynamic eccentricity for whirl ratios of zero and one, with positive pre-swirl, no pre-swirl and negative pre-swirl conditions were measured by Robic (1999). The data collected showed that the pressure field on the seal walls reversed itself between the whirling and non-whirling conditions. As a continuance of the earlier works, the present effort investigates the effect of whirl ratio variation for a 50% eccentric smooth annular seal at a leakage Reynolds number of 24000. An attempt has been made to collect pressure data for negative whirl ratios also under similar test conditions.

A seal test rig capable of handling different eccentricities and whirl ratios simultaneously was designed and constructed for this purpose. Mean and instantaneous wall pressure data were recorded for 50% eccentricity with whirl ratios between ± 1 for a rotor speed of 1800. For a rotor speed of 2700, whirl ratios tested were between ± 0.6 and for 3600 rotor speed, whirl ratios ranging between ± 0.5 were tested. From the collected data a detailed analysis of wall pressures along the seal surface is performed following the technique described by Winslow (1994) and Robic (1999).

DEDICATION

This work is dedicated to my grandparents, parents, Mr. A. Suryanarayanan and Mrs. Devi Suryanarayanan, and my sister, S. Anu Priya, who have been a source of unlimited moral support and encouragement.

ACKNOWLEDGMENTS

The author would like to express his sincere gratitude to Dr. Gerald Morrison for his invaluable advise throughout the project duration. The time I have spent with him has been more than a learning experience. I wish to thank Dr. David Rhode and Dr. Kenneth Hall for being on my committee. My thanks to Mr. Eddie Denk and his assistants for assisting me in assembling up the test set-up, the former for also teaching me the nuances of shop work. Special thanks to my friend Stephen Danczyk for helping me through all phases of the project, the knowledge acquired from him has been very enriching. I also thank my other friends Selvam Raghupathy, Burak Ozturk, Avijit Bhattacharya, Anand Srinivasan, Bharathwaj Kannan, Sherif Abdel Fattah, Dario Rubio, Adolfo Delgado, Vasanth Muralidharan and Nader Berchane for the all the pleasant moments I have had at College Station.

TABLE OF CONTENTS

Page

ABSTRACT iii

DEDICATION.....v

ACKNOWLEDGMENTS.....vi

TABLE OF CONTENTS.....vii

NOMENCLATURE.....viii

INTRODUCTION.....1

LITERATURE REVIEW.....3

EXPERIMENTAL FACILITY.....6

Water Supply Unit.....6
Seal Test Facility.....7
Eccentricity and Whirl Setting Unit.....9
Instrumentation and Data Acquisition System.....10

EXPERIMENTAL PROCEDURE.....12

Steps to Set Eccentricity and Whirl.....12
Phase Averaged Pressure Measurement.....14
Mean Pressure Measurement.....15

RESULTS AND DISCUSSION.....16

Effects of Whirl Ratios and Taylor numbers on Normalized Mean Pressure Distribution and Pressure Drop across the Seal.....16
Effects of Whirl Ratios and Taylor numbers on Phase Averaged Instantaneous Pressure Distribution.....21

CONCLUSIONS.....30

REFERENCES.....33

APPENDICES.....36

VITA.....98

NOMENCLATURE

c	Nominal clearance between rotor and stator
D	Rotor diameter
e	Rotor eccentricity ratio
L	Rotor length
P	Pressure
P*	Nondimensional Pressure, $PL/c\Delta P$
P_{mean}	Time averaged pressure
P^*_{mean}	Nondimensional Mean Pressure $(P_{mean}-P_{Z/L=1.00})/\Delta P$
r	Distance above centered rotor surface
Re	Reynolds number = $2\rho U_{mean}c/\mu$
Ta	Taylor number = $(\rho W_{sh}c/\mu)(2c/D)^{1/2}$
U	Mean axial velocity
U_m	Average mean axial velocity, $Q/\pi Dc$
X	Axial distance from front of seal
Y	Radial distance above rotor tooth top
Z	Axial distance downstream of the seal entrance
ΔP	Pressure drop from seal entrance to exit
μ	Absolute viscosity, 7.84×10^{-4} kg/m-s
ν	Kinematic viscosity
ρ	Density, 999 kg/m^3
< >	Phase averaged quantity
ω	Whirl ratio

INTRODUCTION

It is a well established fact that seals play a vital role in determining the stability and efficiency of rotating machinery. The effective separation of the high and low-pressure zones depends on the geometry of the seal. The physical features of the seal-rotor annulus influences the flow through it and consequently the forces created on the rotor (Brennen, 1976). With time, due to wear and tear, the clearance between the rotor tip and the seal changes non uniformly on the circumference. The flow through such a worn clearance volume changes correspondingly with regions of larger clearances allowing for higher leakage. This varying leakage at the rotor edge contributes to uneven non-axisymmetric loads, deflecting the rotor from the center. Unequal forces on the rotor rim can also give rise to excessive vibrations and noise apart from causing physical wear. Mechanical damage can occur over a period of time if the flow on the seal wall causes concentrated stresses in the rotor. The forces exerted by the flow can greatly influence the stability of the rotor. To minimize the forces acting on the seal and the rotor due to fluctuations in the clearance flow, extensive testing for different system conditions needs to be performed to obtain a viable seal design.

Characterization of the flow measurement inside the seal clearance volume is complicated due to the problems involved with the measurement of flow in small sections. The clearance in real equipment is so small that velocity measurements become cumbersome. Velocity and turbulence measurements for eccentric annular and labyrinth seals for different Reynolds and Taylor numbers were performed by Johnson (1989), Thames(1992), Das (1993) and Shresta (1993). Also, instantaneous and phase averaged wall pressures for an annular and labyrinth seal with dynamic eccentricities and a whirl ratio of one were recorded by Winslow (1994) and for different pre-swirls by Robic (1999).

From the data they collected it was observed that the pressure and suction sides switched positions between the non-whirling and the whirling seal for the same eccentricity. This implied that the pressure forces also changed locations as the whirl ratio varied from

---

This thesis follows the style and format of *Journal of Turbomachinery*.

0 to 1 reaching a minimum at some intermediate whirl ratio and then increasing on the opposite side of the seal. To ascertain the circumstances under which the forces change directions and also to study the effects of fractional whirls on the clearance flow, the current work endeavors to measure the dynamic wall pressures on an annular seal for the following test conditions:

1. Eccentricity: 50% of the seal-stator clearance.
2. Water Flow Rate: 4.86 ±0.05 l/s (corresponding to Re = 24000)
3. Rotor Speeds: 0 rpm or static eccentricity case, 1800 rpm, 2700 rpm, 3600 rpm
4. Whirl Ratio: -1 to +1 at intervals of 0.1 for 800 rpm, -0.6 to +0.6 for 2700 rpm, -0.5 to +0.5 for 3600 rpm.
5. Zero pre-swirl.

Seal design can be improved by incorporating the findings in the wall pressure distribution for different whirls of the rotor. The results obtained can also be used to determine the forces and the moments generated due to the differential flow in the clearance volume. Knowing the pressure distribution along the seal wall for different whirls can possibly assist in determining the appropriate conditions under which the rotor is under minimum stress.

LITERATURE REVIEW

Hirs (1973) proposed a bulk-flow theory as a basis for designing bearings lubricated by fluids of low kinematic viscosity. He compared his model with the law of the wall and mixing length concepts to study the differences. The theory is based on the finding that the relation between the wall shear stress and the mean relative velocity at the point where the shear stress is exerted can be expressed by a formula for drag flow and pressure flow or a combination of both the flows. The model differed from the earlier methods in the empirical constants used. He found that the bulk flow theory was slightly better for the low Reynolds number and matched well for the high Reynolds number in comparison with the law of the wall theory. Brennen (1976) analytically calculated the forces exerted by the fluid in the annulus between concentric cylinders for different annular widths, Reynolds numbers and whirl using a simplified Navier Stoke's equation.

Allaire et al. (1978) extended the Hirs (1973) bulk flow theory to large eccentricities and high axial flow conditions. He included the roughness effects in his analysis. Short annular seals with large axial flows were evaluated experimentally. He used perturbation techniques to solve the flow equations. The friction coefficient was found to affect the load bearing capacity of the seal. The large stiffness and damping coefficients were determined to have a stabilizing effect on high-speed machines.

Kaneko (1984) analyzed annular seals for static and dynamic characteristics in the turbulent and laminar regions based on a mixing length theory. He employed the ordinary Reynolds equation for the laminar region and 2-dimensional turbulent equations for the transient zone. He considered both the circumferential and axial velocities in the turbulent clearance volume unlike bulk flow models. The pressure drop distribution along the seal circumference at the inlet region influenced the seal load carrying capacity and the main stiffness terms. The author determined the coefficients without considering the mass effects of the flow on the seal. The values calculated were in fairly good agreement with the experimental results.

Hashimoto et al. (1988) studied the effects of fluid inertia forces on the dynamic characteristics of short journal bearings. They calculated the whirl onset velocities using

three lubrication theories, namely turbulent theory with inertia effects, turbulent theory without inertia effects and laminar theory. They determined the shaft speeds for which the system became unstable when analyzed using each of the three theories. It was found that inertia effects improved the stability of the system under certain running conditions. Their analysis pointed out that inertia effects dominated the turbulence effects on the transient characteristics of clearance flow in a short journal bearing. Hence, it can be deduced that the journal bearings lubricated by low kinematic viscosity fluids can essentially be modeled based on turbulent theory with inertia effects being considered.

3D laser anemometry measurements in an annular seal were performed by Johnson(1989) for a Re=27000 and Ta=6600 to obtain the mean velocity profiles and the complete Reynolds stress tensor distribution. The inlet velocities and the turbulent kinetic energy were calculated. The flow near the seal inlet was found to be in the turbulent region. The azimuthal velocity at the seal inlet was found to be almost zero. The radial velocity typically was 10% less than the average axial velocity. The axial mean velocities contour showed magnitudes about 20% higher than the average leakage velocity near the entrance region. The magnitude of the mean axial velocity decreased towards the seal exit. The mean radial velocity followed a pattern of low initial velocity, almost going to zero, maximizing somewhere in between and then reducing again. The mean azimuthal velocity increased continuously as the flow progressed downstream. The shear stresses were found to be dominated by the $u'_x u'_r/U$ term. It was also noted that this term steadily increased as the flow progressed towards the seal exit.

Chen and Jackson (1987) put forward a method of directly calculating the dynamic coefficients of a seal at any location on its circumference. They proposed two approaches to determine the dynamic coefficients without actually aligning the minimum clearance location. The leakage model employed by them compensated for the effects of seal surface roughness and misalignment. They experimentally determined the effects of roughness on the leakage rates and the dynamic seal coefficients. Rough stator surface in combination with smooth rotor surface decreased the leakage rate and thus improved the seal performance. It was also found that labyrinth seals had a better sealing performance than rough annular seals. The experimental figures for the dynamic coefficients tallied with the

results from the analytical models used.

Morrison, Johnson and Tatterson (1991), Morrison, DeOtte and Thames (1992), Das(1993),Morrison, DeOtte and Thames (1994) and Morrison and Winslow (1995) measured the flow field inside an annular seal using a 3D LDA system. They observed that the location of maximum and minimum velocity migrated between a non-whirling seal and a seal whirling at a ratio of one. Olivero–Bally et al. (1993), measured the wall pressure fluctuations in turbulent boundary layers and determined that flush mounted pinhole piezoresistive pressure transducers were appropriate for acquiring data in the high frequency or turbulent region of flow. The transducers were exposed to the flow through Ø 0.3mm holes to minimize spatial averaging effects. Nunes (1993) performed a comparison between a ScaniValve system and piezoresistive transducers for measuring wall pressure and found the piezoresistive transducers to work better in the transient pressure zones.

Arghir and Frene (1997a) and (1997b) theoretically investigated a 50% eccentric synchronously whirling seal. The data from Morrison et al. was used as a case study for comparing the results of the analysis. A perturbation technique with averaged Navier-Stoke's equations was used as the method of analysis. The average pressure distribution matched experimental results shown by Morrison et al except at the seal entrance and exit. They also noticed the migration of maximum axial velocity along the seal as found experimentally. They showed perturbation technique can be used for eccentricities as large as 50%.

Robic (1999) experimented with 0%, 10%, 25% and 50% eccentric seals. They conducted the tests with different Reynolds and Taylor's number for annular and labyrinth seals. Mean and phase averaged pressure distribution along the length of the seals were mapped. The location of high pressure was observed to change locations between whirling and non-whirling seals. The mean pressure showed a sudden increase at the seal entrance decreasing to 45% at approximately 10% of the seal length. They also performed force and moment analysis for all the cases. The flow into the seal was regulated by swirl rings, which could impart either positive, negative or zero swirl to the flow. The positive swirl added to the tangential velocity of the flow while the negative swirl reduced it.

EXPERIMENTAL FACILITY

The experiments were conducted at the Turbomachinery Laboratory at Texas A&M University. The test facility used for this work is classified into four distinct units.

1. The water supply system
2. The seal test facility
3. Eccentricity and whirl setting unit
4. Instrumentation

Water Supply Unit

Water to the test rig is supplied by a centrifugal pump driven by a 29.5kW (40hp) motor from a 19m^3 tank. The water supply system is a closed unit in which water exiting the test section flows back to the supply tank through a heat exchanger. To prevent cavitation, pressure inside the test section upstream of the seal is maintained at a minimum of 138kPa (20psi). A gate valve on the inlet line is adjusted to ensure the minimum test section pressure as well as to control the flow. A gate valve on the outlet, nearest to the test section, is left open throughout. A turbine flow meter with 0.25% accuracy and a linear range between 1.6 l/s to 14.2 l/s is used to measure the water flow rate. A frequency counter records the output voltage frequency from the turbine meter. This output voltage frequency is calibrated to measure the flow rate through the test section. The test section pressure is monitored using a Bourdon tube pressure gauge with a rating of 413.7kPa (60psi). The outlet pressure for the supply pump is maintained at 600 ± 30kPa (90±2psi). The water temperature in the test facility is maintained at 30.5 ± 4°C using a 70 kW heat exchanger in order to maintain the thermal expansion of the seal within limits. The supply water temperature is monitored using a copper – constantan thermocouple that has a time constant of approximately 0.5s. The water entering the test section is cleaned of all floating debris by a 10μ filter placed at the pump exit and a wire mesh just ahead of the seal. Water is re-circulated back to the supply tank through two outlets from the test rig.

Seal Test Facility

The test section is comprised of a rotor-stator seal arrangement (Fig.1) in which the rotor is connected to an overhung shaft of diameter 50.8mm run by a 37kW (50hp) variable speed motor capable of speeds up to 5300rpm. The rotor, which also serves as a seal, is enclosed in a stainless steel stator of inner diameter 166.64mm. The stator itself is constrained axially in the housing but is free to oscillate radially within the housing. O-rings on the either side of the stator and on the housing prevent water leakage to the outside. Prior to assembling the stator inside the test rig, a silicone based lubricant is applied to the stator sides and to the housing surface in contact with the stator to prevent wear and to allow for smooth stator oscillation. The outer diameter of the rotor is measured at 164.1 mm. The rotor-stator clearance measures 1.27mm on the radius. To facilitate easy instrumentation work, the simulated clearance of 1.27 mm between the seal and stator is slightly larger than that present in most turbomachines. The seal is made of acrylic and has the following mechanical properties (Johnson, 1989):

Young's Modulus, $E = 1.24 \times 10^{10}$ Pa,
Density, $\rho = 913$ kg / m^3,
Ultimate Strength, $\sigma_{ult} = 9.507 \times 10^{10}$ Pa,
Coefficient of thermal expansion, $\alpha = 41 \times 10^{-6}$mm/ °C.

The seal was made of acrylic to enable LDA velocity measurements near its surface. The plain annular seal is 35.56 mm in length and has a highly polished surface with an anti reflecting coating applied on its surface. The inner plug ensures smooth flow of water up to the seal and also accommodates guide vanes that provide negative, zero or positive swirl to the flow ahead of the rotor region. It should be noted that throughout the current work a zero pre-swirl ring was used. The downstream edge of this ring has a diverging cross section. There is a 5 ± 0.1mm gap between the swirl generating assembly tip and the rotor leading edge. Water entering the test section passes through a plenum where it is filtered. The eddies generated in the piping system are broken down by the Ø3 mm holes in the plug

support.

Das (1993) utilized the “hoop stress analysis for a thin cylindrical body” method to analyze the mechanical growth of the seal. He reckoned that the seal expanded by 0.0386 mm (3% of the clearance), at a rotor speed of 3600rpm and by 0.006 mm/°C (0.4% of the clearance for the 8°C test temperature window) with changes in temperature. As the water temperature in the test section increases, the seal expands based on the coefficient of thermal expansion and causes variation in the clearance volume. It is for this reason that an air cooled heat exchanger is employed to maintain the water temperature within preset limits. Bending of the rotor for maximum tip loading was measured by Robic (1999). The maximum deflection that was observed at the rotor extremity for a load of 88.96 N (20 lbf) was 0.04 mm (1.6 mils) or 3.2% of the clearance. Thus the maximum variation of clearance during the operation of the rig was calculated to be a maximum of 6.6% of the clearance. This implies that under extreme conditions the clearance will have a maximum variation of 6.6% in addition to the 50% eccentricity already being set.

The stator has seventeen flush pressure taps aligned to span the axial length of the seal at two azimuthal positions along its circumference. The pressure tap holes are 0.79 mm (1/32") in diameter on the seal side. They are counter bored from the exterior, the counter bore diameter being 1.59 mm (1/16"), to mount Ø 1.59 mm stainless steel tubes. The ScaniValve pressure taps are connected to these steel tubes via nylon tubes. The nylon tubes are held in position by tiny springs slipped over them. The stator also has a trapezoidal slot on its outer diameter where the instantaneous pressure transducer mounts can be fixed. The slot was earlier used to perform velocity measurements in the seal gap. The rotor speed is measured using a sensor that is triggered by the main shaft key way. The main shaft bearings are oil cooled. An independent cooling system with a gear pump is used to circulate oil through the bearings. Oil temperature inside the bearing is maintained under 147°F using a counter flow water-cooled heat exchanger. Synthetic oil of grade 10W40 is used for this purpose.

Eccentricity and Whirl Setting Unit

Variable whirl ratio is obtained by oscillating the stator independent of the rotor using the cam system shown in the fig.2. The motion is accomplished by removing the locator pins that hold the stator concentric to the housing. Provision for setting the stator eccentricity with respect to the rotor is incorporated in the system oscillating the stator. The conceptualized design is a cheap and reliable method for shaking the stator to simulate different whirl ratios at different eccentricities. Two independent cam operated plunger units are designed to oscillate the stator at varying frequencies and amplitudes. Each plunger unit is comprised of a Ø25mm shaft supported on two pillow blocks, a cam to set the stator eccentricity, plunger housing and a plunger. The plungers are located orthogonally to each other on the stator. The plungers effect the vertical and the horizontal oscillations of the stator as well as making it whirl when working in unison. The head of the plunger is connected to the stator while the threaded end is screwed to the plunger housing which holds the outer race of a bearing on its inside. The inner race of the bearing sits on a cam mounted on the Ø 25 mm shaft driven by a 7.35kW (10hp) constant torque motor with a maximum speed of 1755 rpm. The inner edge of the cam is pressed against the shaft edge and is held in position with four fine threaded screws at 90° to each other. By adjusting these screws the cam can be set for different eccentricities. Castle nuts force the cam to press against the whirl shaft once the eccentricity is set. The maximum cam adjustment corresponds to 1.27 mm on the radius, which is equal to the clearance.

The phase between the two plunger units is set by changing the length of the timer belt driving the system, using an idler pulley positioned between the two plunger shafts. The whirl motor speed is controlled using a 36.8kW (50hp) Omega AC drive and can be made to spin in clockwise and counter clockwise direction by a switch on the drive. The whirl motor speed is indicated by a readout on the drive. A whirl ratio of one for rotor speeds up to 3600 rpm can be obtained using a 1:1 and a 2:1 pulley combination. The stator is whirled by setting the eccentricity and then running the cam-plunger shafts at different speeds. For static testing, a circular graded scale similar to a protractor and with a least count of 1° was designed and mounted concentric with one of the whirl pulleys. The eccentric stator was

held at a known reference and mean pressure readings were acquired at every 20° angular increments for a rotor speed of 1800rpm. The data was analyzed in the same manner as the dynamic whirl data.

Instrumentation and Data Acquisition System

The instrumentation consists of pressure transducers to measure the instantaneous and the mean wall pressures of the seal, the associated signal conditioners and the data acquisition system. The mean pressure distribution along the seal length is measured using a ScaniValve system. The ScaniValve is connected to the pressure taps on the stator by nylon tubes. The ScaniValve indexes sequentially to measure pressures at each of the thirty-four pressure taps. A Validyne pressure transducer is used to measure the average pressure. Since the maximum pressure encountered across the seal is between 96.5-110.5kPa (13.0 to 16 psi), the Validyne transducer is fitted with a 137.9kPa (20.0psi) diaphragm to obtain maximum resolution. An 8-channel computerized data acquisition board, CIO-DAS802/16, with a maximum sampling rate of 100kHz is used to record the pressure readings. The ScaniValve is indexed using CIO-Relay16 and CIO-DIO/24 controller boards. The acquired data is averaged over 1024 samples to obtain the mean wall pressure at each tap position along the seal. The accuracy on the data output from the system is 1.5% of the measured value.

According to Olivero – Bally et al. (1993), who measured the wall pressure variations in turbulent boundary layers, flush mounted pinhole piezoresistive pressure transducers were found to be suitable for acquiring data in the high frequency range. Nunes (1993) measured the pressure distribution along the walls of a smooth annular seal for flow rates of 2.44 and 4.81 l/s using a ScaniValve system and also a flush mounted pin hole piezoresistive transducer system. An examination of the results from the two systems showed that the piezoresistive transducers were better at measuring transient wall pressures than the ScaniValve system. The ScaniValve system was found to be inadequate in accurately measuring and quantifying the dynamic or the instantaneous pressures due to their low frequency response. Piezoresistive Kulite pressure transducers rated for 172.5 kPa

(25 psi gauge) and having a rated sensitivity of 0.35 mV/kPa (2.5 m V/psi) and a frequency response of 120 kHz were chosen for the purpose. These transducers can be used to measure pressures up to 276.0 kPa (40psi) safely.

Brass plugs (fig.3) with 0.3mm pinholes were manufactured to hold the Kulite transducers such that they fit in the trapezoidal slots made for laser measurements. Four such plugs with holes at different axial positions were drilled and tapped to hold the flush mounted pressure transducers. The brass blocks provide several axial measurement locations along the entire length of the seal with one upstream and five downstream positions. The length of the seal (L) is used to normalize the axial position of the transducers along the seal. The axial positions are represented as a Z/L coordinate with zero being the entrance of the seal and one being the exit. The brass plug measurement surfaces were machined to fit level with the stator inner surface so as not to interfere with the flow. Data from the Kulite transducers are amplified using a 10X gain setting on OMNI AMP™ III instrumentation amplifiers and then processed through an 8 bit, 4-channel Rapid Systems A/D converter unit and a computer at the rate of 2000 samples per second. The Rapid system has a maximum frequency response of 500 kHz. The external trigger to the Rapid system is provided when a reflector strip on the cam-plunger shaft activates an optical sensor. The system starts acquiring data when it receives the trigger from the optical sensor. By fixing the timing of the trigger(positioning the reflector strip at a known location) with respect to a known shaft or stator position the collected data can be phase averaged. The whirl motor speed can also be measured using the output from the optical sensor and a frequency counter. The Validyne and the Kulite transducers are calibrated against a dead weight tester. Two Bentley Nevada proximity probes are used to determine the stator position. The probes are connected to the Proximitor® via 5m cables. They are calibrated for the specific material of the stator on a lathe. These probes can also be used for triggering the Rapid System for phase averaging purposes. The rotor speed is controlled by a Dynamatic variable frequency drive system.

EXPERIMENTAL PROCEDURE

Steps to Set Eccentricity and Whirl

- To begin with the part of the housing pressing the stator against the downstream section of the housing is pulled out using shims to facilitate easy stator oscillations. Care must be taken to ensure that the shimming does not lead to leakage near the seal.
- The cam is set outside to zero run-out with respect to the whirl shaft using a dial indicator.
- The cam is inserted into the plunger housing with the plunger fastened to the stator. The entire plunger setup is mounted on the support frame.
- The plunger unit pillow blocks are shimmed to center the stator with respect to the rotor. A dial indicator is fixed to a large nut screwed on to the shaft for this purpose.
- The castle nut holding the cam is loosened slightly and the eccentricity on the stator is set by adjusting the fine threaded screws. The dial indicator screwed on to the rotor shaft is used to quantify the eccentricity. The castle nuts are re-tightened to hold the cam tightly against the shaft in the set position.
- To set the 90° phase between the two plungers, the plunger units are clamped such that when one plunger reaches the maximum or minimum eccentricity, the other reaches the middle value. Then the timing belt is run over the three pulleys and the belt slack is minimized by pushing the whirl motor using jack screws. The idler pulley is also tightened at its current location.
- The nut on the rotor is removed and the annular seal is mounted on the shaft with the zero eccentricity bushing. A torque of 33.9N-m(25ft-lbf) is used to tighten the nut holding the seal on the rotor.
- The whirl motor is spun manually and the clearance is checked using feeler gauges.
- The profile of the stator oscillation is studied by connecting the two proximity

probes to the 'X' and 'Y' terminals of an oscilloscope and can also be recorded on the Rapid data acquisition system. If the profile is circular and the oscillation is equal to what was set using the dial indicator, then the system is ready to be run. Else eccentricity readjustment is required.

The Validyne and the Kulite pressure transducers are calibrated using a pneumatic dead weight tester. The incoming flow rate is adjusted to 4.86 ± 0.05 l/s corresponding to Re = 24,000, with an upstream pressure of at least 138kPa(20psi) and not more than 275kPa(40psi). The seal is set for 50% eccentricity using the fine adjustment screws on the cams. The phase between the two cams is maintained at 90° to obtain a circular orbit for the stator when it is whirling. The stator is then whirled at ratios between 0 to 1, 0 to 0.6 and 0 to 0.5 for rotor speeds of 1800 rpm, 2700 rpm and 3600 rpm respectively with one of the four brass plugs fixed in the trapezoidal slot. A whirl ratio interval of 0.1 is considered. A set of instantaneous and mean pressure data is acquired. The whirl motor is then run in the direction opposite to that of the main rotor to produce negative whirls and another set of instantaneous and mean pressure readings is collected. The same steps are repeated for the remaining six plug positions. The average pressure drop across the seal is used to normalize the instantaneous and mean pressures during data reduction. Once all the plug positions with the 1:1 pulley setting are completed, the 2:1 pulley setting is prepared to produce the higher whirl ratios. To maintain the Reynolds number constant, physical properties such as density and viscosity of water are maintained as constant as possible. Temperature of water is maintained at 30.5 ± 4° C by employing the heat exchanger and the two fans.

Every time the brass plug's orientation is changed, the nylon pressure tubes connecting the pressure taps and the ScaniValve are flushed to clear any trapped air. This is done to eliminate any inaccuracies in the pressure measurement due to trapped air bubbles.

Nature of data acquired

1. Mean pressure readings for different eccentricities and whirl ratios.
2. Instantaneous pressure readings for different eccentricities and whirl ratios.

Parameters monitored

- Water temperature
- Bearing oil temperature
- Main motor speed
- Whirl motor speed
- Stator eccentricity
- Water flow rate

The procedure followed in collecting the mean and phase average pressure distribution with the necessary precautions adopted prior to testing are explained below. As mentioned earlier, a Rapid System data acquisition system along with Kulite transducers and signal conditioners were used to acquire the instantaneous pressure data and a DAS802/16 board along with a Validyne transducer and ScaniValve system were used to measure the mean pressure along the stator length. Care was taken to avoid drift of the Validyne electronics the Validyne by leaving it on for at least a day before acquiring data and throughout the entire data acquisition period. Water bubbles were cleared from the ScaniValve tubes to eliminate errors.

Phase Averaged Pressure Measurement

A sampling rate of 2 kHz was used with the rapid Systems data acquisition system as per Winslow [94]. A total of 1024 data points and 1024 data sets were acquired for each whirl, shaft rpm, flow rate and eccentricity. The number of cycles of rotor rotation or cycles per data set for different whirls ranged from 1.65 to 16.5 and are given in appendix A. Signal from an optical encoder mounted near the vertical whirl shaft provided a once per revolution signal which was used for phase averaging the data. The acquisition was triggered when the high clearance zone was at the top most position. The gain for each of the four transducers used to acquire the instantaneous pressures was set independently for each case to obtain maximum output resolution. The correct gain was determined by trial and error method to avoid chopping of the peak rms pressure amplitudes. The OMNI

AMP™ III was set for a 10X gain to amplify the signal output from the transducers. This gain was also set based on the raw output voltage from the transducers. A C++ program was written to convert the binary output from the Rapid system into readable decimal format. Post processing to convert voltage readings to obtain pressure was performed using Excel macros with graphs of the data created in TecPlot

Mean Pressure Measurement

A sampling rate of 128 Hz was used to acquire 1024 voltage readings for each of the seventeen axial positions along stator. The mean axial pressure distribution was calculated for these values. The gain setting was selected appropriately to get maximum data resolution. Data was acquired directly into Excel sheets using a macro. Installation of DAS Wizard and Instacal was required for the Excel macros to work. Instacal was used to sense the CIO- DAS802/16 and the relay cards and also to calibrate the DAS board. The mean pressure plots were created using TecPlot after applying the calibration values and normalizing the mean pressures on Excel spreadsheets. The range setting for the Validyne transducer can be set on the power supply/control unit.

RESULTS AND DISCUSSION

The annular seal was tested for a constant Reynolds number of 24000 corresponding to 4.86±0.05 l/s flow rate for positive and negative whirls and rotor speeds 1800 rpm, 2700 rpm and 3600 rpm(Ta=0,3300,4950,6600). The axial positions (Z) along the seal were normalized using the seal length (L), Z/L=0 corresponding to the seal entrance and Z/L=1 the exit. The axial mean pressures along the length of the stator were normalized by the seal inlet and the outlet pressures using the following equation:

$$P^*_{mean} = (P_{mean} - P_{out})/(P_{in} - P_{out})$$

Similarly the axial rms pressures were normalized using the seal length, L, mean pressure drop ΔP across the seal and the seal nominal clearance, c. The equation used is as given below:

$$< P^* >_{rms} = P(\theta, Z)_{rms} L / c\Delta P$$

Effects of Whirl Ratios and Taylor numbers on Normalized Mean Pressure Distribution and Pressure Drop across the Seal

The general mean pressure distribution for all the positive and negative whirl ratios and the three Taylor numbers follow the trend observed by Robic(1999) and Winslow(1994). The normalized mean pressure distribution experiences a rapid increase near the inlet region, undergoes a drop in pressure as the flow enters the small clearance volume annulus and before seeing a minor pressure recovery. Beyond this region of pressure recovery the normalized mean pressure profile follows a linear path. The influence of the diverging section on the flow at the exit is not discernible as the mean pressure continues to decrease. The pressure increase observed near the seal entrance is primarily due to the radial step the flow runs into in the face of an eccentrically whirling rotor and

also due to the diverging profile of the no- swirl ring at the downstream edge closest to the seal inlet. The entrance constriction encountered by the flow due to the rotor eccentricity affects the flow up to an axial position of Z/L=0.1-0.15 before the flow recovers. According to Morrison et al. (1994) the pressure recovery observed along the seal axis between Z/L=0.3-0.4 can be attributed to the "vena contracta" effect giving rise to a region of re-circulation on the rotor and the seal. This effect manifests itself as a recovery in pressure, enabling the mean pressures to overcome the subduing influence of the wall's frictional forces. The flow past this region is influenced by the wall friction alone and the pressure decreases almost linearly.

Reynolds number =24000, Ta=3300, Positive Whirl Ratios between 0 and 1

Fig.4 shows the mean axial pressure distribution for ω =0.0 to 1.0 for a shaft speed of 1800rpm. As the flow approaches the seal inlet, the pressure experiences a sharp increase up to Z/L=0.15 for all the whirl ratios. Between Z/L=0.15 to 0.25 a large drop in the mean pressure occurs. The pressure reduces by 70% of its value from Z/L=0.15 to 0.30. A small pressure recovery occurs at Z/L=0.22-33 after which the pressure reduces almost linearly from Z/L=0.4 to 1.3, well past the end of the seal. The normalized axial mean pressure distributions for all the whirl conditions coincide with each other indicating that the mean pressure distribution is independent of the rotor whirl. The findings of Robic(1999) that the ratio of dP^*_{mean}/ dZ/L was mainly dependent on the Reynolds and Taylor number matches our result which shows that the whirl ratio has no influence on the normalized average axial pressure distribution. Fig.5 represents the overall pressure drop across the seal for whirl ratios between 0.0 and 1.0 measured from the inlet plane of the seal to the exit plane. The general trend shows that as the whirl ratio increases the pressure differential increases slightly. ΔP reaches a maximum of 23.5kPa at ω=0.8and then decreases for further increases in ω. The variation of the pressure drop seen at this whirl ratio could be representative of the changes occurring in the instantaneous pressure field as it migrates along the cycle and the length of the seal.

Reynolds number =24000, Ta=3300, Negative Whirl Ratios between 0 and -1

Fig. 6 shows the normalized axial pressure distribution for the negative whirl ratios between 0 and -1 for Ta=3300. The mean pressure distribution shows a sudden increase in pressure as the flow enters the seal. This high pressure region extends up to Z/L=0.18 along the length of the seal. Between Z/L=0.18 and 0.28 the pressure experiences a 70% drop before making a small recovery at Z/L=0.28-38 for all whirls between 0.0 and -1.0. The rise and fall in the mean pressure at the entrance follow the pattern observed with the positive whirl ratio case for the same Taylor number. The slope of the mean plot beyond Z/L=0.4 is almost constant with minimal variations, following an almost linear path up to the end of the seal. It is also seen that all the normalized mean pressure curves for all the whirl ratios concur with each other indicating the independence of the mean pressure distribution from the negative rotor whirl also.

The pressure drop(ΔP) measured across the seal inlet and the exit plane for the negative whirl cases and Ta=3300 is shown in Fig 7. ΔP is seen to vary between a minimum of 20.6kPa at ω= -0.1 and a maximum of 21.7kPa at ω= -0.9. Between ω= -0.1 and -0.7 the pressure drop increases gradually and linearly. The pressure drop for the positive whirl ratios in the same range interestingly had very little change with the average at 23.5kPa. Between -0.8 and -1.0 the pressure drop appears to reach a plateau. Over all it is seen that the pressure drop for all the negative whirl ratios is lower than that for the same positive ratios.

Reynolds number=24000, Ta=4950, Positive Whirl Ratios between 0 and 0.6

Fig. 8 shows the mean axial pressure distribution for the rotor spinning at 2700rpm. The plot follows the previously observed trend where the pressure increases steeply near the inlet, drops between Z/L=0.12 to 0.22, recovers a little between Z/L=0.22 to 0.35 and then decreases almost linearly up to the exit. The distribution for all the measured whirl ratios converge including the one for ω= 0.0. Pressure decrease occurring immediately after the entrance was measured at 85% of the peak pressure, which is higher than the 70%

observed for Ta=3300. A mild wavy pattern in the profile beyond Z/L=0.4 is also observed. $dP^*_{mean}/dZ/L$ is also observed to have a lower gradient than Ta=3300 and is believed to be dependent on the Taylor number.

Fig. 9 shows the overall axial pressure drop across the seal for the different whirl ratios for Ta=4950. The zero whirl case is seen to have the maximum pressure drop amongst all whirl ratios. For the other whirl ratios the pressure drop across the seal remains relatively constant ranging between 28-29kPa. The pressure drop for the whirl ratios between ω=0.1 to 0.6 varies slightly and has a maximum of 28.76kPa for ω=0.4. ΔP has increased from 22-24kPa range for Ta=3300 compared to 28-29kPa for Ta=4950, which complies with Robic's(1999) findings of increasing pressure drop with higher Taylor numbers.

Reynolds number=24000, Ta=4950, Negative Whirl Ratios between 0 and -0.6

Fig 10. contains the mean pressure distribution along the axis of the seal. The effects of changing the whirl ratios on the mean pressure distribution is found to be negligible as the contours for all the pressures coincide with each other. The flow experiences an increase in pressure as it enters the seal. The increase in pressure is neutralized to some extent by the higher rotor speed and also due to the higher pressure drop across the seal and hence the high pressure rise observed for the lower Taylor numbers is not seen here. The pressure as observed earlier drops between Z/L= 0.13-0.22 and recovers between Z/L=0.23-0.36 is significantly less than in the previous cases. The gradient of the distributions from Z/L=0.4 to the end is almost constant and is higher than the Ta=6600 case but lower than Ta=3300. Fig 11. shows the pressure drop the flow undergoes across the seal length when subjected to the different whirl ratios. The static whirl case causes the maximum pressure drop at 35.75kPa. The whirl ratios between ω=0.1 to 0.5 produce a smaller pressure drop ranging between 27-29kPa. The ΔP magnitudes are comparable to the pressure differential experienced by the flow for the positive whirl cases and the same Taylor number.

Reynolds number=24000, Ta=6600, Positive Whirl Ratios between 0 and 0.5.

Fig 12. represents the average axial pressure distribution for positive whirl ratios at Ta=6600. The flow experiences a smaller pressure increase near the entrance compared to the smaller Taylor numbers. The higher tangential velocity of the fluid and the higher angular momentum gained by the fluid stifles the pressure increase seen for Ta=3300 and 4950. But the pressure drop between Z/L=0.15 and 0.25 is higher for Ta=6600. A small part of the lost pressure is redeemed between Z/L=0.25 and 0.35. The profile of the distribution beyond Z/L=0.4 is wavy but appears to have a linear contour along the mean path. The slope of the mean path is smaller compared to that of the lower Taylor numbers. Once again all the curves for the different whirl ratios converge. The wavy pattern observed after Z/L=0.4 is believed to be due to the possible generation of alternate rows of low and high pressure azimuthal vortices. At Z/L=0.23 the value of P^*_{mean} is slightly lower than zero and occurs due to the rapid acceleration of the fluid as it flows past the entrance of the eccentrically whirling seal giving rise to suction pressures over a small region. Beyond this small region the vena contracta effect comes into play causing a pressure recovery and restoring the positive pressures.

The pressure drop across the seal for the different whirl ratios for Ta=6600 is shown in fig 13. The general trend shows decreasing pressure drop with increasing whirl ratio for a shaft speed of 3600rpm. The highest drop occurs for the zero whirl case and the lowest for ω=0.5. The range of the pressure reduction the flow sees for all the individual whirl ratios lie within 42kPa to 44kPa and is much larger than those for the lower Taylor numbers. This is expected due to the higher angular momentum the fluid acquires at Ta=6600, undermining the effect of the axial momentum, providing a greater resistance to flow across the seal. Between ω=0.2 and 0.4 the drop in pressure appears to be constant before it starts reducing again. The reduction observed could be precursor to the changing pressure field and also a pointer towards determining the location of the peak dynamic pressures.

Reynolds number=24000, Ta=6600, Negative Whirl Ratios between 0 and -0.5

Fig 14. represents the axial pressure distribution for negative whirls at Ta=6600. The trend shows a smaller pressure rise at the inlet in comparison to that for the lower Taylor numbers. It closely resembles the plot for the positive whirls for Ta=6600 but has a lower pressure drop between Z/L=0.12-0.24. The pressure recovery and the waviness seen for the positive whirls is present in the negative case and occur almost at the same axial locations . These could be due to the formation of alternate azimuthal vortices in the flow. Also dP/dZ/L for the curve beyond Z/L=0.4 is greater in comparison to that seen for the positive whirls for the same Ta. The saw tooth nature of the distribution beyond Z/L=0.4 is amplified and appears to increase with higher Taylor number. As has been the trend so far with the other Ta and positive whirl ratios, the pressure distribution is unaffected by the changes in the whirl ratios. Fig 15. shows the pressure drop for the negative whirl and Ta=6600 case. The flow undergoes a lower pressure drop for the zero whirl case. For ω=0.1-0.4 it is seen to increase and is almost a constant. At 50% whirl the pressure drop the fluid undergoes is lower and appears to be decreasing. The changing pressure drop distribution can be an indicator of the continuously changing pressure field the fluid is subjected to. It is of interest to note that the negative whirls offer higher resistance to flow for this Ta than the positive whirls as the pressure drop across the seal for the negative whirls is seen to be higher in comparison with the higher whirls.

Effects of Whirl Ratios and Taylor numbers on Phase Averaged Instantaneous Pressure Distribution

The experimental results for the phase averaged pressure for Ta=3300, 4950 and 6600 are discussed in the following section. The rotor spins in the counter-clockwise direction when viewing it from the front of the test rig. Positive whirl ratios are obtained by spinning the stator in the same direction as the rotor. Each cycle is considered with respect to one complete stator rotation. The cycle begins with the maximum clearance location (0%), followed by the "pressure side" of the seal (0-50%) where the clearance is decreasing,

the minimum clearance occurring at 50% stator cycle and then the "suction side" of the seal (50-100%) where the clearance is increasing. An analysis of the contour plots of the phase averaged instantaneous pressures will assist in understanding the effects of whirl ratio on the fluctuating and mean wall pressures. Since no-swirl ring was used, the flow entering the seal is assumed to possess primarily the axial velocity. Winslow (1994) determined that the radial forces on the rotor due to the azimuthal shear stresses were two to three orders of magnitude lesser than the forces created by the pressure forces. Hence, to obtain a close approximation of the forces created by the flow through the clearance volume, information on the pressure distribution on the seal walls is thought to be sufficient.

Reynolds number =24000, Ta=3300, Positive Whirl Ratios between 0 and 1

The phase averaged rms pressure distributions for the rotor speed of 1800 rpm(Ta=3300) with positive whirl ratios between zero and one are shown in figures 16. to 26. The zero whirl case corresponds to a journal bearing type condition where the eccentricity is static. For the zero whirl case it is interesting that the pressure distribution near the seal inlet is very similar to the Sommerfield journal bearing pressure distribution. However, the axial velocity along the length of the seal causes the viscous driven pressure variations to decrease in magnitude to almost zero at the seal exit. The addition of whirl greatly disrupts the journal bearing type pressure field by decreasing the amplitude of the pressure variance and by decreasing the steep azimuthal pressure gradient at the minimum clearance location near the seal inlet. The overall trend points to the regions of high and low pressures migrating axially along the seal walls near the exit from the “pressure zone” to the “suction zone” between no whirl (static eccentricity) and synchronous whirl condition. The switch in the pressure distribution at the seal exit appears to occur between ω=0.8to0.9, when ΔP decreases. The migration is not as distinct or as complete as seen by Robic(1999). The maximum variation in magnitude of $\langle P^* \rangle$ for static eccentricity is between ±7. The peak positive and negative pressures have the highest magnitudes for zero and synchronous whirl. The whirl ratios between 0.1 and 0.6 have pressures fluctuating in the ±3 range. The whirl ratios from 0.7 to 0.9 exhibit a gradual increase in the magnitude of the peak

pressures, reaching a maximum between ω=0.9 and 1.0, the range being within ±7. Characteristically, for all whirls it is observed that the positive pressure zone occupies between 45% to 60% of the stator cycle while the remaining portion is occupied by the low pressure zone. The maximum positive pressure distribution along the cycle is typically around the 40% mark for all ω.

For ω=0.7, discrete axial peak pressure patches emerge at 20% and 65% between Z/L=0 to 1.0.This could be the manifestation of Taylor vortices which caused the axial banding described by Robic(1999) and Winslow(1994) except in the present case it is observed at a Ta=3300. The formation of these tiny pressure regions is evident even in ω=0.8 and 0.9 where the axial striations seem to be breaking up. Lessen (1987) indicated the presence of Taylor vortices in the boundary layer of the rotor and stator. Earlier, Schlichting (1968) pointed out to the existence of Taylor vortices inside the boundary layer. The differential energy gained by the fluid flowing through the clearance volume due to the whirling rotor could possibly drive the vortices.

The entrance effect where the flow is subjected to a sudden entry into a small annular region is distinctly visible for all whirl ratios between 0.1 to 0.6. The high turbulence at the entrance for these whirls manifests as random pressure fluctuations throughout the cycle up to an axial distance of Z/L=0.1 on the seal surface. This effect was also noticed by Thames (1992) and Robic(1999). For the higher whirls(0.7 to 1.0) the entrance region does not show as appreciable variations as the lower whirls since the relative angular velocity between the rotor and stator is lower. Also, for the higher whirls the rotor imparts more azimuthal momentum to the flow subduing the external fluctuations caused by the sudden entry. Greater relative velocity between the stator and the rotor for the lower whirl ratios offer rapidly changing entrance zone to the incoming flow when compared to the higher whirl ratios, causing the instantaneous pressures to fluctuate sharply. The disturbance in the pressure distribution noticed near the inlet is not observed at the exit section of the seal. The static whirl or the zero whirl ratio condition(fig.6) has the peak positive pressure around the 150° angular location corresponding to 40% of the stator cycle at Z/L=0.2. The high pressure zone extends up to the end of the seal remaining on the pressure side up to the exit. The lower pressures, as expected, occur in the suction zone

where the clearance is increasing. The pressure distribution does not follow Bernoulli's inviscid flow principle according to which a larger clearance would give rise to higher pressures. In our case, the flow is viscous dominated as in a journal bearing and the rotor's viscous drag creates a pumping effect which transmits higher momentum to the flow, squeezing the fluid in the smaller region and increasing the pressure. Between 60% and 65% of the stator cycle the low pressure extends along the entire axial length of the seal. The higher pressure overlaps about 10% into the suction zone.

A sharp 50% drop in amplitude of peak pressure between zero and 0.1 whirl ratio is noticed. The same pressure range is present up to a ω=0.6. The overall pressure drop across the seal is relatively constant over this whirl ratio range from 0.1 to 0.6. Contour plots for ω=0.1 and ω=0.2 show discrete azimuthal shifts in the maximum pressure locations at Z/L=0.4, 0.7 and Z/L=0.2,0.9 respectively. This could possibly be the emergence of a system resonance which shows up clearly at the lower whirls due to the relatively smaller forces involved. This could also be some type of vortex structures generated by the flow. Between ω=0.1 to 0.6, the higher pressures remain on the pressure side both at the inlet and the exit. The pressures also remain uniform throughout the cycle along the seal axis with occasional regions of high and low pressures. The maximum pressures on the "suction"and "pressure" regions start increasing in amplitude between ω= 0.7 and 1.0. The shift in the exit pressure magnitude begins from ω=0.8 where the high pressure in the "pressure" zone at the seal exit is inclining towards the "suction" zone. It becomes more evident for ω=0.9 before closely resembling a shift for ω=1.0.

Reynolds number=24000, Ta=3300, Negative Whirl Ratios between 0 and -1

Fig. 27 to fig.37 show the phase averaged pressure contour plots for negative whirl ratios between 0.0 to -1.0. The zero whirl case is the same for both the positive and the negative whirl ratios. As mentioned earlier the pressure distribution for the zero case follows a typical statically eccentric journal bearing model. The phase averaged rms pressure magnitude for ω=-0.1 to -0.5 ranges between ±1.5. Between ω= -0.6 and -1.0 the peak pressure amplitudes increases as the whirl ratio increases and fluctuates in the ±3

range. In comparison with the positive whirl ratios, for the same Ta, the peak pressures for the negative ratios are smaller by a factor of two. The fact that the instantaneous pressures are smaller for the negative case implies that the forces acting on the seal-rotor for the negative ratios are lower and hence under minimal stress and bending moment. Lower forces on the rotor may also be a major contributor to the stability of the system for the negative whirl ratios. The reasons for the smaller forces encountered for the negative whirl ratios could be that the azimuthal momentum imparted by the rotor is countered to a certain degree by the negative azimuthal momentum the fluid gains from the stator spinning in the opposite direction.

The same cycle of operation as the positive whirl ratios was considered for the negative case. A 50% drop in instantaneous pressures is observed between the zero whirl and ω= -1 case. The ω= -0.1 to -0.6 exhibit pressures which are a third of the peak pressures observed for the zero whirl but the location of the high pressure zone remains on the "pressure side" as in the static case. The picture gets interesting for ω= -0.7 to -1.0 where the high and low pressure zones have their locations floating along the cycle. For ω= -0.7, the high pressure distribution which consistently occupied "pressure side" of the seal for ω= -0.0 to -0.6, migrates to 30%-75% along the cycle. For the next few whirl ratios the magnitude of the peak instantaneous pressures increase gradually while the location of the positive pressures moves towards the end of the cycle. For ω= -1.0 the higher pressures return to the "pressure zone" covering up to 30% of the new cycle. A portion of the higher pressures still occupies the "suction zone" between 75% to 100% of the cycle. It is noticed that typically 50% of the stator cycle is occupied by each of the positive and negative pressure regions.

The "entrance effect" is also visible for the negative whirl case. The high fluctuations and the disruptions in the pressure distribution at and around the entrance (Z/L=0.0 to 0.2) for ω= -0.1 to -0.7 are the result of the rapidly changing flow volume the fluid runs into and also due to the differential surface speed it is subjected to by the rotor and stator spinning in the opposite directions. The effects are more prominent for the lower whirls where the pressure forces are smaller. For ω= -0.8 to -1.0 the pressure variations near seal entrance is mild and not disruptive to the nature of flow. For ω= -0.8 to -1.0 the larger

viscous forces and the higher azimuthal momentum the fluid gains from the rotor-stator dampen the pressure variations that occurs near the seal entrance. ω= -0.7 has tiny patches of peak pressures at Z/L=0.4, 0.8 and 1.1 corresponding to 40% and 60% of the stator cycle. Similar patches are observed for ω= -0.9 at Z/L=0.3 and 0.7 at 5% and 60% of stator cycle. The tiny regions of pressures could be the manifestation of axial Taylor vortices seen for ω= +0.7. ω= -0.6 and -0.8 show traces of formation or disintegration of these patches. For ω= -0.1 the azimuthal disturbances in flow at Z/L=0.3, 0.6 and 1.0 are noticed. Similar structures are seen for ω= -0.2 at Z/L=0.2 and 1.0. These could be analogous to the projections seen for some of the smaller positive whirl ratios and are possibly occurring for the same reasons.

Reynolds number=24000, Ta=4950, Positive Whirl Ratios between 0 and 0.6

Fig. 38-44 show the phase averaged pressure contour plots for positive whirl ratios between 0.0 to 0.6 at Ta=4950. As expected, the overall pattern shows high and low pressure regions to remain within the "pressure zone" and "suction zone" for the whirl ratios measured. The zero whirl case has the peak pressures fluctuating between ±9. The magnitude of the pressures falls to 50% of the zero whirl case for ω=0.1 to 0.6. For the same Ta and Re, Robic(1999) saw the pressure fluctuating between ±21 for ω=1.0. The introduction of rotor whirl is seen to reduce the magnitude of the instantaneous pressures but the pressures rise again as the whirl ratios increases. The dynamic pressures may approach the values seen for static eccentricity conditions as the rotor approaches synchronous whirl conditions. The high pressure zones cover up to 50% of the cycle and are noticed to be floating along the cycle.

The zero whirl ratio condition exhibits a higher pressure range than the other whirl ratios tested. The peak positive pressure occurs at 25-30% of the stator cycle while for Ta=3300 it was located at 40-45%. It is possible for the Taylor number to have such an effect on the flow. ω=0.1 to 0.4 have extremely low pressures compared to the zero whirl. The distribution is also observed to be even along the axis of the seal throughout the cycle. The forces acting on the rotor for these whirls will be low and more uniformly spread out.

All the whirl ratios between ω=0.1-0.4 exhibit the entrance effect. For these whirl ratios, at the seal inlet the pressure distribution appears discontinuous with a high degree of fluctuations. Between ω=0.1 to 0.4 the location of the higher pressures appears to be drifting between 25% to 75% of the stator cycle. For ω=0.2 and 0.3 the seal inlet has the high pressures between 25% to 75% while the exit shows high pressures between 40% and 80%. The amplitude of the pressure appears to be increasing for ω=0.5 and 0.6. Also the position of the low and high pressure regions stabilize and remain in the "suction" and "pressure" zones. The azimuthal structure seen for Ta=3300 is more subdued and appears only for w=0.2 at Z/L=0.2 and 0.6. The higher relative forces observed for Ta=4950 could possibly be suppressing the angular flow structures. The axial or the Taylor vortices are not noticed in the measured lower whirl ratios.

Reynolds number=24000, Ta=4950, Negative Whirl Ratios between 0 and -0.6

Fig 45-51. shows the cyclically averaged rms pressure contours for negative whirls at rotor speed of 2700rpm. The static eccentricity case is common with the positive whirl for the same Taylor number. Typically the positive and the suction pressures occupy 50% each of the stator cycle. For ω= -0.1,-0.2 and -0.3 the positive pressures cover between 0% to 50% of the cycle. The pressure drops by 85% once the pseudo stator starts whirling. ω= -0.6 shows signs of the instantaneous pressure recovering after being low for the smaller whirls. Between ω= -0.4 and -0.5 the pressure balances out and the differentiation between the high and the low pressure zone ceases to exist. The "suction" and the "pressure" zones have nearly the same magnitude of instantaneous pressures and the pressure distribution along the seal's axis and circumference is uniform.

For this shaft speed the flow at the inlet seems to be affected for all ω. The <P*> disturbances are distinct and show up between Z/L= 0.1 to 0.25 for the different whirl ratios. Though the pressures for the whirl ratios look evenly distributed, the flow could possibly be turbulent giving rise to the patchy pressure profiles. Azimuthal vortices are seen at Z/L= 0.2, 0.65 and 1.0 for ω= -0.1, -0.2 and -0.3. The vortices which are not clear for ω= -0.1 become more grow in size and become more apparent for ω= -0.3. It starts

disintegrating for ω= -0.4 and -0.5 and almost disappears for ω= -0.6. ω= -0.6 shows the <P*> increasing though the patchiness still remains. The negative suction pressure now exists between 25% to 50% of the stator cycle.

Reynolds number=24000, Ta=6600, Positive Whirl Ratios between 0 and 0.5

The phase averaged instantaneous pressure contour plots for the positive whirls and Ta=6600 are shown in fig 52-57. It is interesting to note that the pressure zones follow the pattern similar to Ta=4950 where the positive peak sections remained within the "pressure zone" for the zero whirl and floated around the stator cycle for the other whirls. For the zero whirl case the magnitude of the pressure ranges between +9kPa to -12kPa. The amplitude drops between ±4kPa for ω=0.1 to 0.5.

For ω= 0, peak positive and negative pressure patches exist at Z/L=0.25-0.35. As we pass from the seal inlet to the exit the axial pressures decrease in magnitude due to the increase in axial velocity of the fluid. A distinct separation in the positive and negative pressures is seen at the 50% cycle mark. The maximum positive pressure is seen to occur at 35% cycle, just ahead of the minimum clearance location and the negative peak spreads between the 55% - 75% cycle. The location of the pressure zones remains the same at the exit as at the inlet. For ω=0.1 the positive pressure occupies between 25% to 50% cycle which is partly into the "suction zone". The plot shows the presence of tiny portions of pressure distribution which could again be a form of azimuthal vortices or the manifestation of a system fundamental frequency. The position of the positive pressures near the exit shows evidence of migrating more towards the end of the cycle. ω=0.2 appears similar to ω=0.1 with the peak pressures located at the same positions along the cycle. The little pressure patches in the ω=0.1 case are more distinct, larger and are of a higher magnitude. The 0.3 whirl ratio shows the disintegration of the vortices and the migration of the high pressure from the "pressure zone" at the inlet to the "suction zone" at the exit. The high pressures move back to the "pressure zone" and occupy between 5%-60% of the stator cycle for ω=0.4. Traces of the high pressures still exist near the seal exit. For ω=0.5 a distinct flow of high pressure from the seal inlet to the outlet is observed. There is almost zero trace

of vortices in ω=0.4 and 0.5. The disturbance in the distribution near the inlet is visible only for ω=0.2 and 0.3.

Reynolds number=24000, Ta=6600, Negative Whirl Ratios between 0 and -0.5

Fig 58-63. show the phase averaged pressure plots fro the negative whirl ratios for a rotor speed of 3600rpm. The <P*> distribution follows the typical trend of high positive pressures in the "pressure zone" and lower negative pressures in the "suction zone". Unlike the positive whirls, for the same Taylor number, the positive pressures consistently occupy between 0% to 50% of the stator cycle for ω= 0 to -0.5. The zero or the static eccentricity case is the same for both the positive and negative whirl ratios. The maximum pressure for the zero whirl case ranges between +9 and -12. For the other whirl ratios <P*> drops between ±4kPa. The magnitude of the peak pressure increases as the whirl ratio increases. The maximum positive and negative pressures occur at Z/L=0.15 to 0.25. For ω=0.1 the azimuthal disturbances occur at Z/L =0.2.5, 0.6 and 0.9. At ω=0.2 the vortices are suppressed and appear only at Z/L=0.6 and 0.9. As the whirl ratio increases these structures disappear completely. The signs of migration of the "pressure" zone and the "suction" zone are not distinct and may occur more prominently at the higher Taylor numbers.

CONCLUSIONS

The present work explores the effects of the fractional whirl ratio and Taylor number upon the mean and transient wall pressure distribution for a 50% eccentric smooth annular seal. The test section was designed and modified to accommodate fractional whirl ratios. The provisions were made in the test facility design to handle both positive and negative whirl ratios. The stator was altered to provide eccentricity settings and rotation independent of the rotor. The tests were performed for Re=24000 and Ta=3300, 4950 and 6600. Both negative as well as positive whirl ratios were tested and the mean and dynamic pressures were measured using a ScaniValve system and high frequency piezoelectric Kulite pressure transducers respectively.

The overall trend showed that for any one particular direction of rotor rotation the normalized mean axial pressure distributions were independent of the rotor whirl irrespective of the Taylor number. Fig 64-74 show the fluctuation of mean axial pressures for the three Taylor numbers for all their tested whirl ratios. From these figures and the ones analyzed in "Results" section, it is noted that the pressure rise between Z/L=0.0 to 0.2 and the drop between Z/L=0.2 and 0.4 were affected by the changes in Taylor number. Ta=4950 had the maximum pressure rise at the inlet while Ta=6600 had the lowest for both positive and negative whirls between $\omega = \pm 0.1$ to ± 0.5. The pressure differential between the axial locations Z/L= 0.2 and 0.3 was found to increase as the Taylor number increased and was unaffected by the direction of the rotor whirl. Figure 75. clearly shows that the direction of the rotor whirl has very little influence over the normalized mean axial pressure distribution for the smaller Ta. But for Ta=4950 and 6600, fig 76-77., the profile between Z/L=0.2 to 0.75 appears to be spreading with the positive whirls exhibiting a greater drop in pressure between Z/L= 0.1 and 0.2. The slope of the mean pressure profile beyond Z/L=0.4 to the exit is maximum for the lower Taylor number for the same whirl and is found to decrease with increasing Ta. The variation of ΔP for the positive and negative whirl ratios and the three Taylor numbers are shown in fig 78, 79 and 80. From these figures it is clear that the pressure differential across the seal inlet and exit increases with increasing Taylor numbers. Between the different whirl ratios for the same Taylor number only slight fluctuations are

noticed. The important thing to be noted in these figures is the changing values of the pressure drop with the direction of the rotor whirl, as we move from a lower to a higher Taylor number. The negative whirl ratios which have a lower pressure drop across the seal than the positive whirl ratios for Ta=3300 has almost the same ΔP as positive whirl ratios for Ta=4950 and a greater drop in comparison to the positive whirls for Ta=6600.

The significant finding of this study was the determination of the whirl ratios at which the peak instantaneous pressures switched sides from the "pressure zone" to the "suction zone" at the seal exit between an eccentric static seal and a synchronously whirling seal for the positive and negative whirl ratios for Ta=3300. For the positive whirl ratios the switch occurred between ω=0.8 and 0.9, though the reduction in the amplitudes of the peak pressure was noticed between ω=0.1 to 0.6. For the negative whirls the entire pressure field was observed to be drifting around the seal azimuth for whirl ratios between -0.7 to -1.0. The magnitude of the pressures remained in the same range for both the positive and negative whirl cases. The negative whirls also had lower rms pressure fluctuations between ω= -0.1 and -0.6. It was not possible to arrive at a similar conclusion for Ta=4950 and 6600 as all the whirl ratios were not tested due to design constraints on the test rig. The entrance effects were prominent for $\omega=\pm0.1$ to ±0.5 for all Taylor numbers. For the higher whirl ratios the disturbances experienced by the flow seal inlet were subdued and less vivid.

At ω=0.7 structures similar to Taylor vortices as reported earlier by Robic(1999) were observed for the positive whirls of Ta=3300. Similar structures were seen between ω= -0.7 and -0.9 for the negative ratios and the same Ta. The lower whirls did not exhibit these vortices. Due to the lower pressures for ω=0.1 to 0.6 for almost all the Ta, it is believed that running the seal in this whirl range will have a minimum force on the rotor. For 1800 shaft rpm and positive whirl ratios of ω=0.1 and 0.2, conical structures of high pressures project into the "suction zone". These structures are thought to be either some type of azimuthal vortices or disturbances caused in the flow by the excitation of the system fundamental frequency, which are normally suppressed by the damping effect of water but showed up in the measurements due to the lower forces involved in the flow at those whirls. Typically for all the Taylor numbers, the phase averaged plots exhibited high peak pressures for the static and synchronously whirling case. The whirl ratios between 0.1 and 0.6 had almost

60%-80% smaller and more evenly distributed peak pressures. The peak pressures were seen to rise for whirl ratios beyond 0.6. For the higher whirls the azimuthal momentum gained by the fluid caused the instantaneous pressures to increase. For Ta = 4950 and 6600 it is critical to note that a conclusive result as to how the pressure distribution behaved was not measured. The constraints in the design of the cam eccentricity setting fine screws prevented the testing of the positive and negative whirl ratios between 0.7 - 1.0 and 0.6 - 1.0 for Ta = 4950 and 6600 respectively and thus obtaining a comprehensive result.

Future research can be focused towards studying the effects of Reynolds number on the pressure, force distribution and the bending moments on the seal walls for different Taylor numbers and whirl ratios. The reasons for the appearance of azimuthal vortices seen for Ta=3300 can be investigated. Numerical simulations for the tested cases can be performed to reduce the cost of experimentation. Different types of seals with smaller clearance volume can also be tested. Similar measurements can be performed for more eccentricities. An interesting and challenging work of determining the rotordynamic seal coefficients from the pressure, force and rotor displacement data acquired can be pursued.

REFERENCES

Allaire, P.E., Lee, C. C., and Gunter, E. J., 1978, "Dynamics of Short Eccentric Plain Seals with High Axial Reynolds Numbers," *Journal of Spacecraft and Rockets*, Vol. 15, pp. 341-347.

Arghir, M, and Frêne, J., April 1997a, "Forces and Moments due to Misalignment Vibration in Annular Liquid Seals Using the Averaged Navier-Stokes Equations," *Journal of Tribology*, Vol. 119, pp. 279-290.

Arghir, M, and Frêne, J., July 1997b, "Analysis of a Test Case for Annular Seal Flows," *Transactions of the ASME*, Vol. 119, pp. 408-414.

Brennen, C., 1976, "On the Flow in an Annulus Surrounding a Whirling Cylinder," *Journal of Fluid Mechanics*, Vol.75, No 1, pp. 173-191.

Chen, W.C., and Jackson, E.D., 1984, "Eccentricity and Misalignment Effects on the Performance of High-Pressure Annular Seals," *ASLE Transactions*, Vol. 28, pp. 104-110.

Chen, W.C., and Jackson, E.D., 1987, "A General Theory for Eccentric and Misalignment Effects in High-Pressure Annular Seals," *ASLE Transactions*, Vol. 30, pp. 293-301.

Das, P. G., 1993, "3-D Laser Doppler Velocimetry Measurements of Eccentric Annular and Labyrinth Seals," M.S. Thesis, Texas A&M University, College Station.

Hashimoto, H., Wada, S., and Sumitomo, M., 1988, "The Effects of Fluid Inertia Forces on the Dynamic Behavior of Short Journal Bearings in Super Laminar Flow Regime," *Journal of Tribology*, Vol. 110, pp. 539-547.

Hirs, G. G., 1973, "A Bulk Flow Theory for Turbulence in Lubricant Films," *Journal of*

Lubrication Technology, April, pp. 137-146

Johnson, M. C., 1989, " Development of a 3-D Laser Doppler Anemometry System: With Measurements in Annular and Labyrinth Seals," Ph.D. Dissertation, Texas A&M University, College Station.

Lessen, M., 1987, "Turbulent Flow in Shaft Seals and Bearings," *STLE Tribology Transactions*, Vol. 31, pp. 391-396.

Morrison, G. L., Johnson, M.C., and Tatterson, G.B., 1991, "Three-Dimensional Laser Anemometer Measurements in an Annular Seal," *Journal of Tribology*, Vol. 113, pp. 421-427.

Morrison, G. L., DeOtte, R.E., and Thames, H. D., 1992, "Turbulence Measurements of High Shear Flow Fields in a Turbomachine Seal Configuration," *1992 Conference on Advanced Earth-To-Orbit Propulsion Technology*, Huntsville, Alabama.

Morrison, G. L., DeOtte, R.E., and Thames, H. D., 1994, "Experimental Study of the Flow Field Inside a Whirling Annular Seal," *STLE Tribology Transactions*, Vol. 37, pp. 425-429.

Morrison, G.L., and Winslow, R. B. 1995, "Forces and Moments Generated by Pressure and Shear Stresses on the Stator of a Whirling Eccentric Seal," *31st Joint Propulsion Conference and Exhibit*, San Diego, California, AIAA 95-2766.

Nunes, S.J., 1993, "A Comparison of Pressure Measurement Systems for an Annular Seal with Whirl," Senior Honor's Thesis, Department of Mechanical Engineering, Texas A&M University, College Station.

Olivero-Bally, P., Forestier, B.E., Focquenoy, E., and Olivero, P., 1993, "Wall-Pressure Fluctuations in Natural and Manipulated Turbulent Boundary Layers in Air and Water,"

ASME FED-. 168, *Flow Noise Modeling, Measurement, and Control, Winter Annual Meeting*, New Orleans, Louisiana, pp. 63-74.

Thames, H. D., 1992, "Mean Flow and Turbulence Characteristics in Whirling Annular Seals," M.S. Thesis, Texas A&M University, College Station.

Robic, B. F., 1999, "Experimental and Numerical Analysis of the Effect of Swirl on the Pressure Field in Whirling Annular and Labyrinth Seal," Ph.D. Dissertation, Texas A&M University, College Station.

Robic, B. F., 2000, " Experimental Analysis of the Effect of Swirl on the Pressure Field in Whirling 50% Eccentric Annular Seal," *Proceedings of ASME IGTI TURBO EXPO 2000*, 2000-GT-0286.

Shresta, S. 1993, "The Effects of Pre-swirl on Flow Through Centered and Eccentric Annular Seals," M.S. Thesis, Texas A&M University, College Station.

Winslow, R. W., 1994, "Dynamic Pressure and Shear Stress Measurements on the Stator Wall of Whirling Annular Seals," M.S. Thesis, Texas A&M University, College Station.

APPENDICES

APPENDIX A: FIGURES AND GRAPHS

APPENDIX B: AutoCAD DRAWINGS

APPENDIX C: TABLES AND PHOTOS OF THE SEAL TEST FACILITY

Appendix D:C++ CODE

APPENDIX A

FIGURES AND GRAPHS

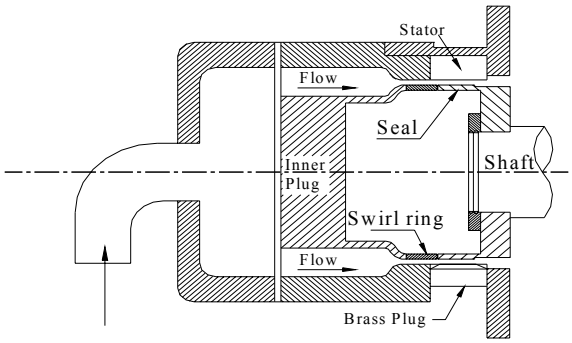

Fig1. Cross sectional view of the seal test rig

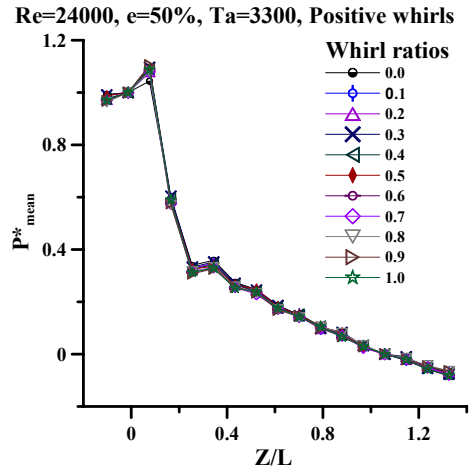

Fig 4.Effect of Whirl Ratio on Normalized Mean Pressure

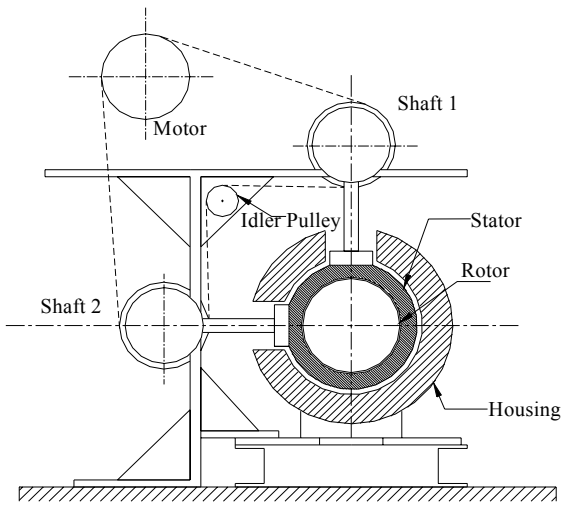

Fig 2. Basic sketch of the test rig with whirl setup

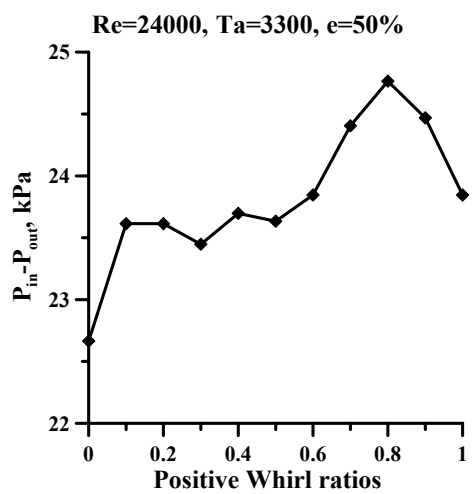

Fig 5. Effect of Whirl Ratio on delP across seal inlet and exit

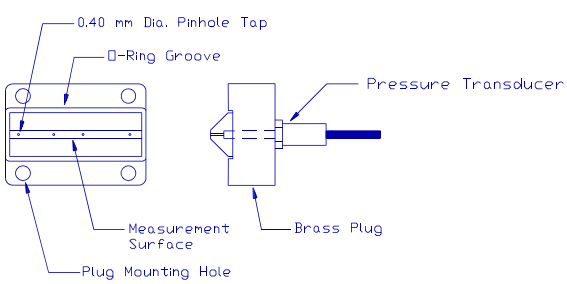

Fig 3. Piezoresistive pressure transducer mounting brass block

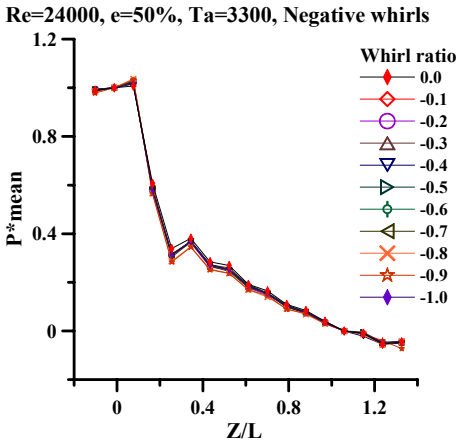

Fig 6. Effect of Whirl Ratio on Normalized Mean Pressure

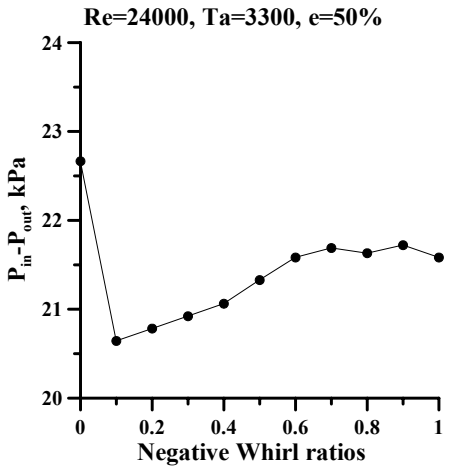

Fig 7. Effect of Whirl Ratio on delP across seal inlet and exit

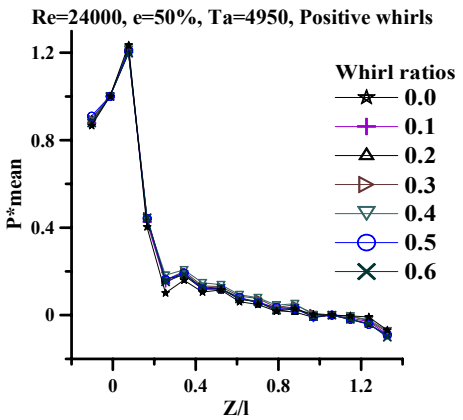

Fig 8. Effect of Whirl Ratio on Normalized Mean Pressure

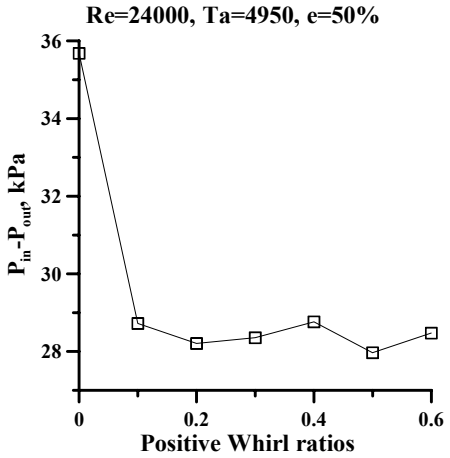

Fig 9.Effect of Whirl Ratio on delP across seal inlet and exit

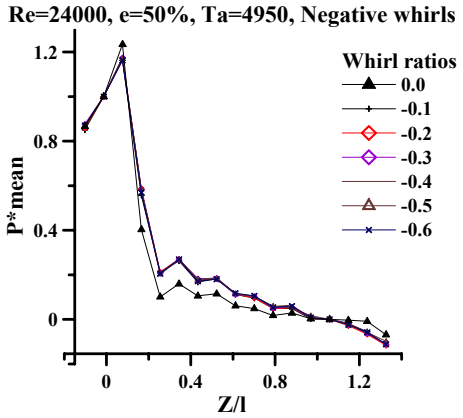

Fig 10. Effect of Whirl Ratio on Normalized Mean Pressure

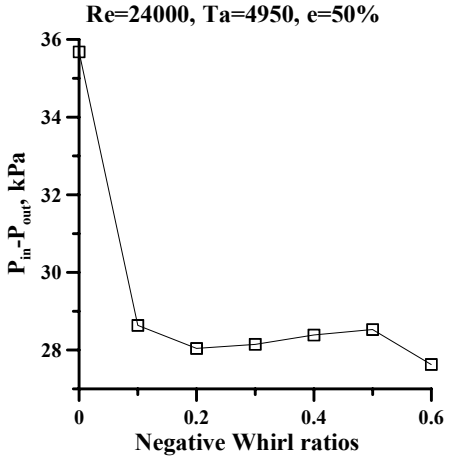

Fig 11. Effect of Whirl Ratio on delP across seal inlet and exit

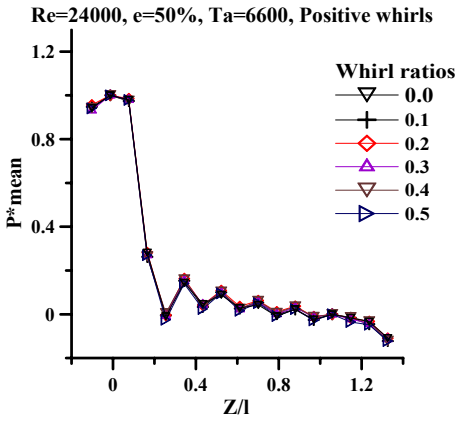

Fig 12. Effect of Whirl Ratio on Normalized Mean Pressure

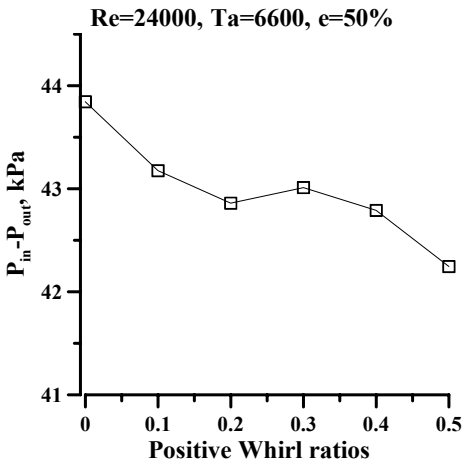

Fig 13. Effect of Whirl Ratio on delP across seal inlet and exit

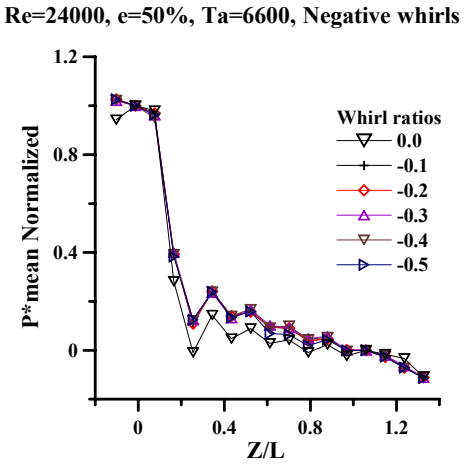

Fig 14. Effect of Whirl Ratio on Normalized Mean Pressure

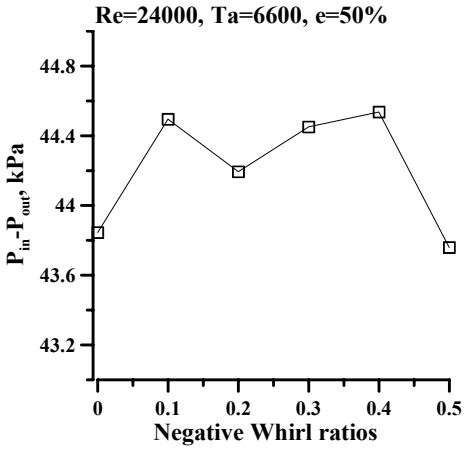

Fig 15. Effect of Whirl Ratio on delP across seal inlet and exit

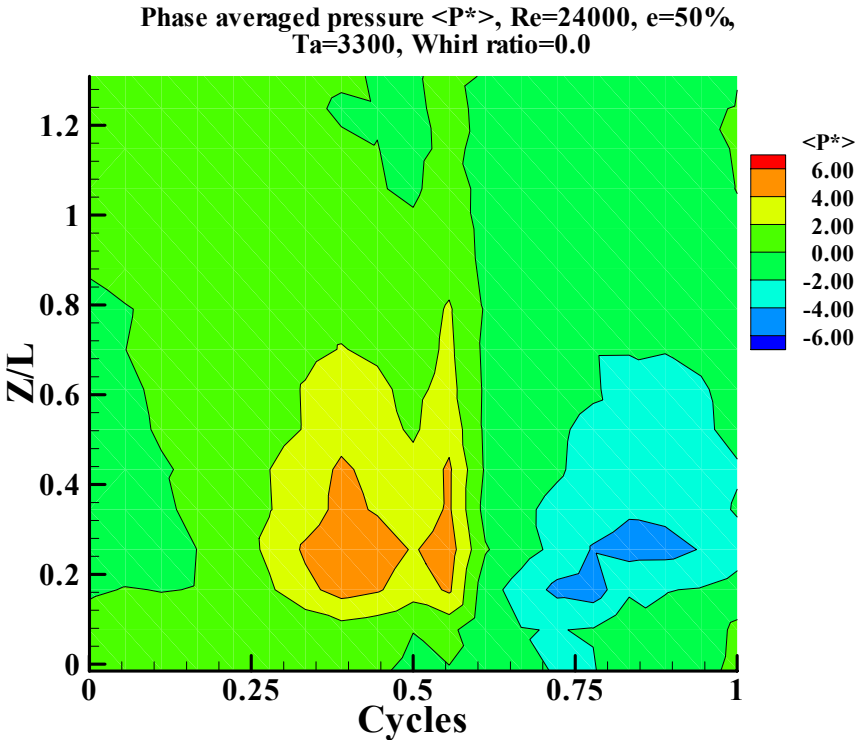

Fig 16. Phase averaged pressure contours, whirl ratio 0.

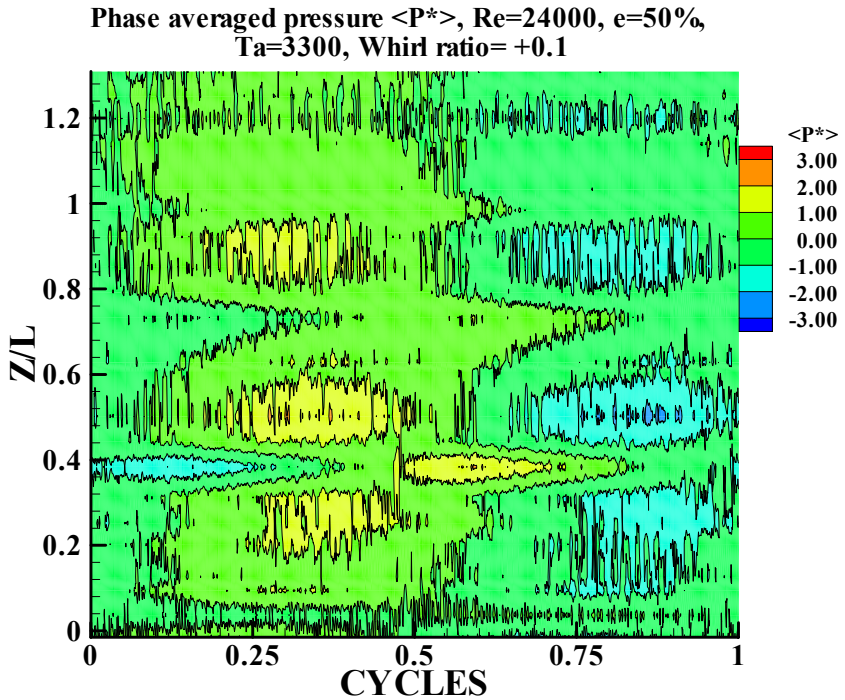

Fig 17. Phase averaged pressure contours, whirl ratio 0.1.

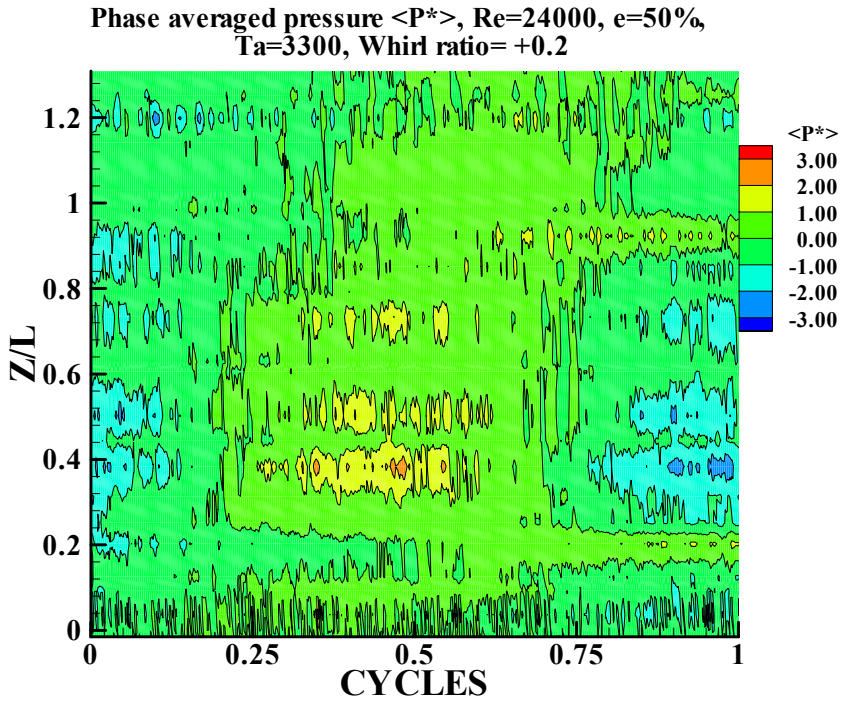

Fig 18. Phase averaged pressure contours, whirl ratio 0.2.

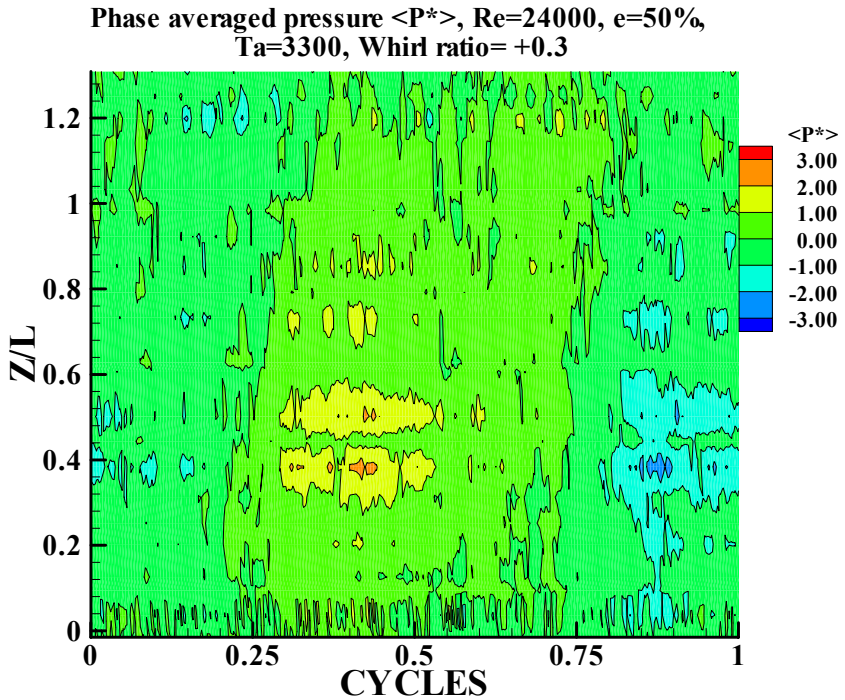

Fig 19. Phase averaged pressure contours, whirl ratio 0.3.

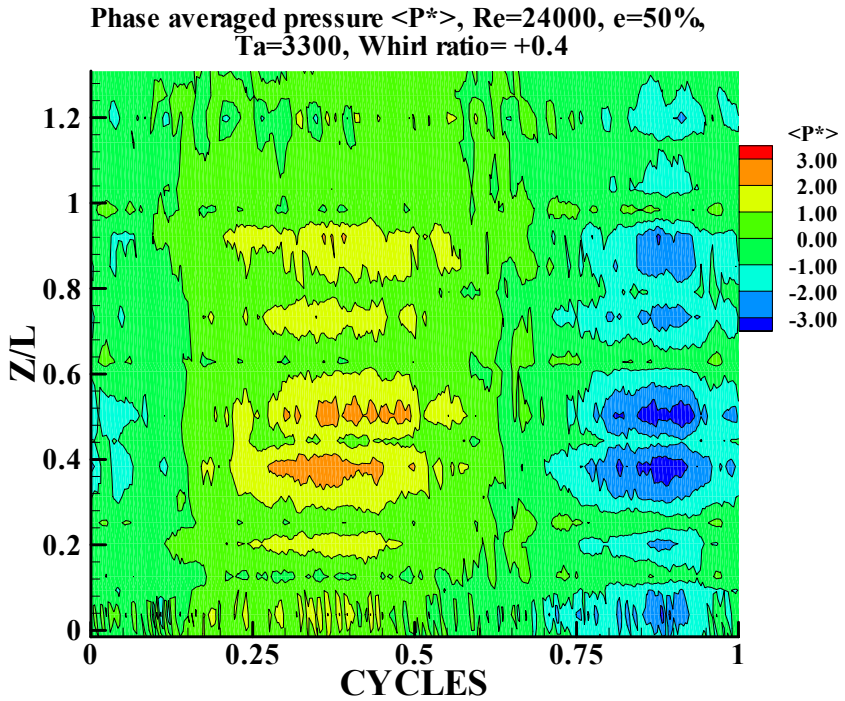

Fig 20. Phase averaged pressure contours, whirl ratio 0.4.

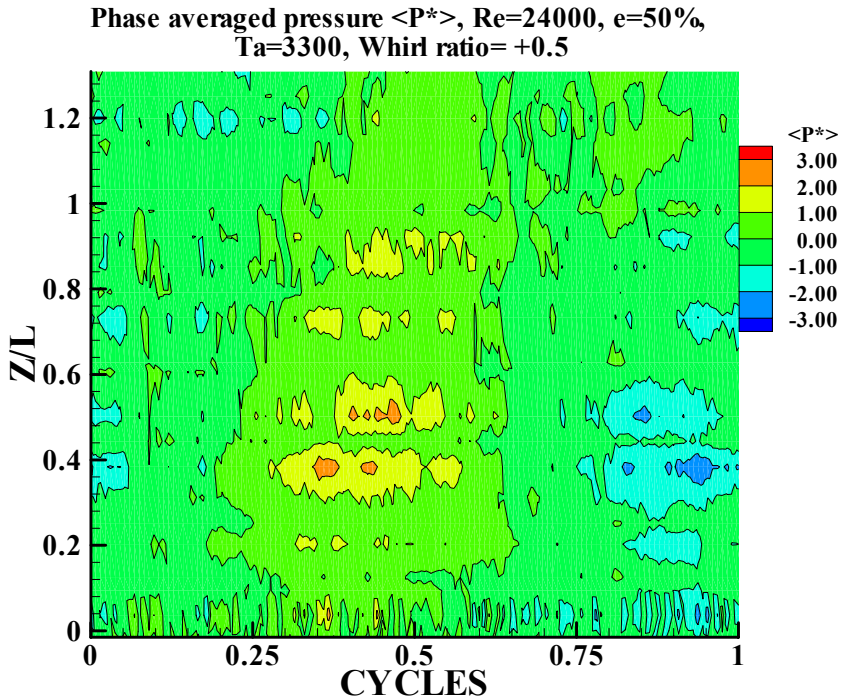

Fig 21. Phase averaged pressure contours, whirl ratio 0.5.

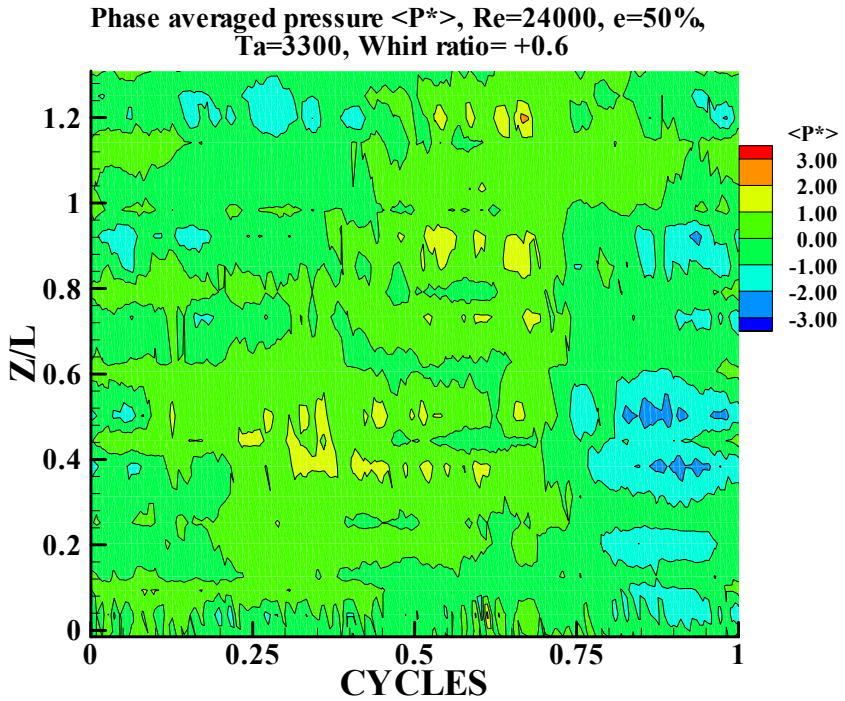

Fig 22. Phase averaged pressure contours, whirl ratio 0.6.

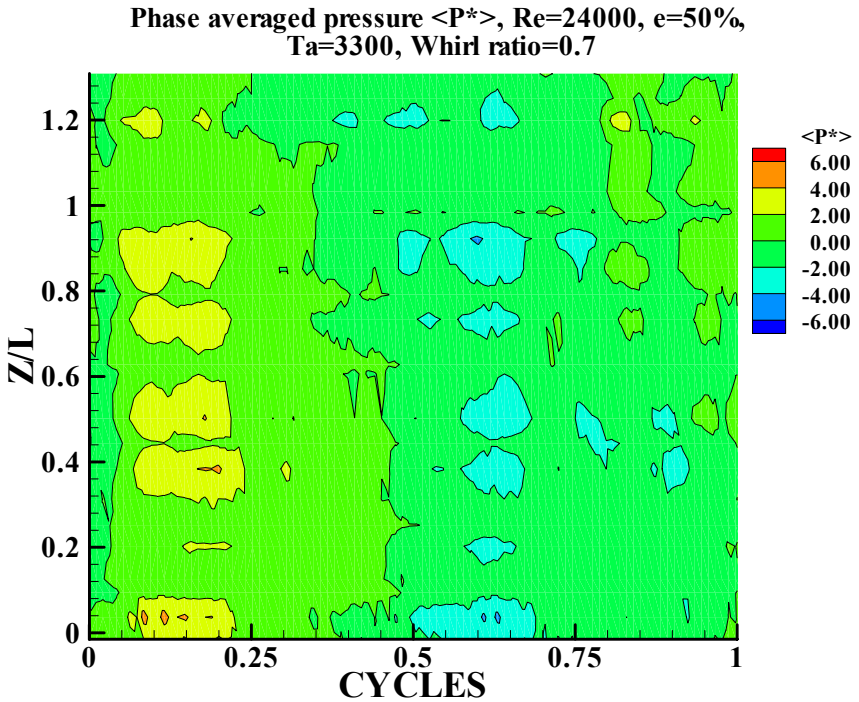

Fig 23. Phase averaged pressure contours, whirl ratio 0.7.

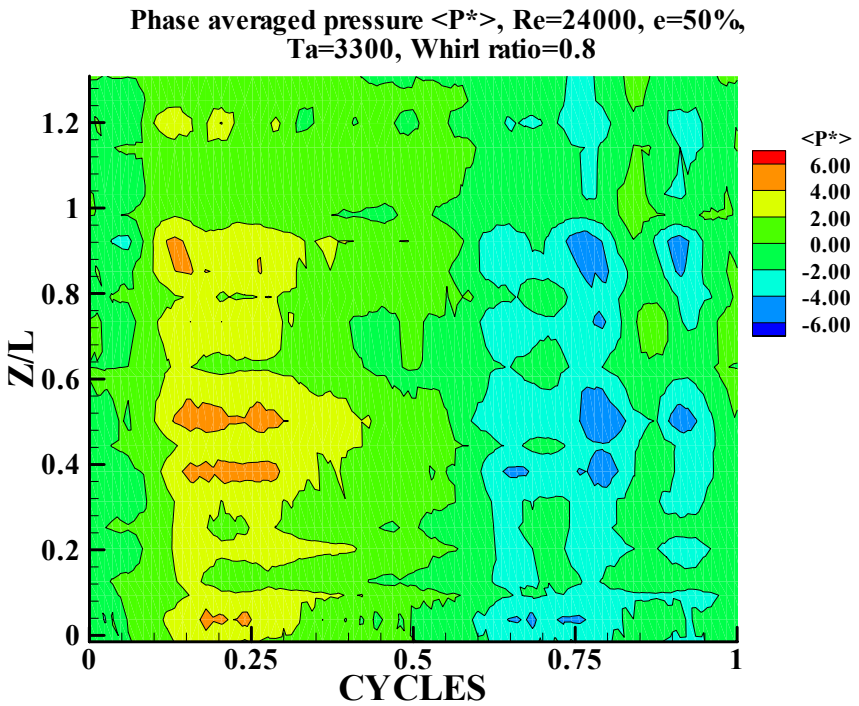

Fig 24. Phase averaged pressure contours, whirl ratio 0.8.

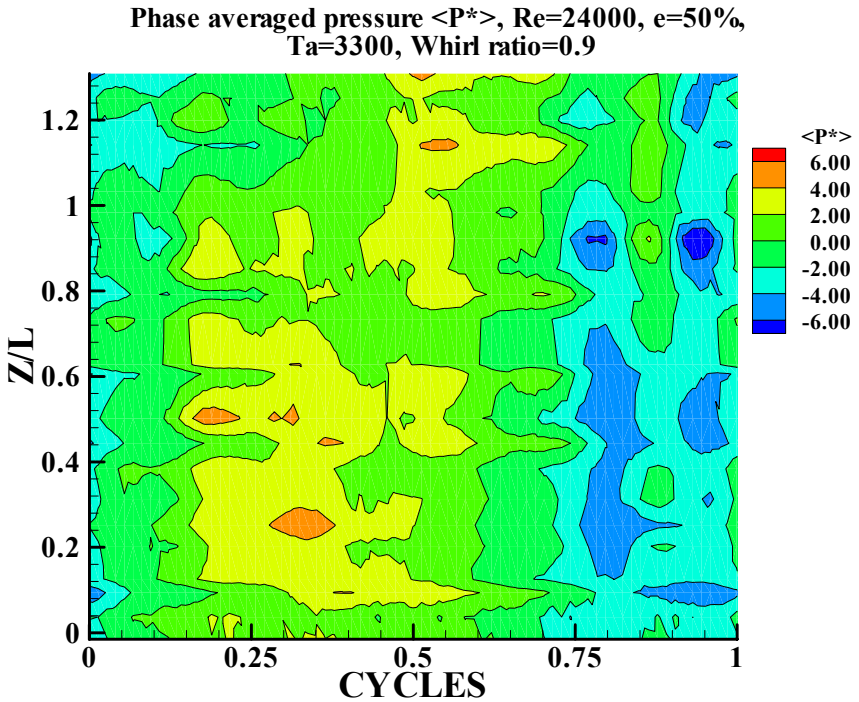

Fig 25. Phase averaged pressure contours, whirl ratio 0.9.

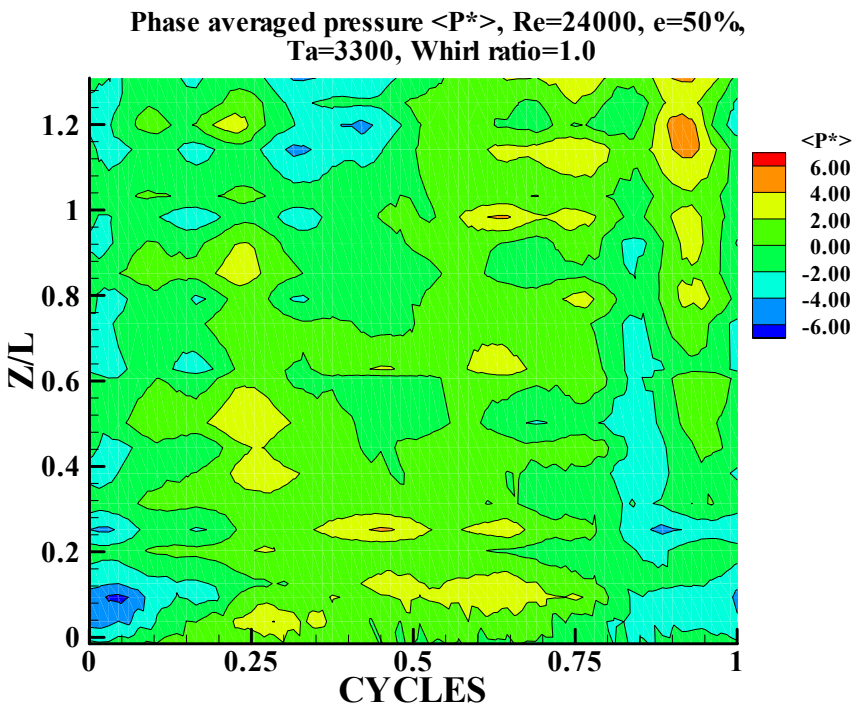

Fig 26. Phase averaged pressure contours, whirl ratio 1.0.

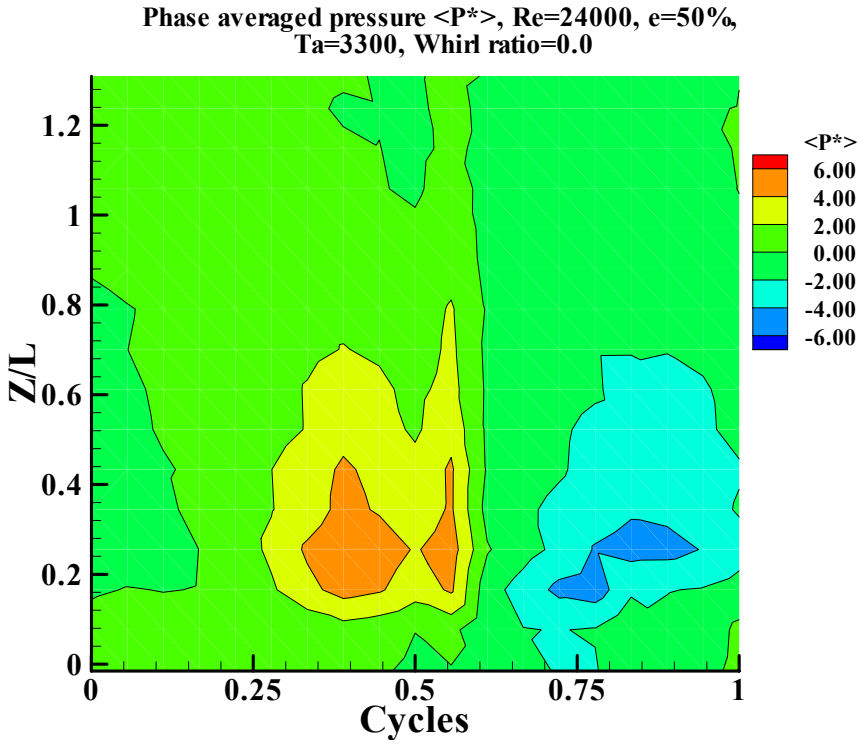

Fig 27. Phase averaged pressure contour, whirl ratio 0.0

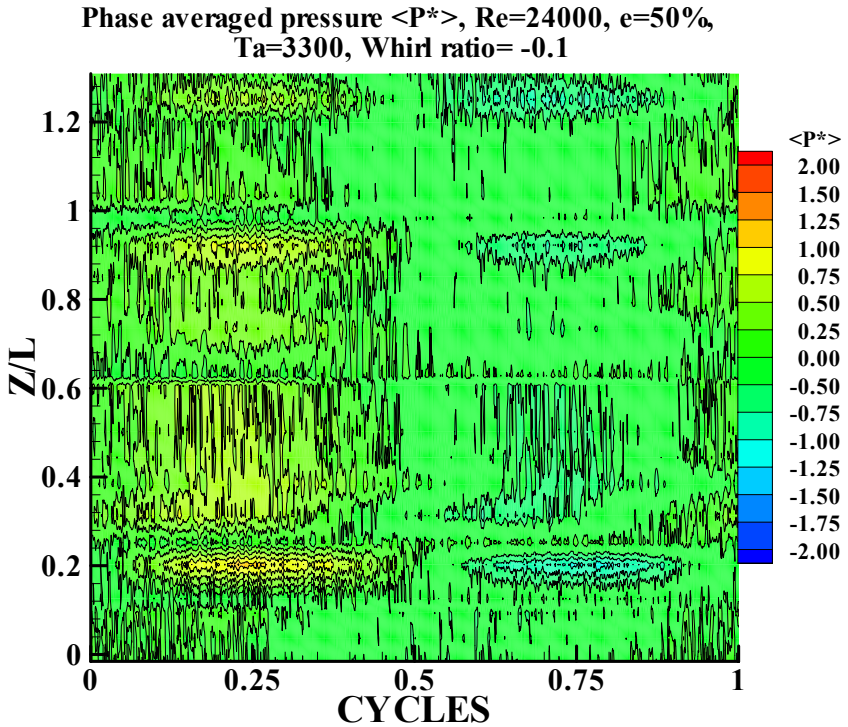

Fig 28. Phase averaged pressure contour, whirl ratio -0.1

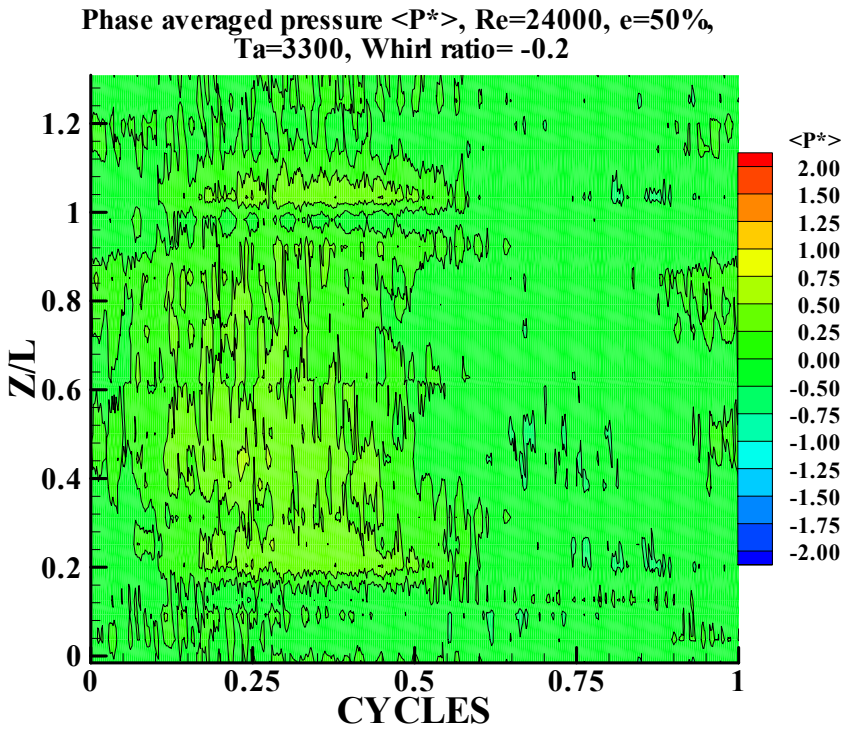

Fig 29. Phase averaged pressure contour, whirl ratio -0.2

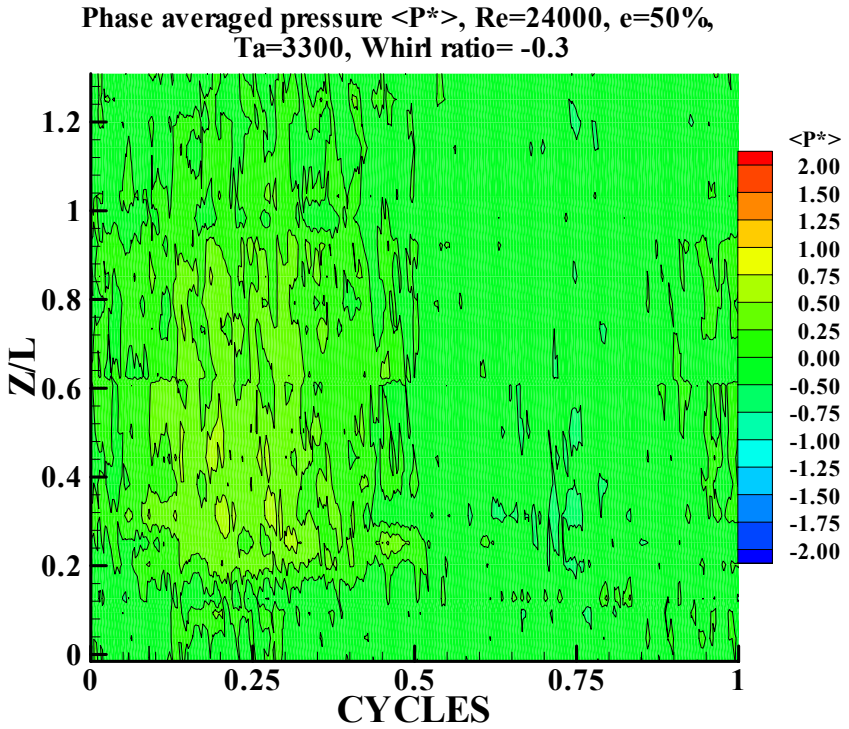

Fig 30 . Phase averaged pressure contour, whirl ratio -0.3

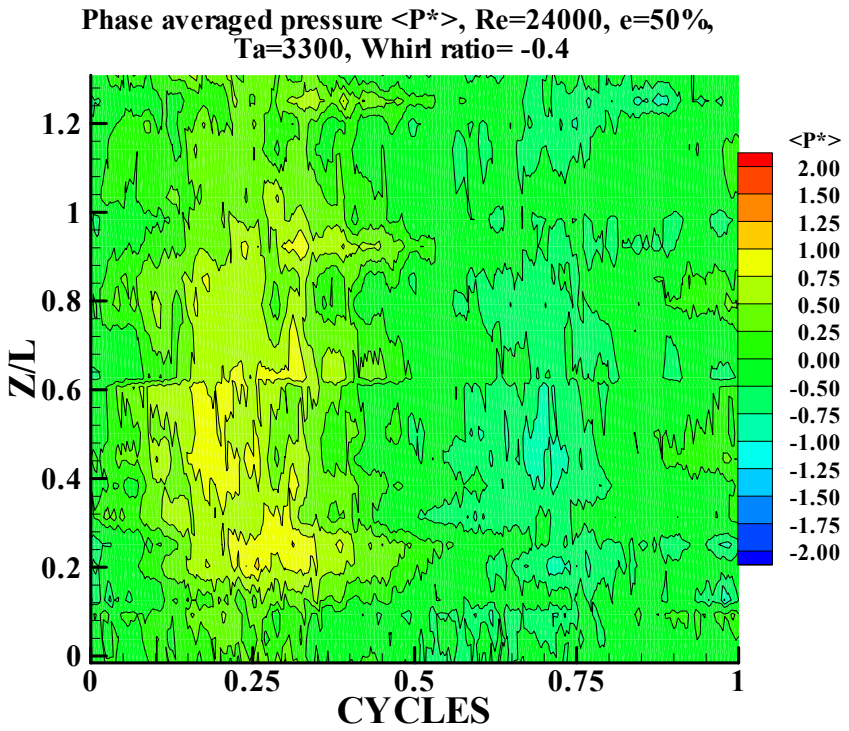

Fig 31. Phase averaged pressure contour, whirl ratio -0.4

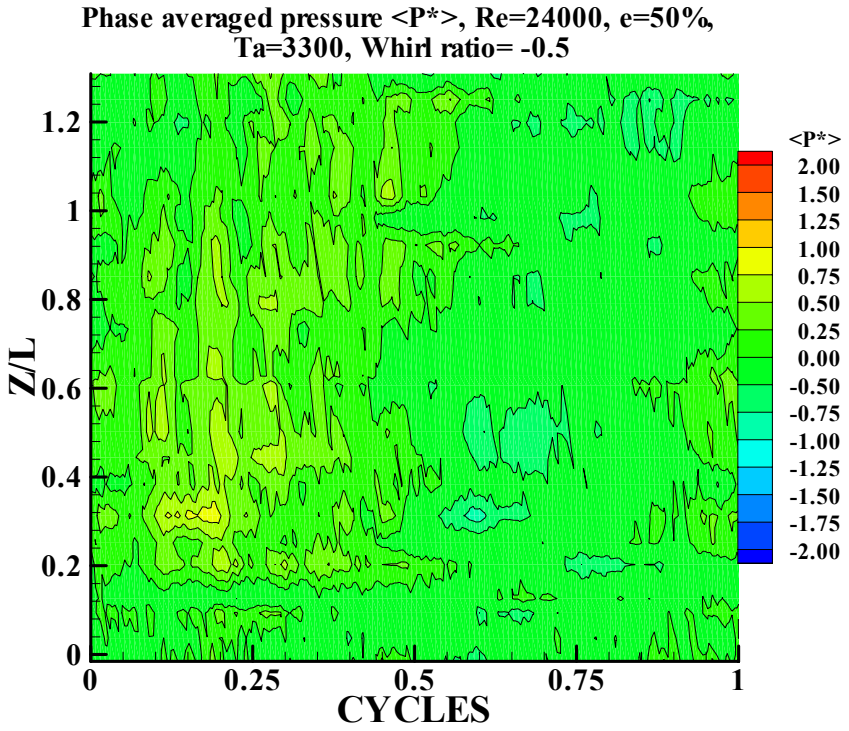

Fig 32. Phase averaged pressure contour, whirl ratio -0.5

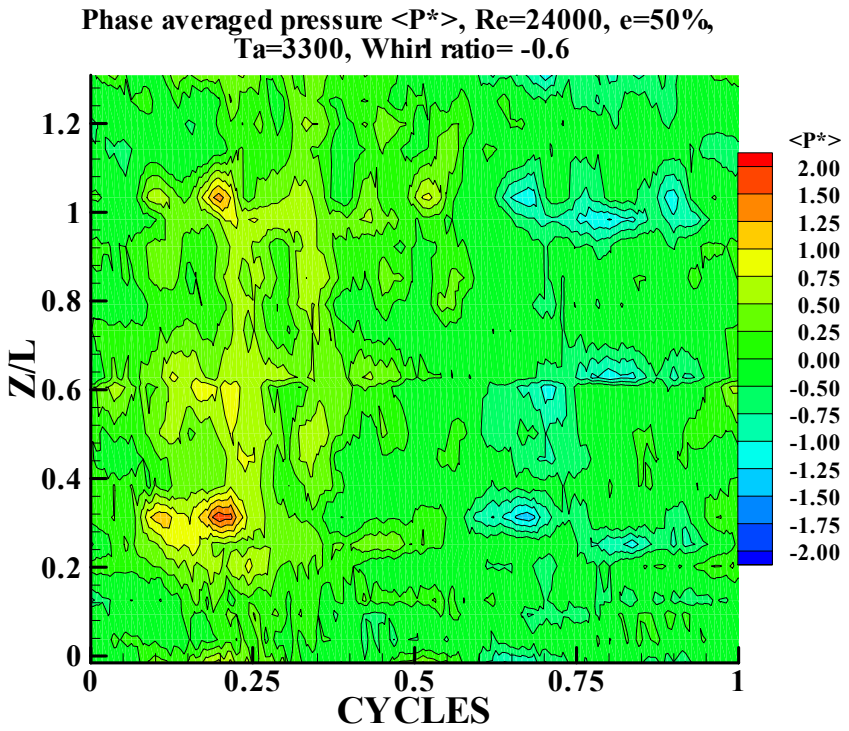

Fig 33 . Phase averaged pressure contour, whirl ratio -0.6

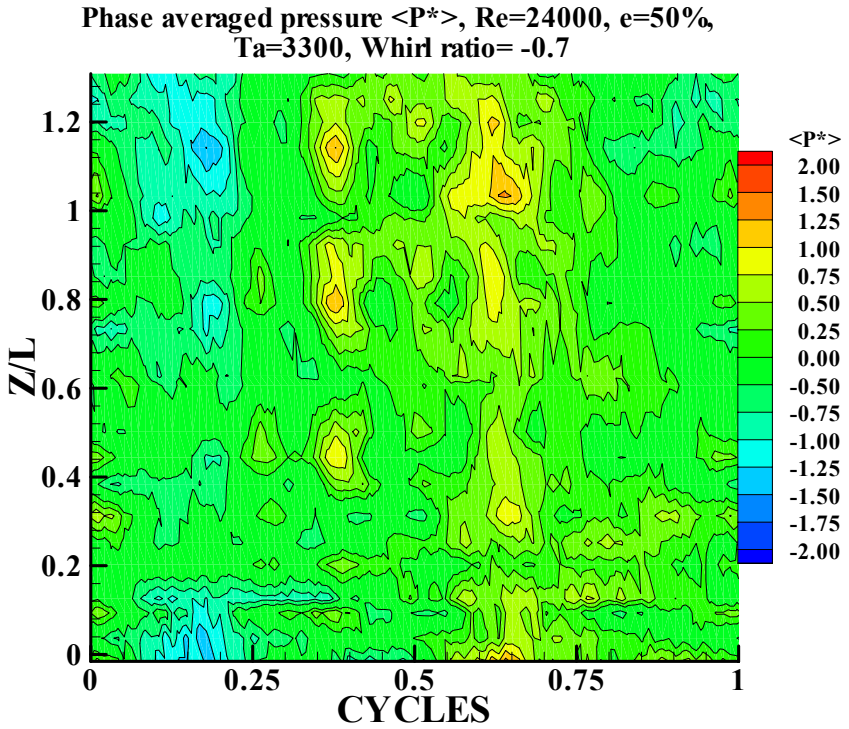

Fig 34. Phase averaged pressure contour, whirl ratio -0.7

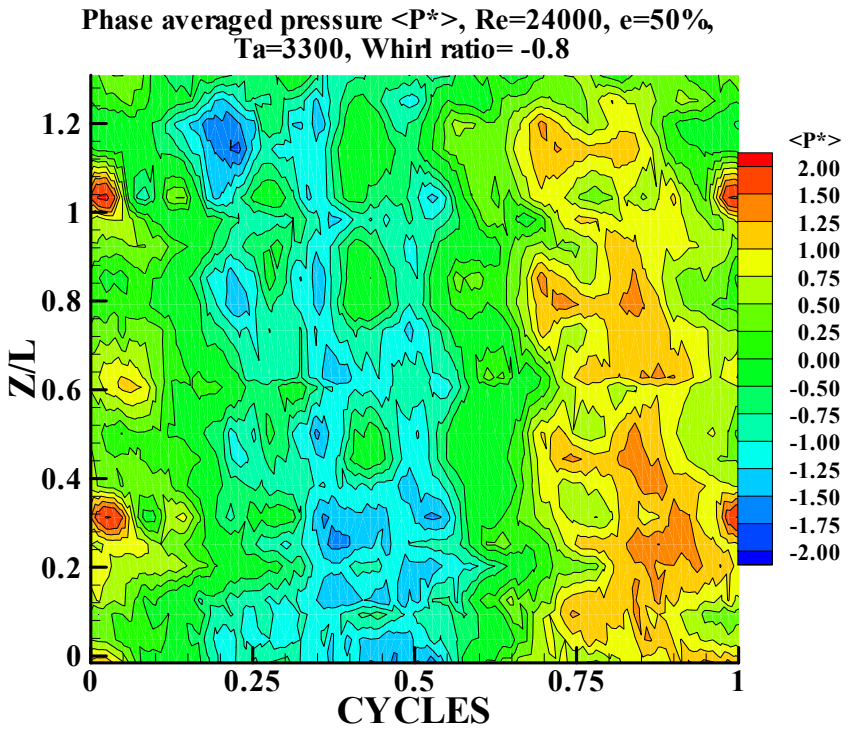

Fig 35. Phase averaged pressure contour, whirl ratio -0.8

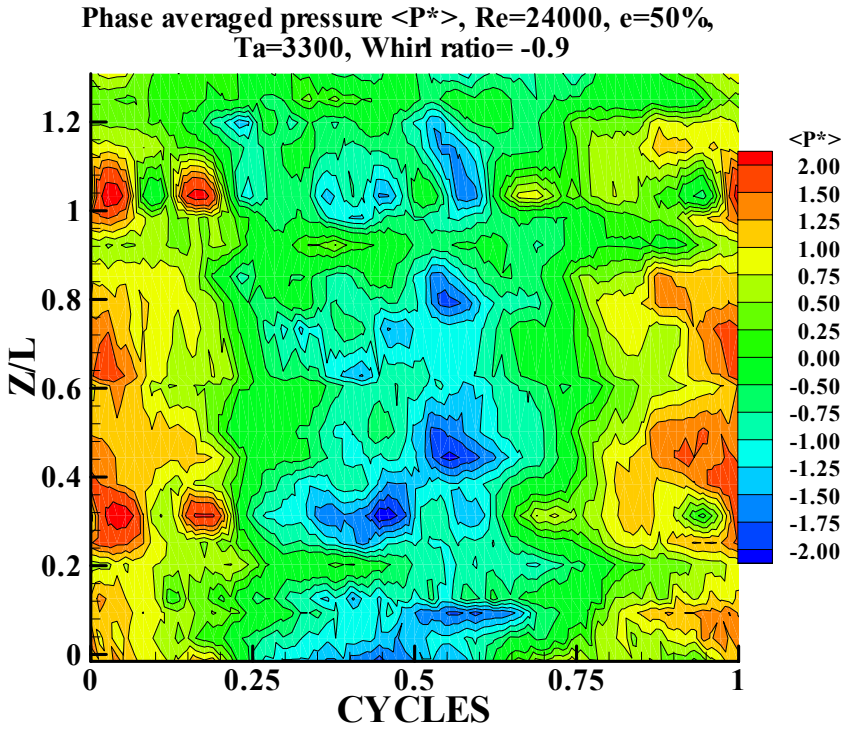

Fig 36. Phase averaged pressure contour, whirl ratio -0.9

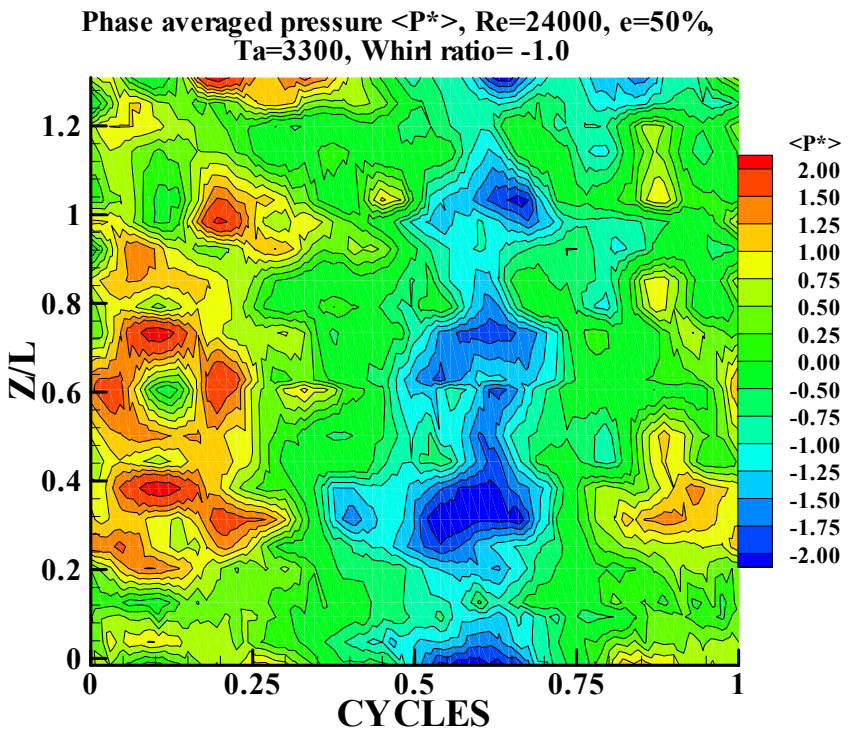

Fig 37. Phase averaged pressure contour, whirl ratio -1.0

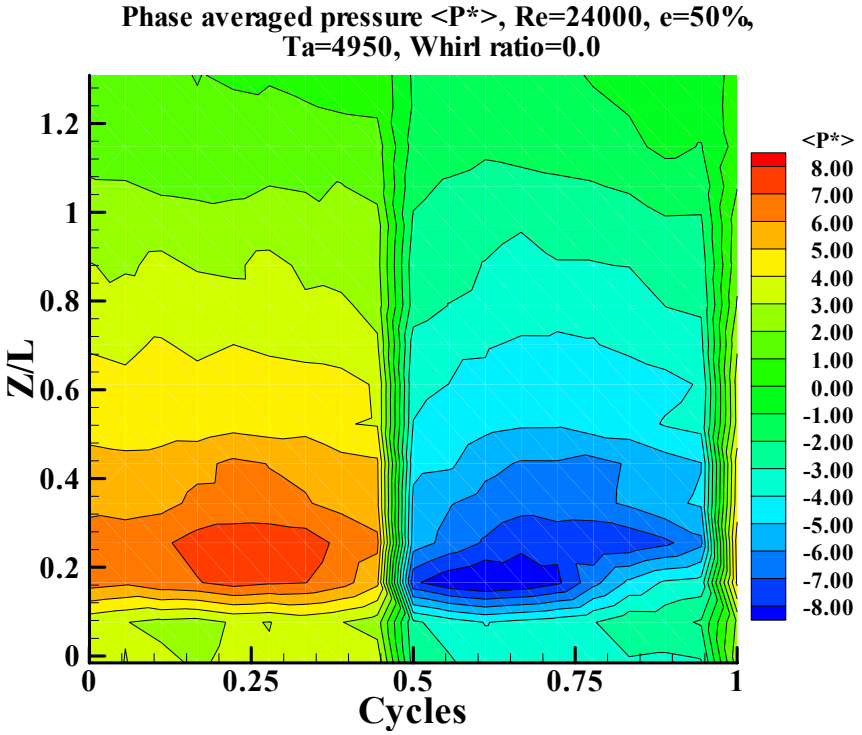

Fig 38. Phase averaged pressure contour, whirl ratio 0.0

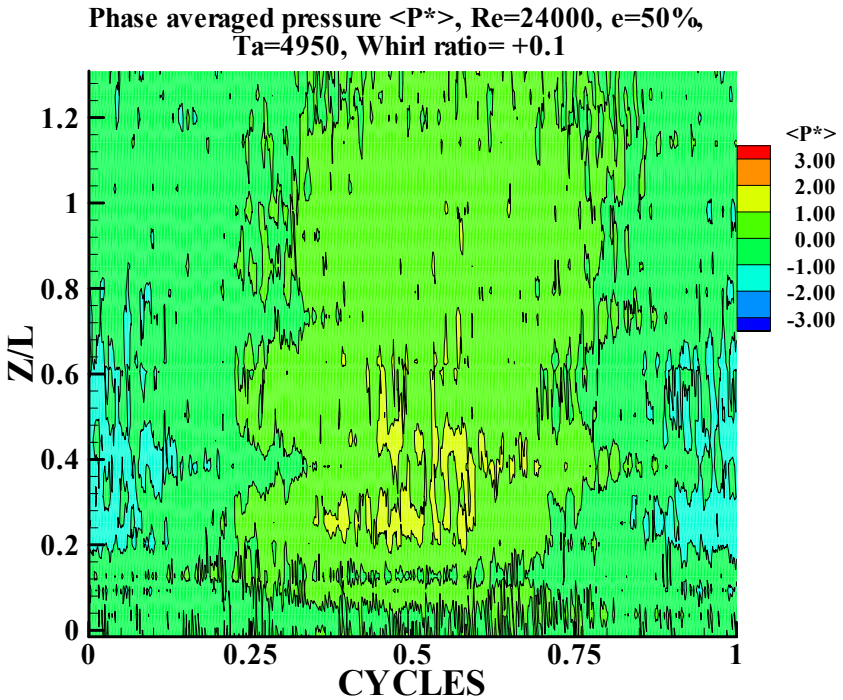

Fig 39. Phase averaged pressure contour, whirl ratio 0.1

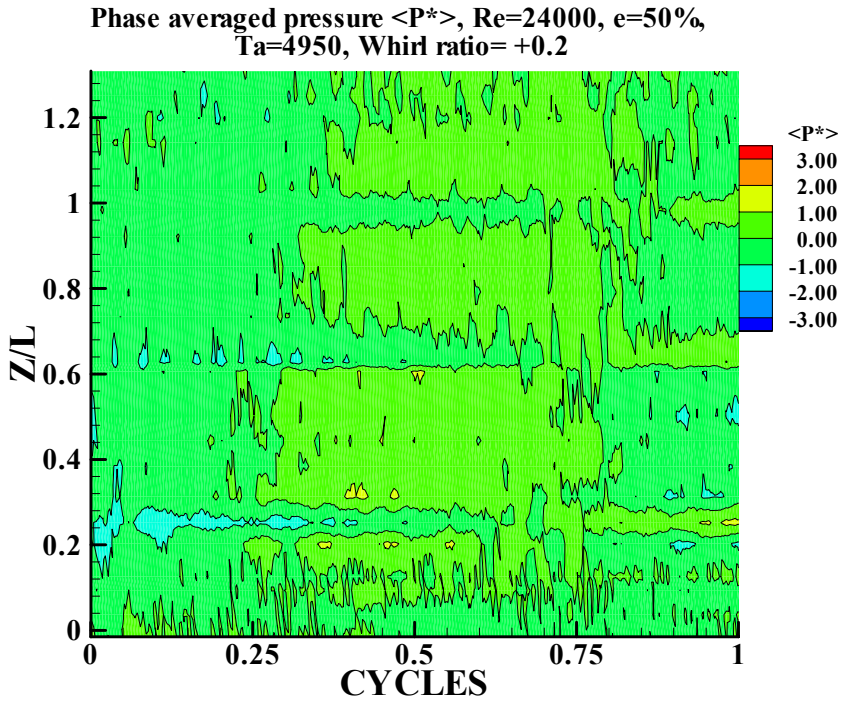

Fig 40. Phase averaged pressure contour, whirl ratio 0.2

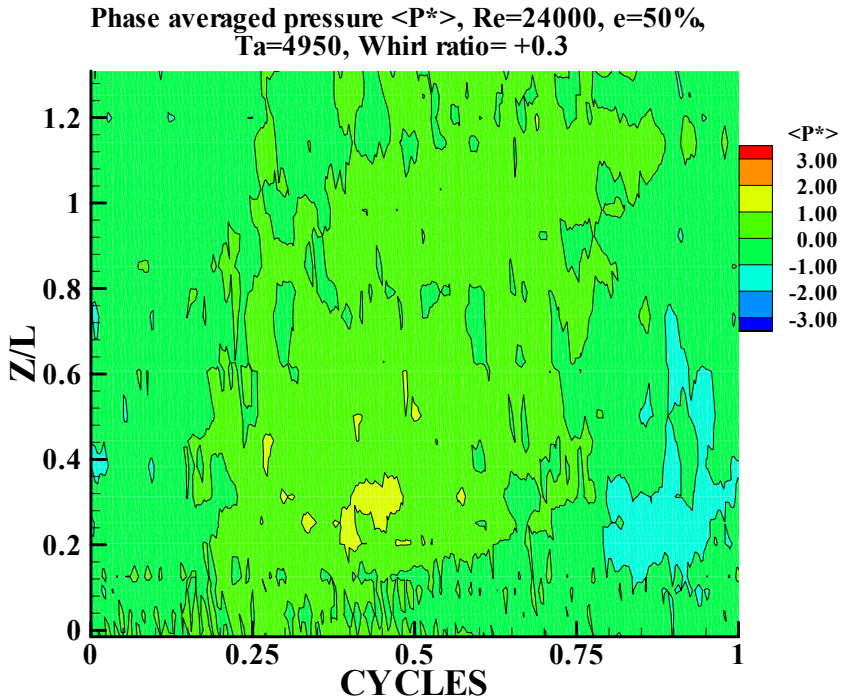

Fig 41. Phase averaged pressure contour, whirl ratio 0.3

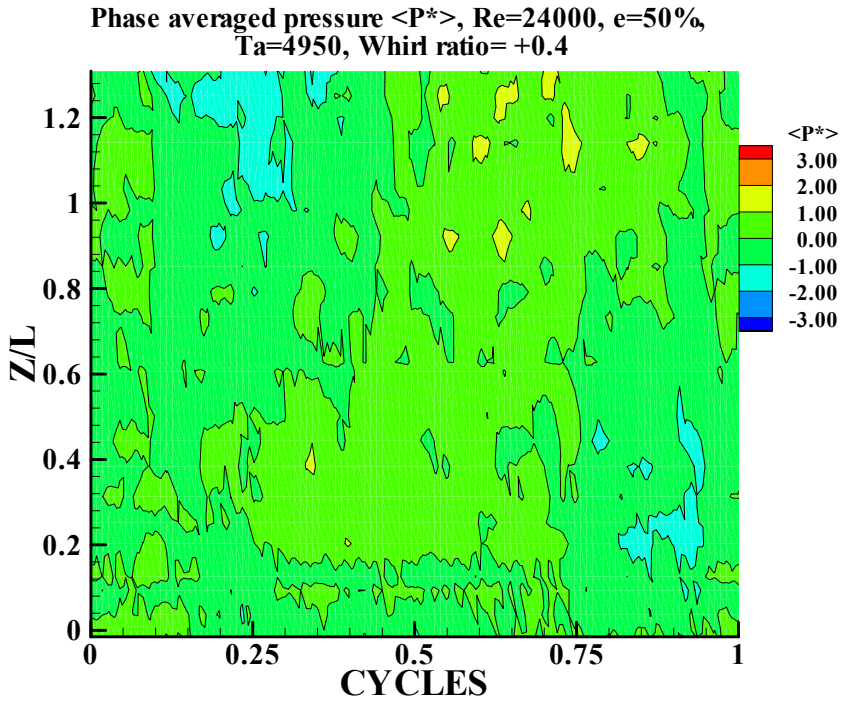

Fig 42. Phase averaged pressure contour, whirl ratio 0.4

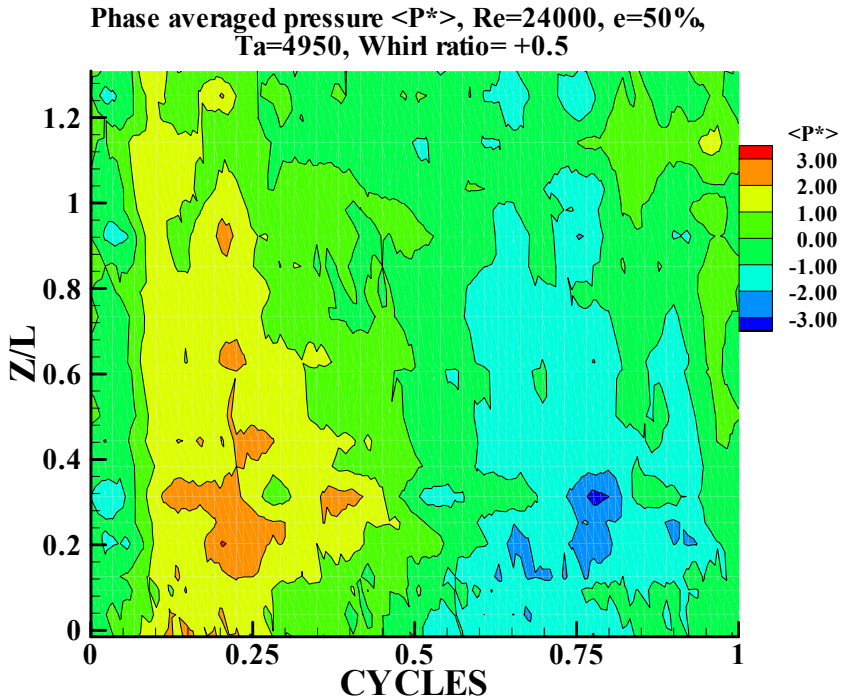

Fig 43. Phase averaged pressure contour, whirl ratio 0.5

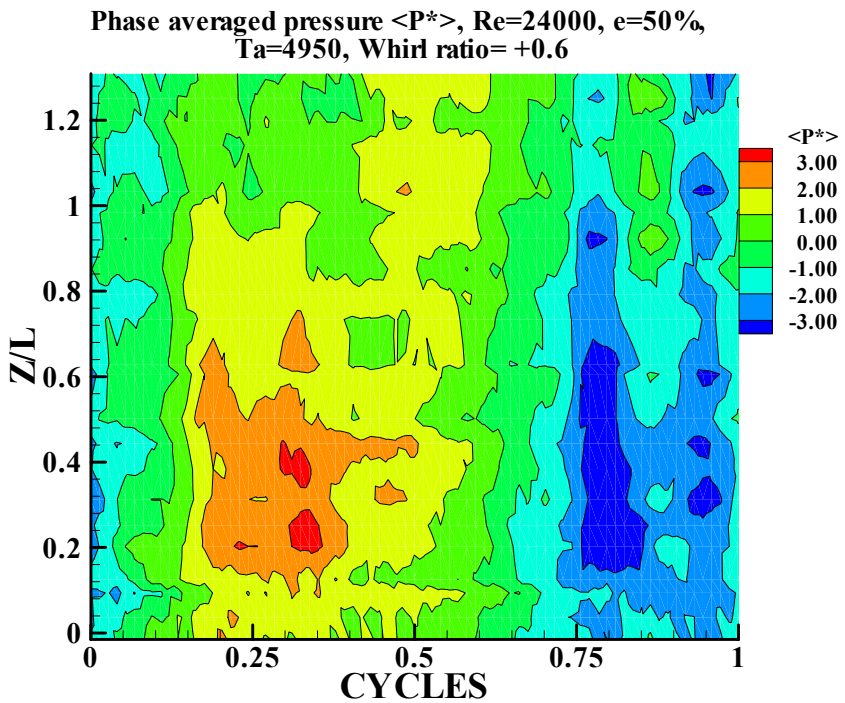

Fig 44. Phase averaged pressure contour, whirl ratio 0.6

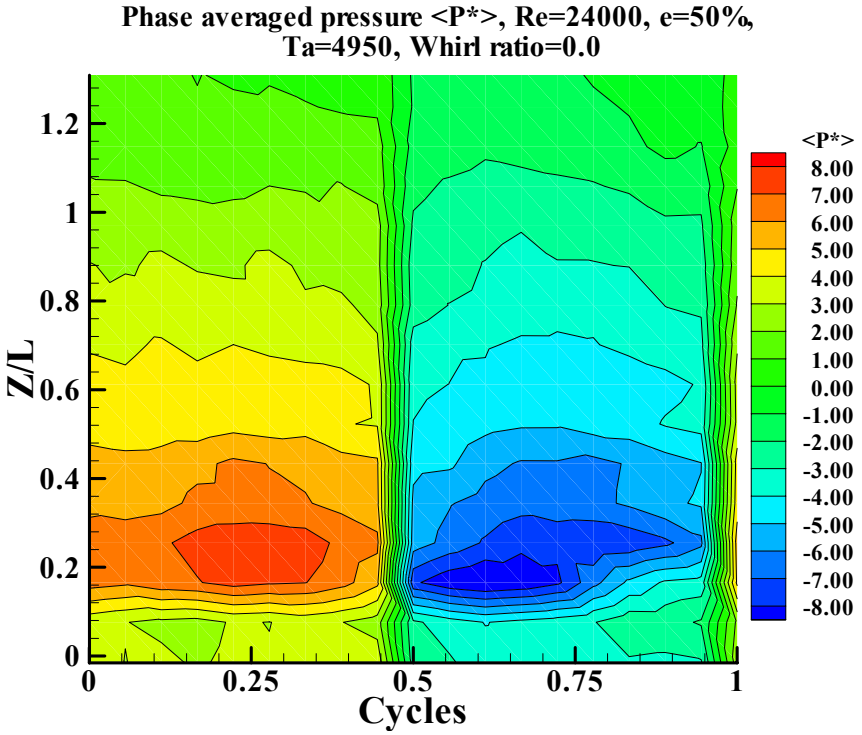

Fig 45. Phase averaged pressure contour, whirl ratio 0.0

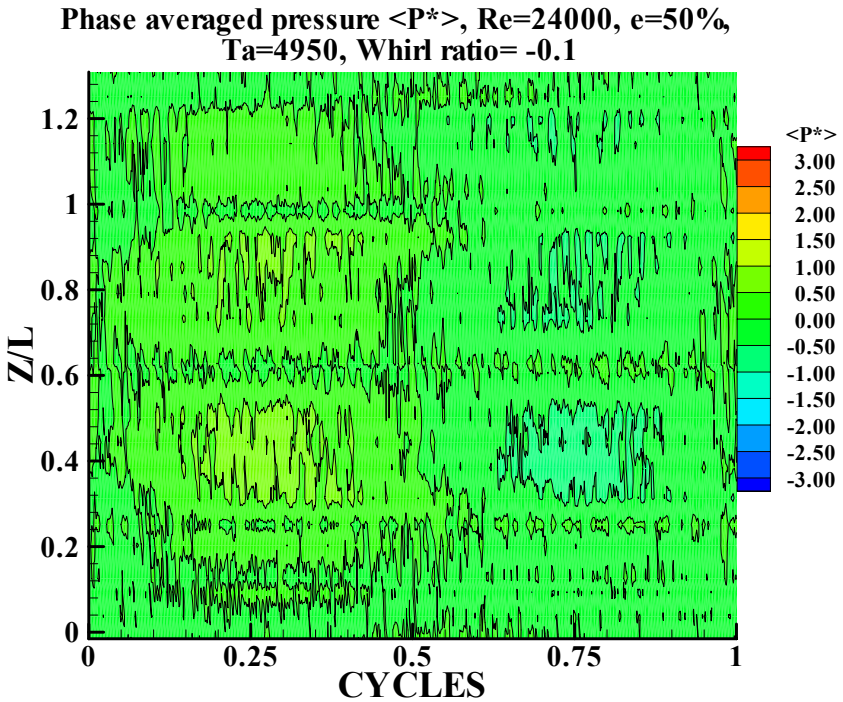

Fig 46. Phase averaged pressure contour, whirl ratio -0.1

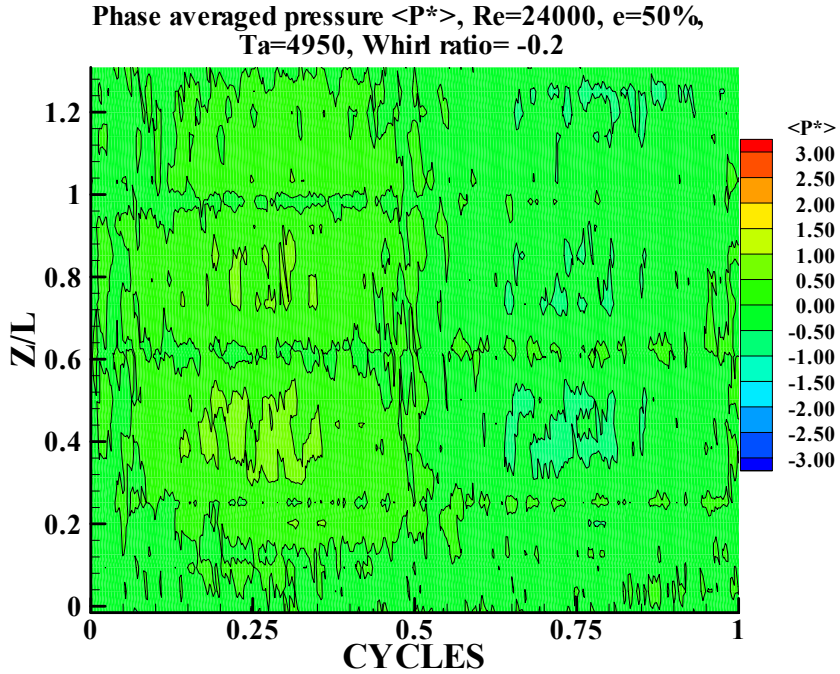

Fig 47. Phase averaged pressure contour, whirl ratio -0.2

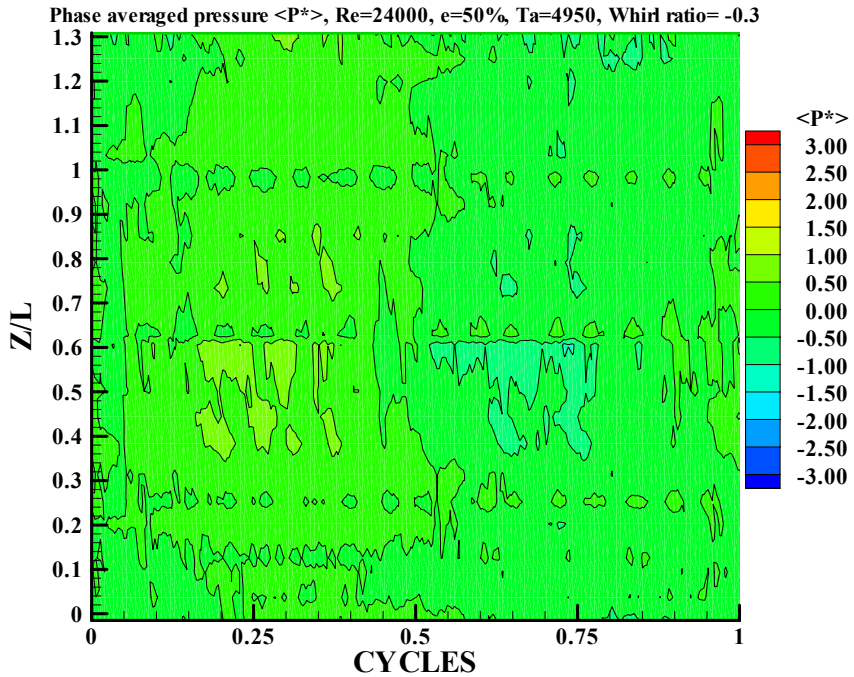

Fig 48. Phase averaged pressure contour, whirl ratio -0.3

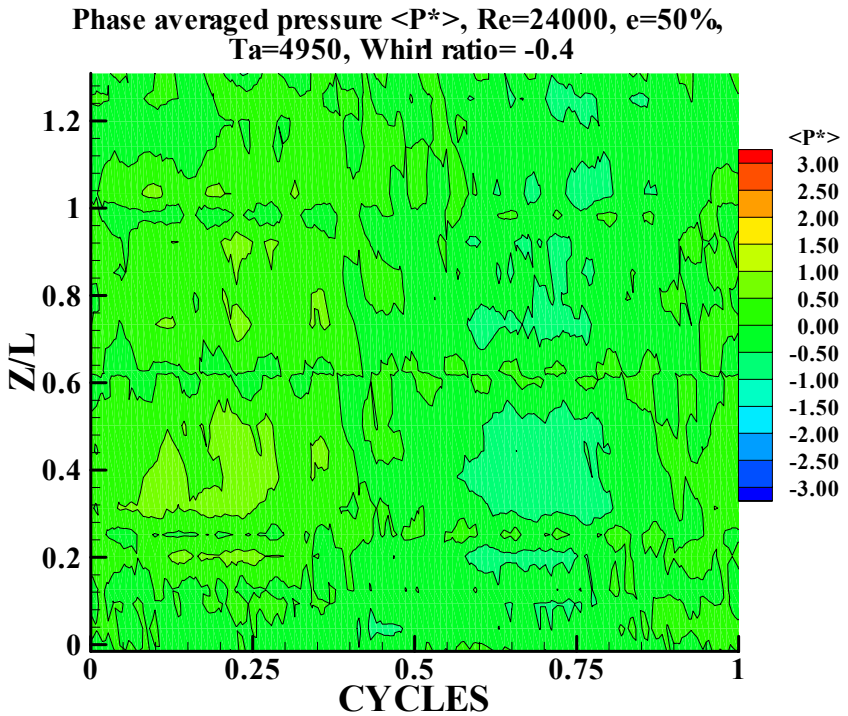

Fig 49. Phase averaged pressure contour, whirl ratio -0.4

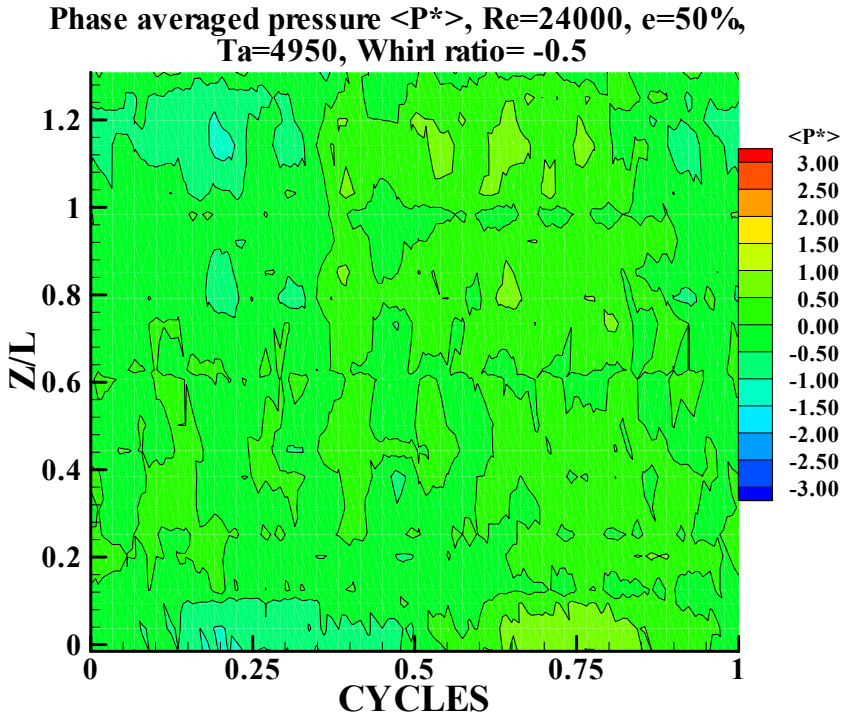

Fig 50. Phase averaged pressure contour, whirl ratio -0.5

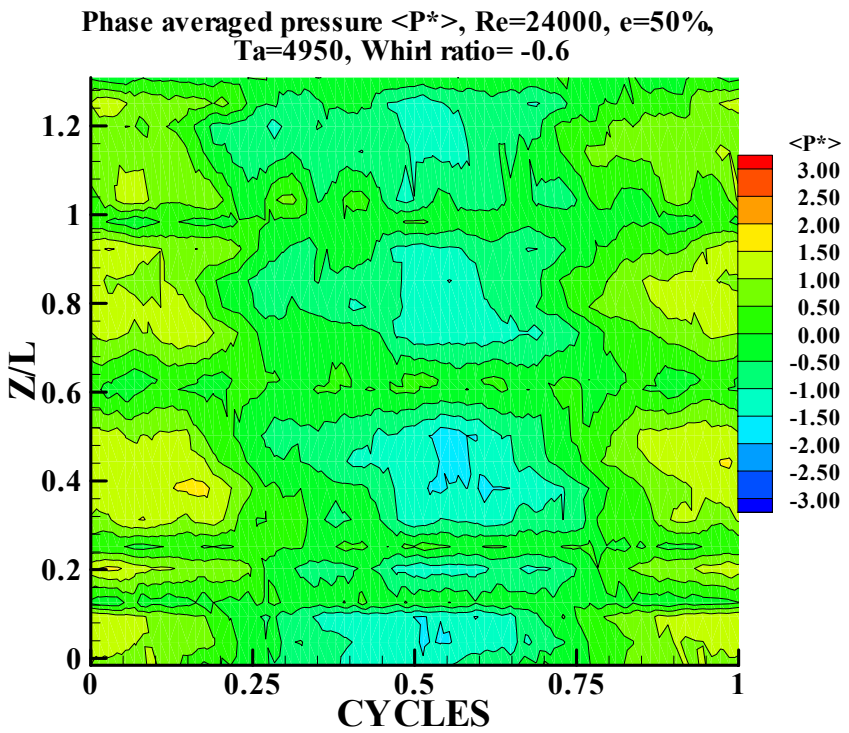

Fig 51. Phase averaged pressure contour, whirl ratio -0.6

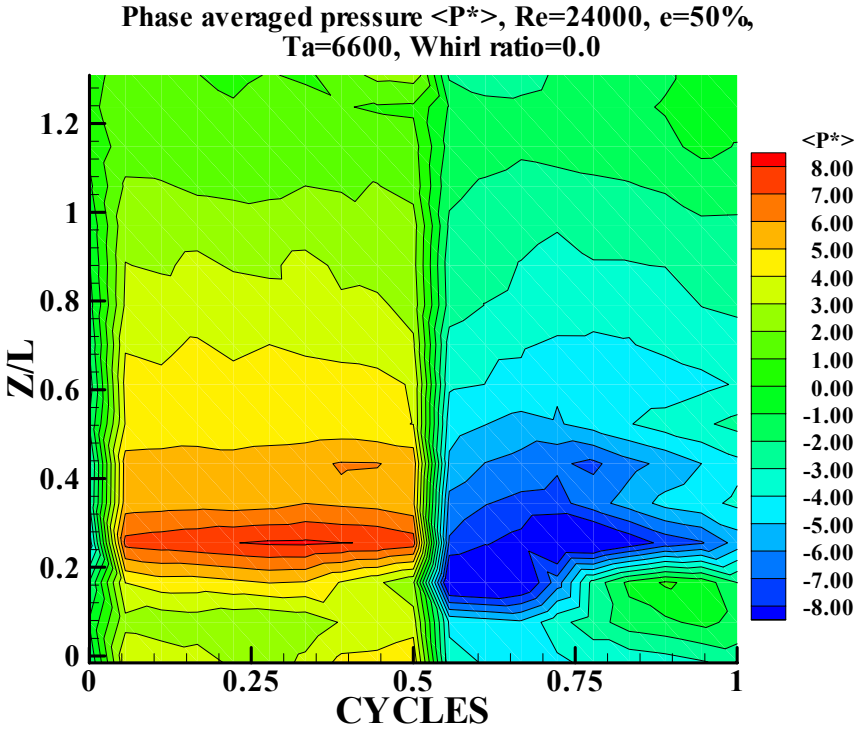

Fig 52. Phase averaged pressure contour, whirl ratio 0.0

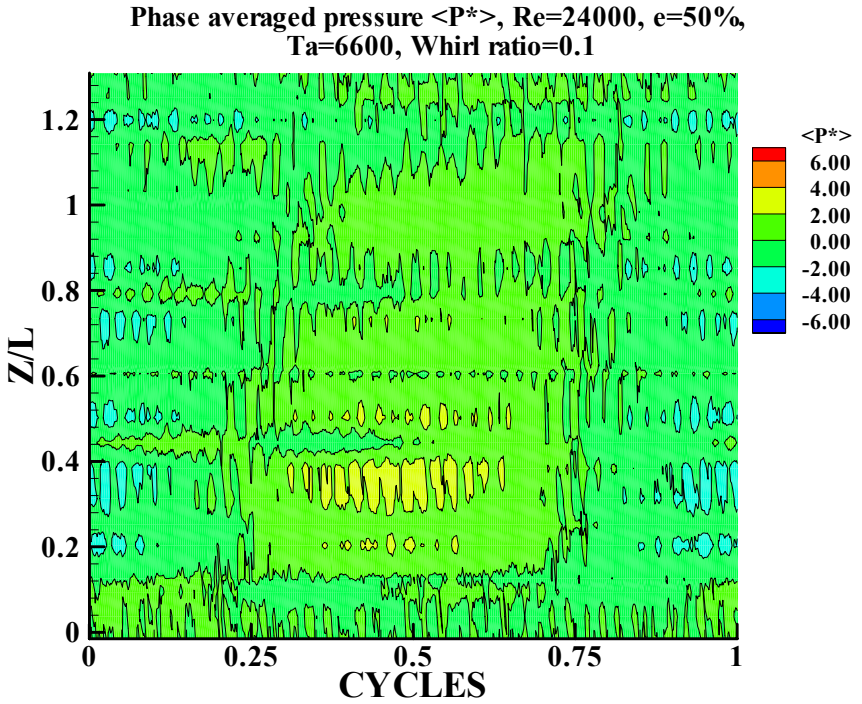

Fig 53. Phase averaged pressure contour, whirl ratio 0.1

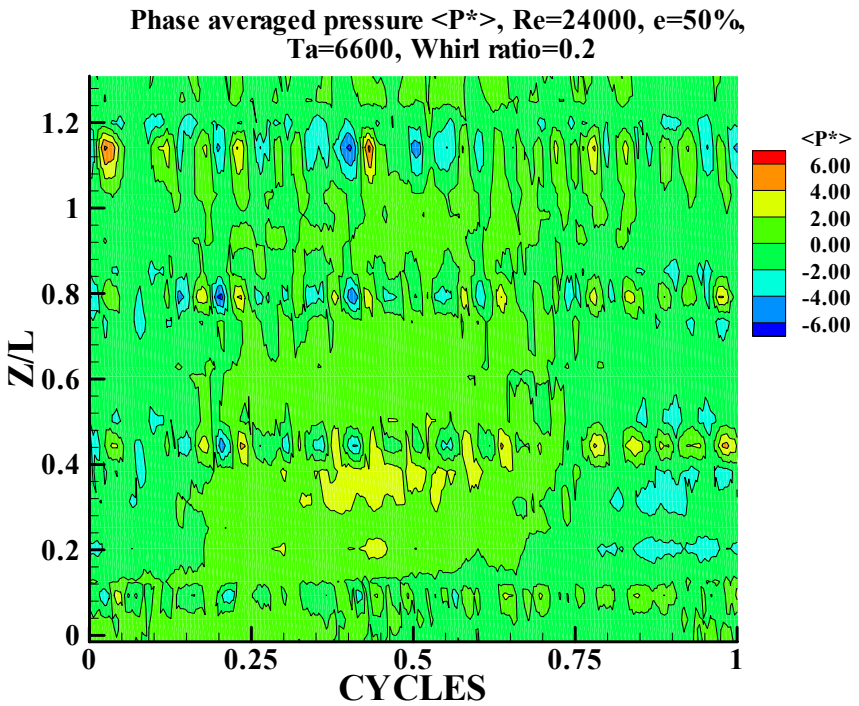

Fig 54. Phase averaged pressure contour, whirl ratio 0.2

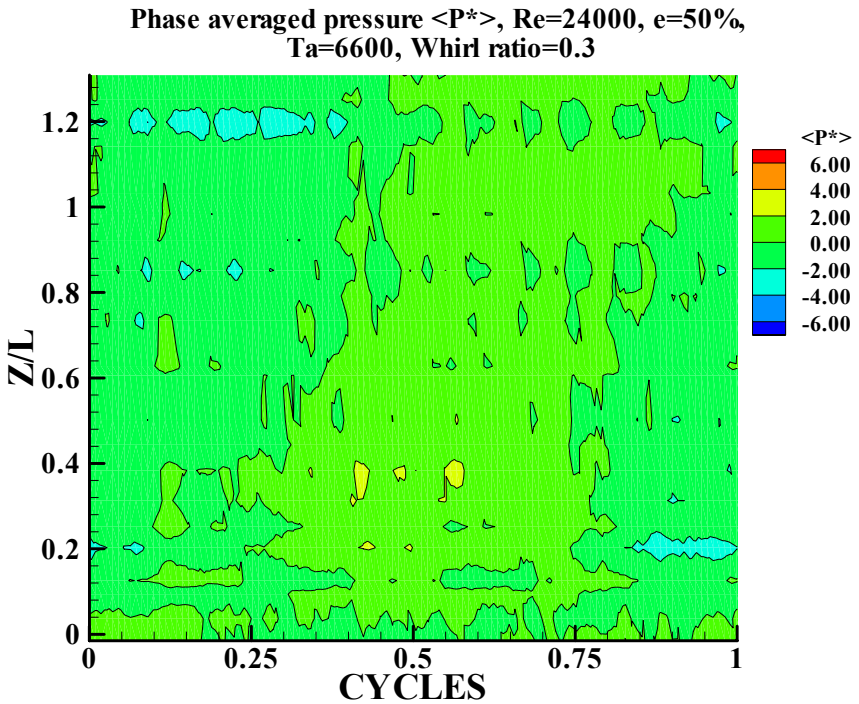

Fig 55. Phase averaged pressure contour, whirl ratio 0.3

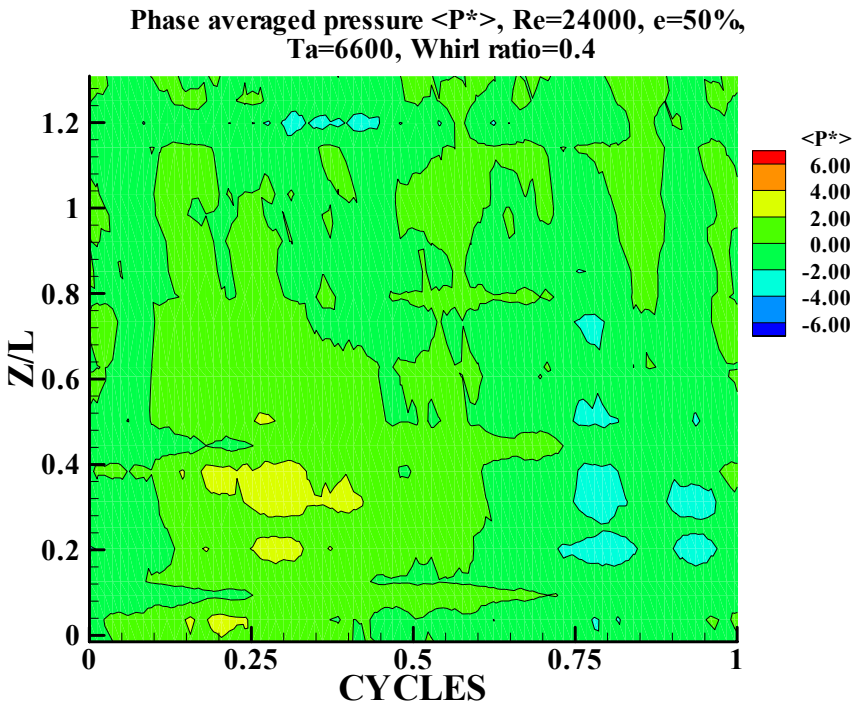

Fig 56. Phase averaged pressure contour, whirl ratio 0.4

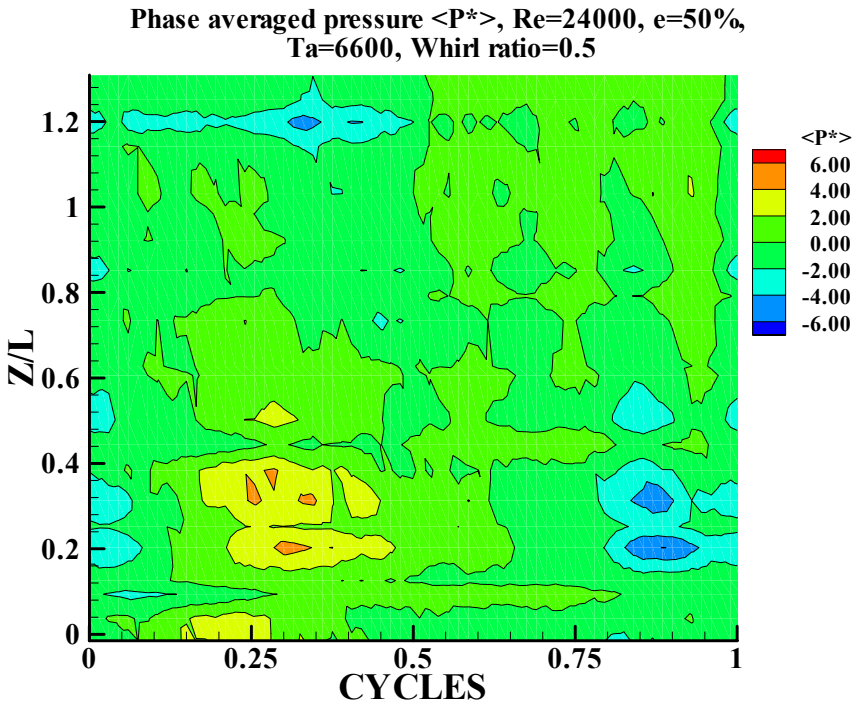

Fig 57. Phase averaged pressure contour, whirl ratio 0.5

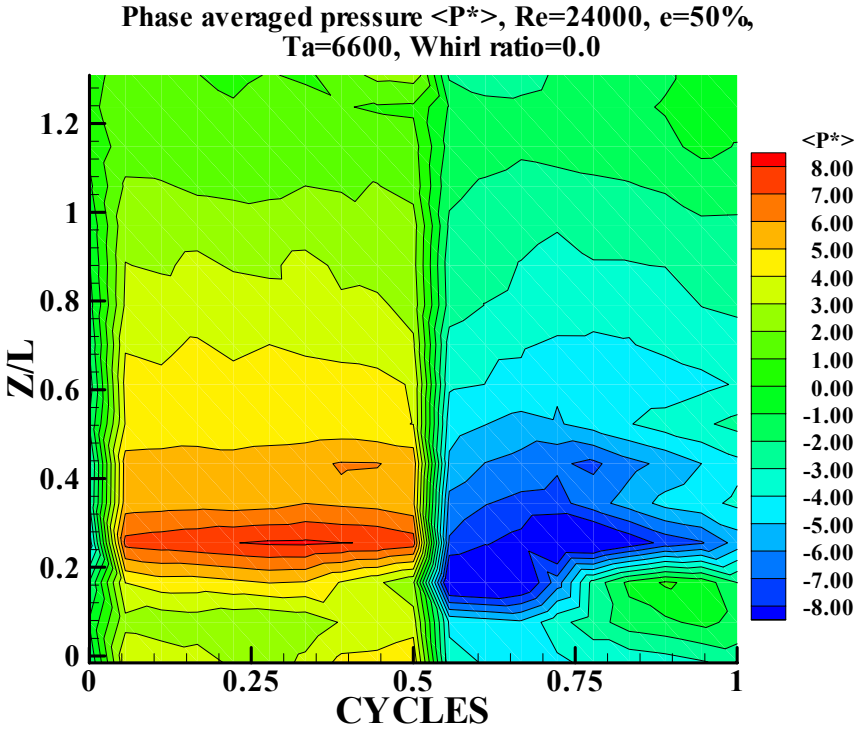

Fig 58. Phase averaged pressure contour, whirl ratio 0.0

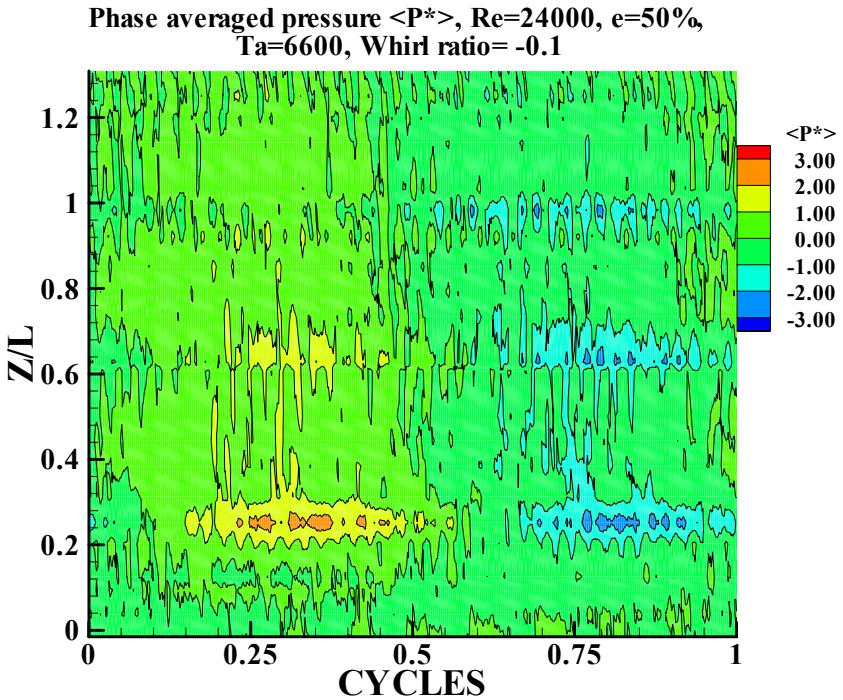

Fig 59. Phase averaged pressure contour, whirl ratio -0.1

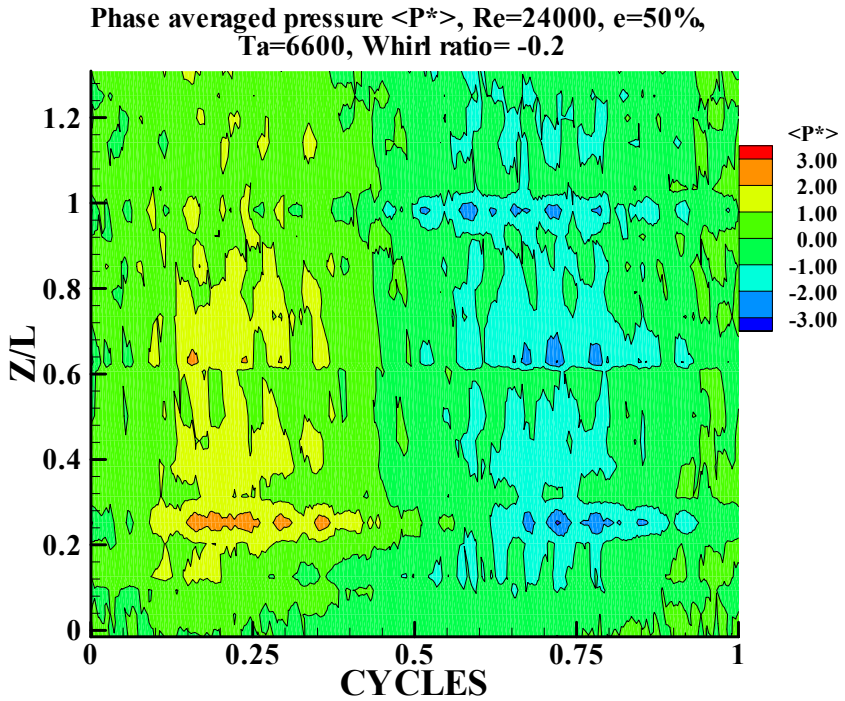

Fig 60. Phase averaged pressure contour, whirl ratio -0.2

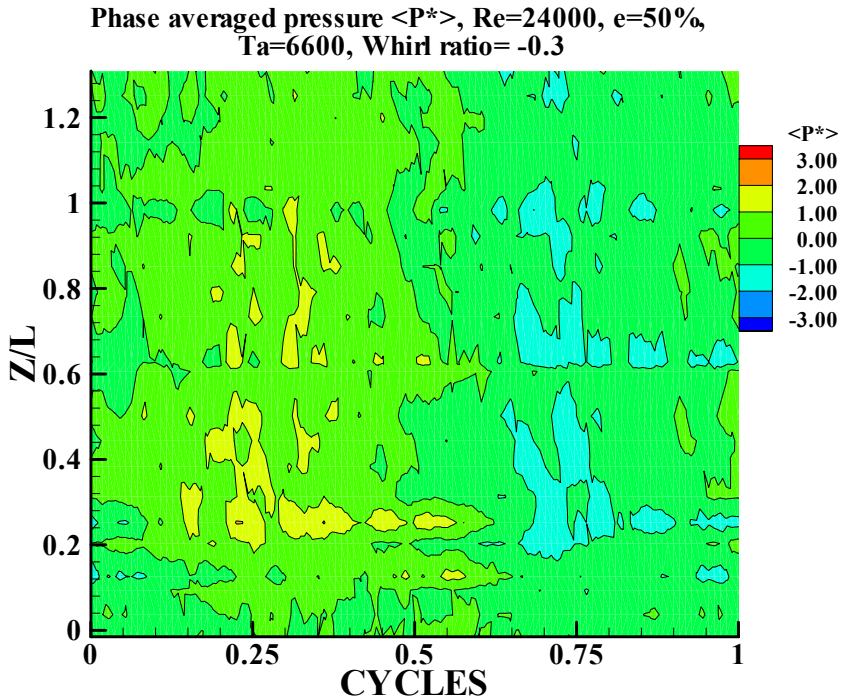

Fig 61. Phase averaged pressure contour, whirl ratio -0.3

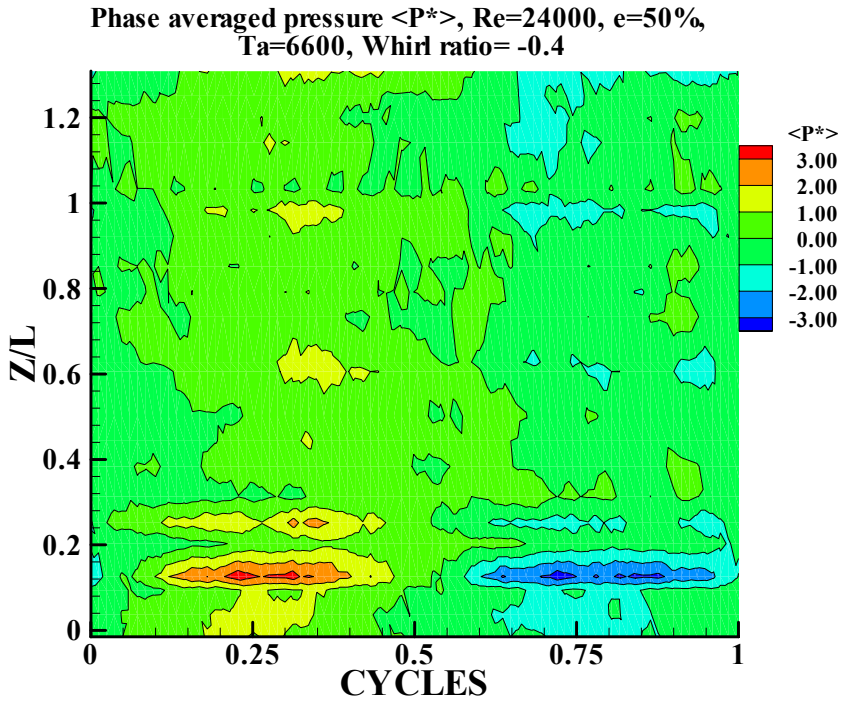

Fig 62. Phase averaged pressure contour, whirl ratio -0.4

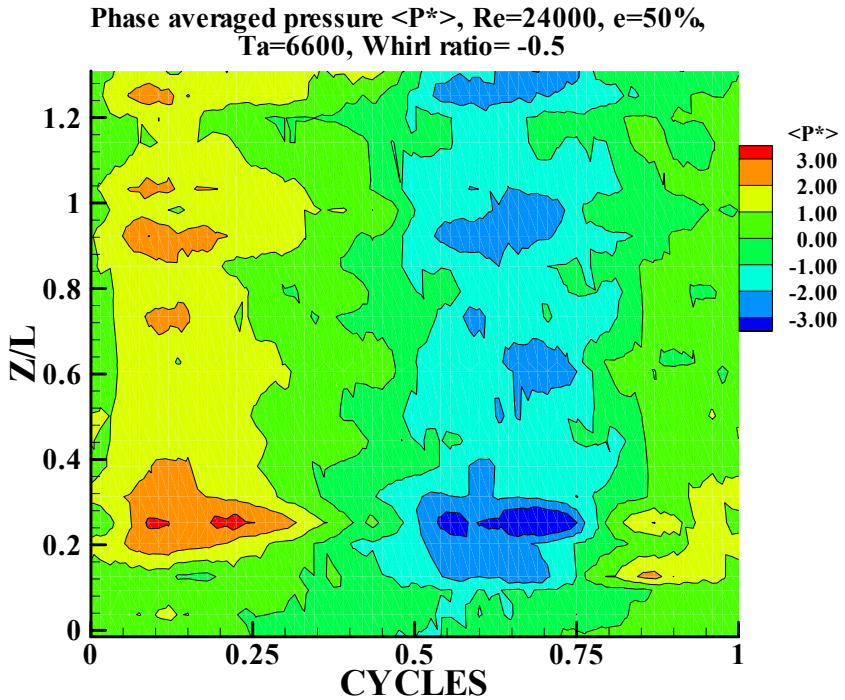

Fig 63. Phase averaged pressure contour, whirl ratio -0.5

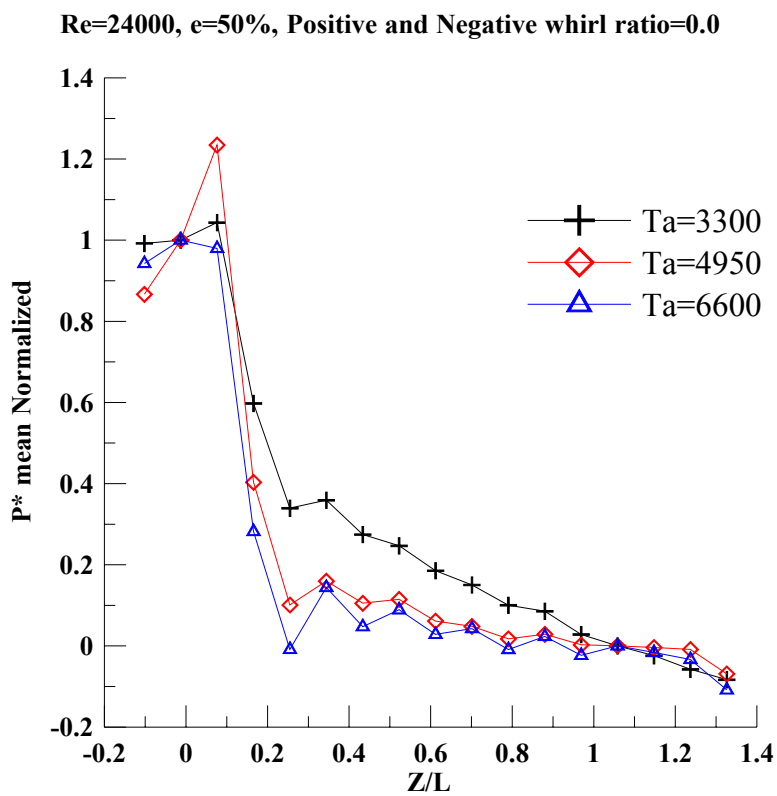

Fig 64. Effect of ω on ΔP across the seal inlet and exit

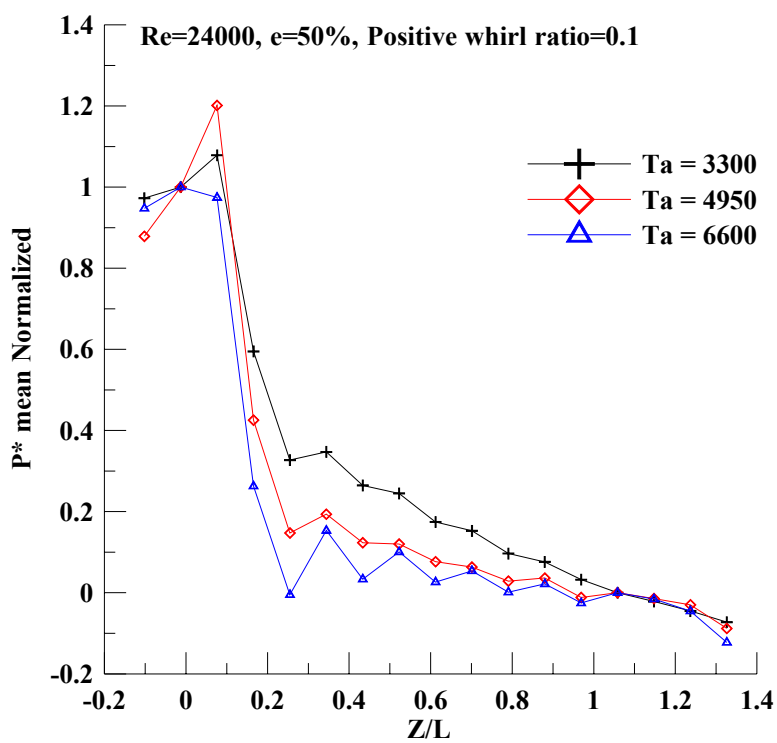

Fig 65. Effect of ω on ΔP across the seal inlet and exit

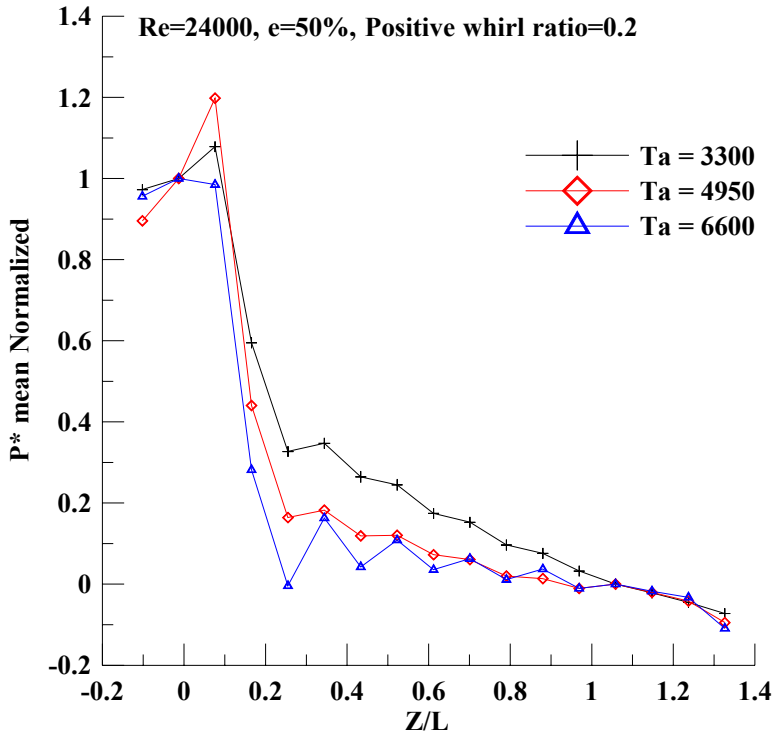

Fig 66.Effect of ω on ΔP across the seal inlet and exit

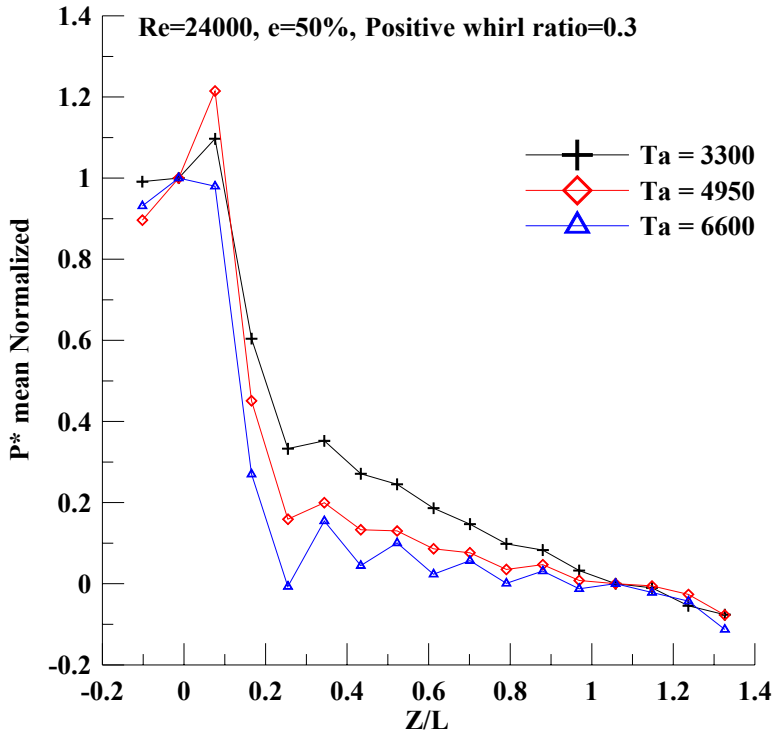

Fig 67.Effect of ω on ΔP across the seal inlet and exit

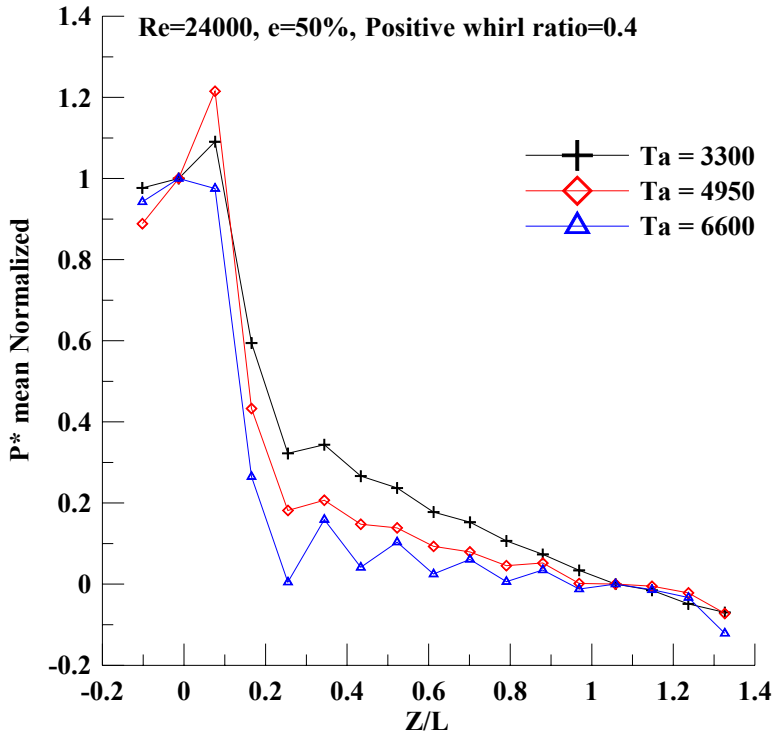

Fig 68.Effect of ω on ΔP across the seal inlet and exit

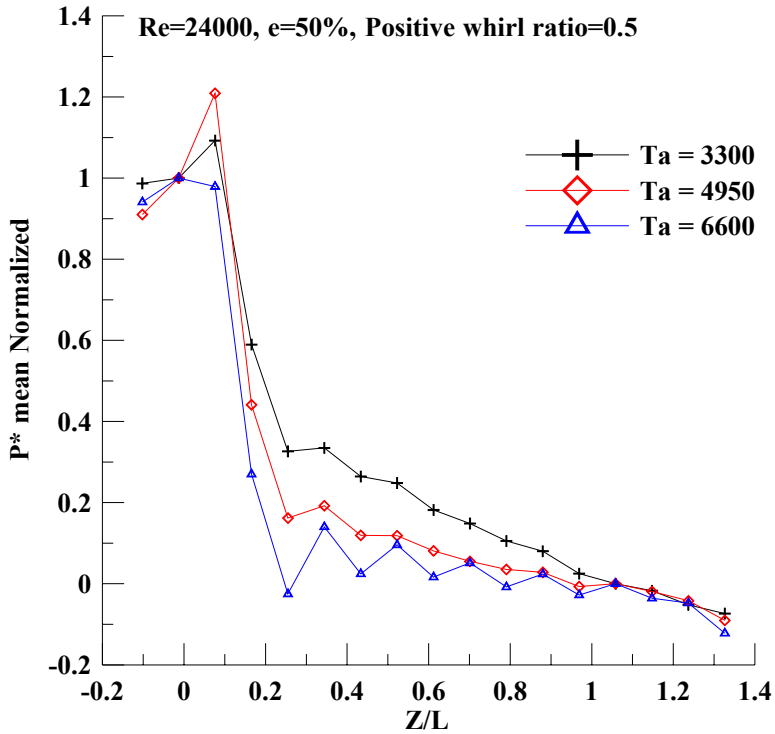

Fig 69.Effect of ω on ΔP across the seal inlet and exit

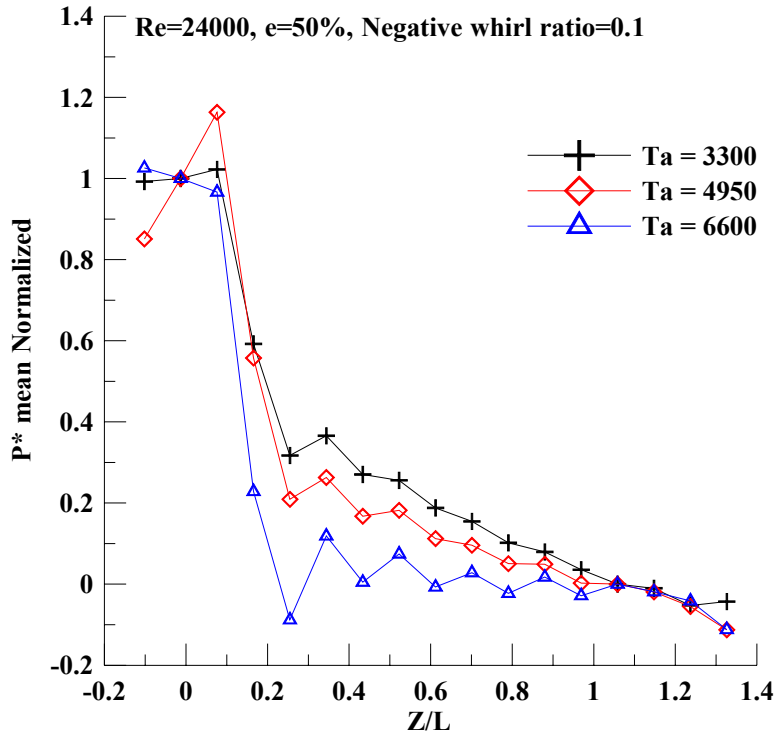

Fig 70.Effect of ω on ΔP across the seal inlet and exit

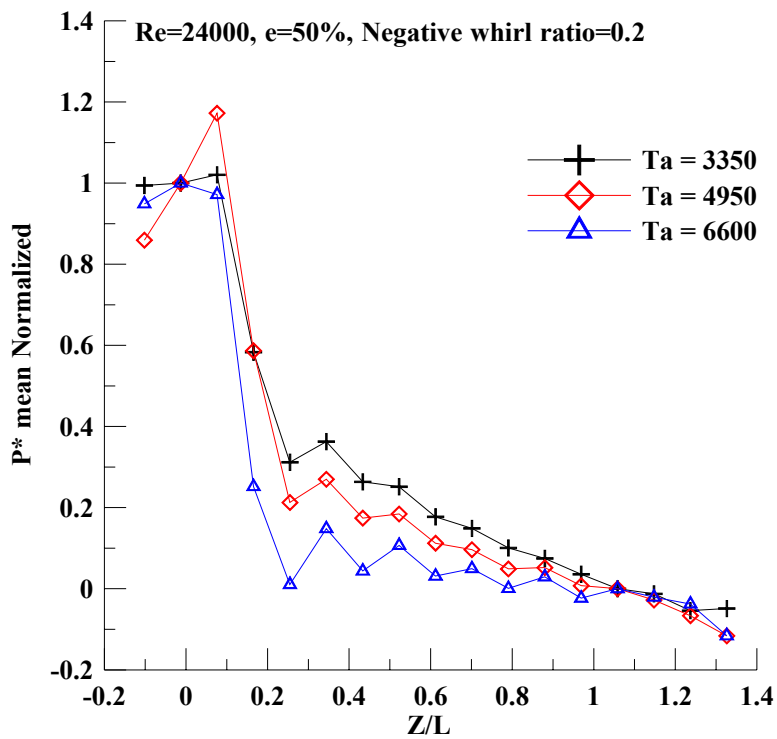

Fig 71. Effect of ω on ΔP across the seal inlet and exit

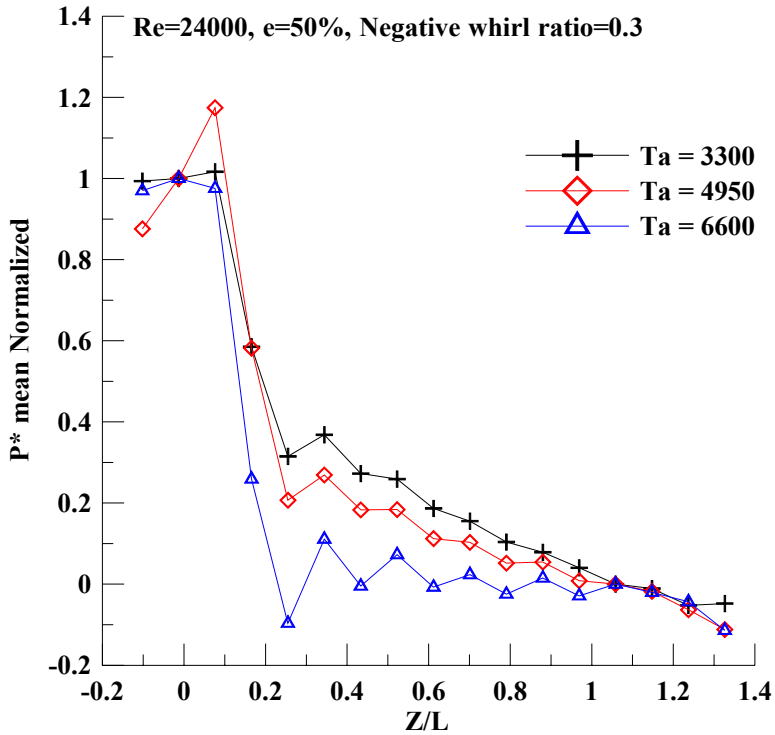

Fig 72.Effect of ω on ΔP across the seal inlet and exit

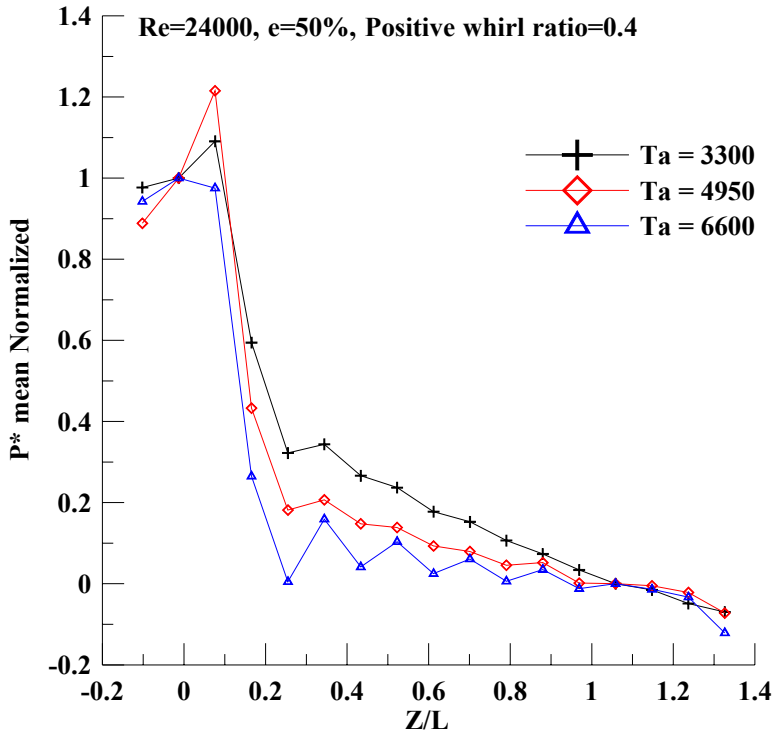

Fig 73.Effect of ω on ΔP across the seal inlet and exit

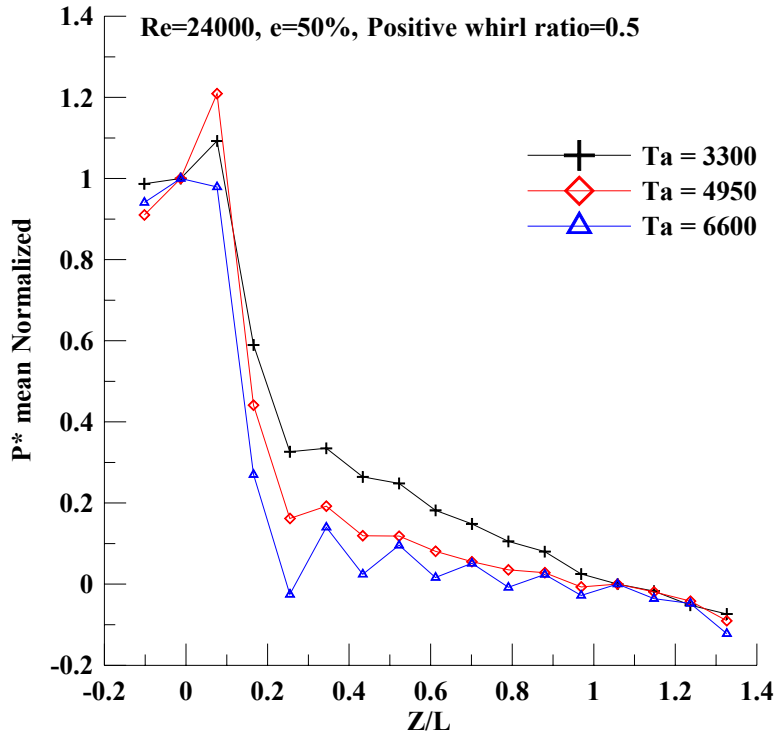

Fig 74.Effect of ω on ΔP across the seal inlet and exit

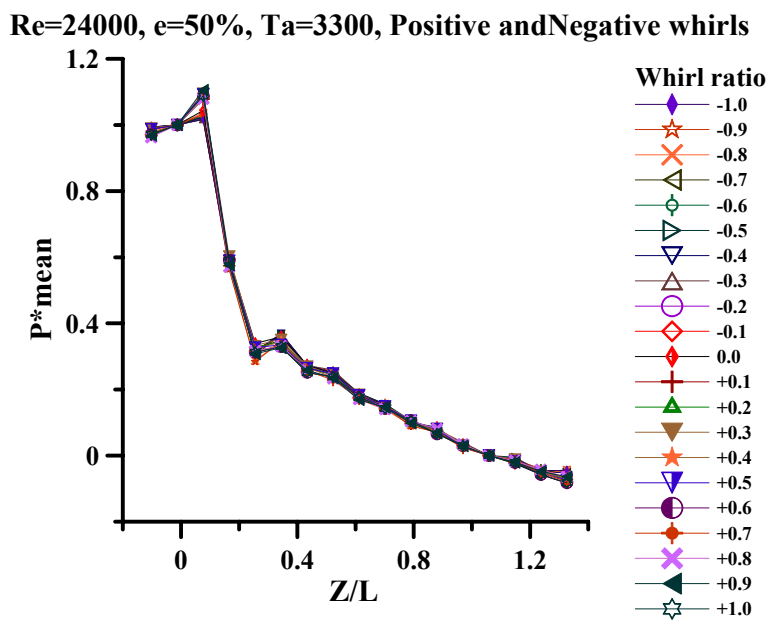

Fig 75. Effect of positive and negative ω on normalized axial pressure distribution

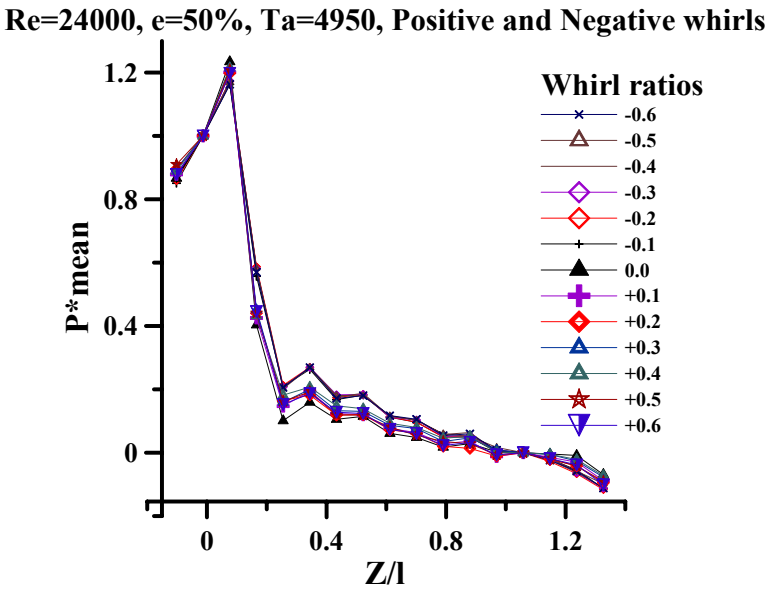

Fig 76. Effect of positive and negative ω on normalized mean axial pressure distribution

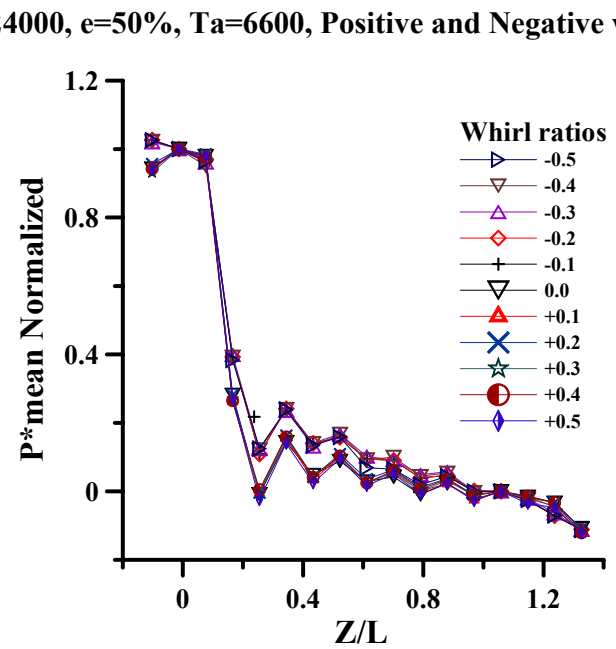

Fig 77. Effect of positive and negative ω on normalized mean axial pressure distribution

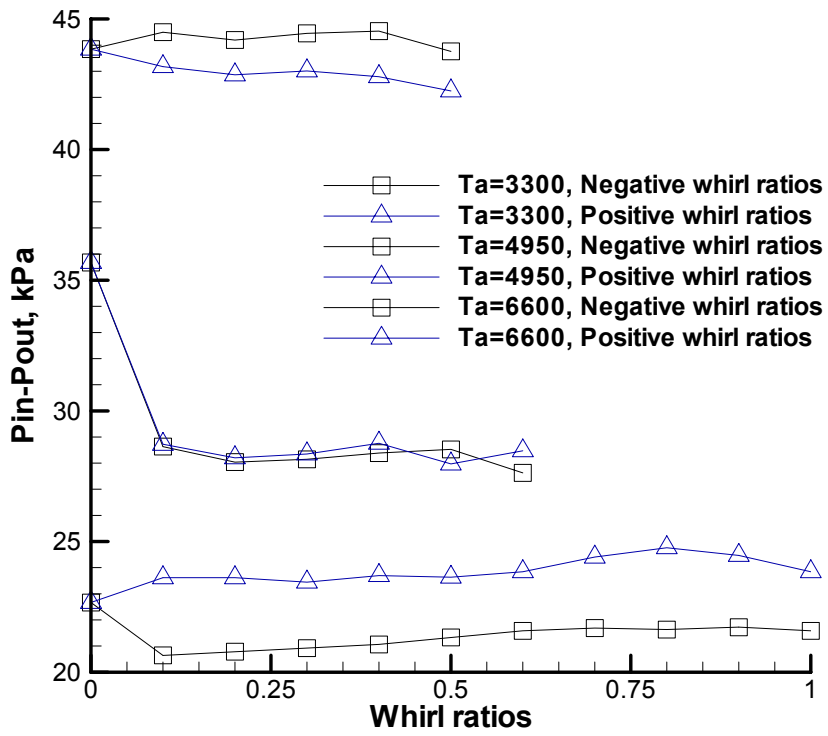

Fig 78. Variation of Del P with whirl ratios

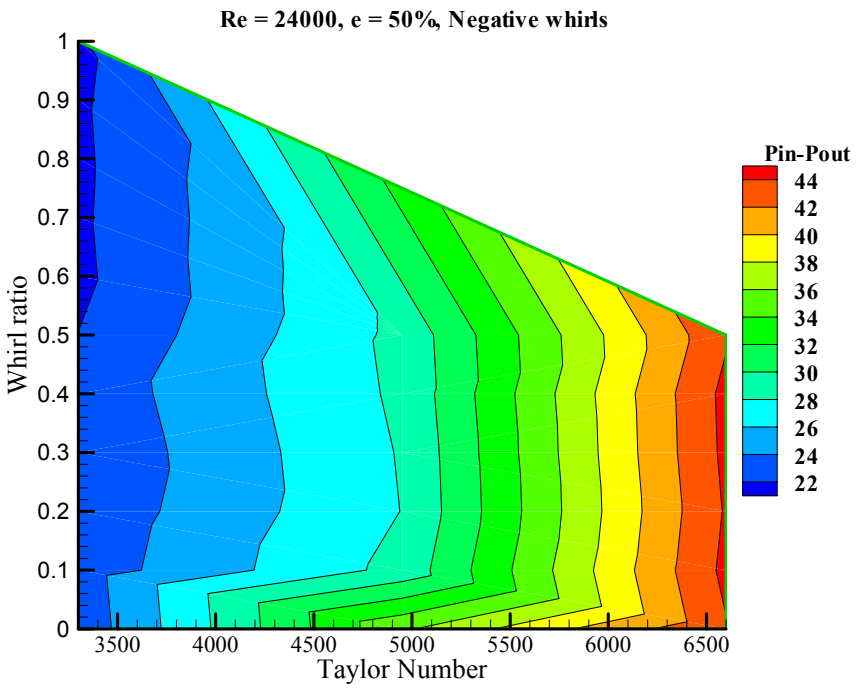

Fig 79. Effect of whirl ratio and Ta on ΔP

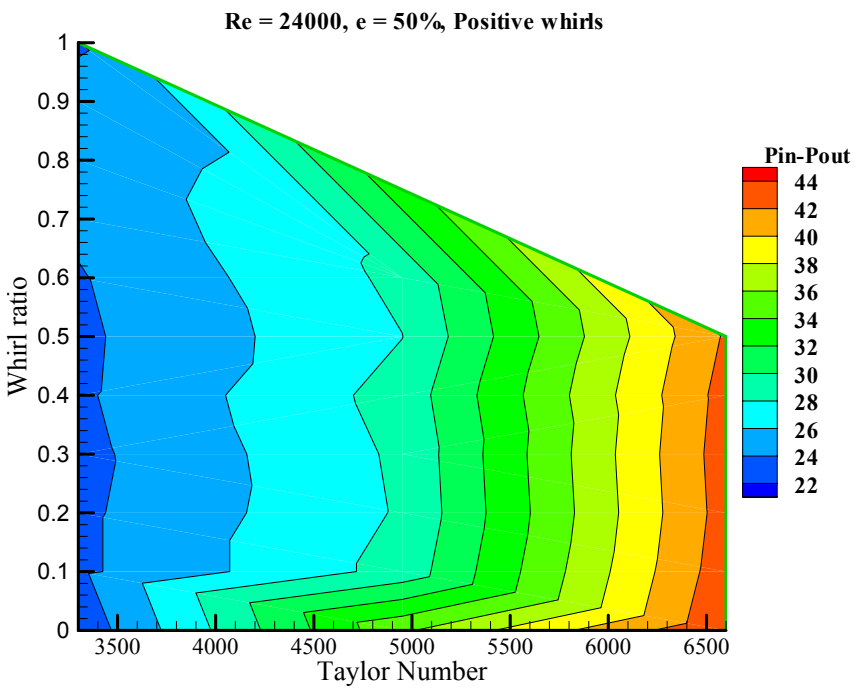

Fig 80. Effect of whirl ratio and Ta on ΔP

Appendix B

AutoCAD DRAWINGS

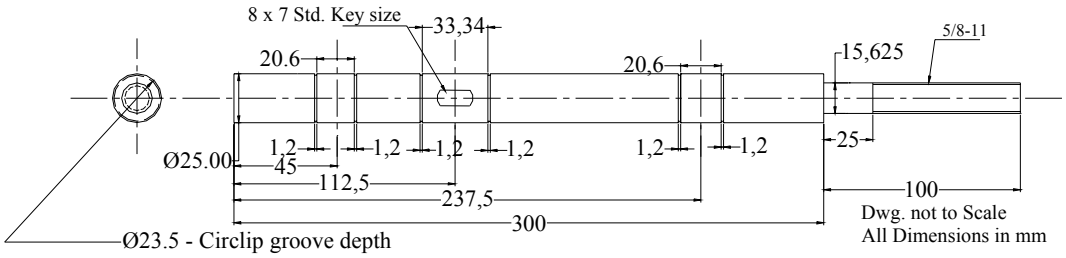

Fig 81. Whirl shaft

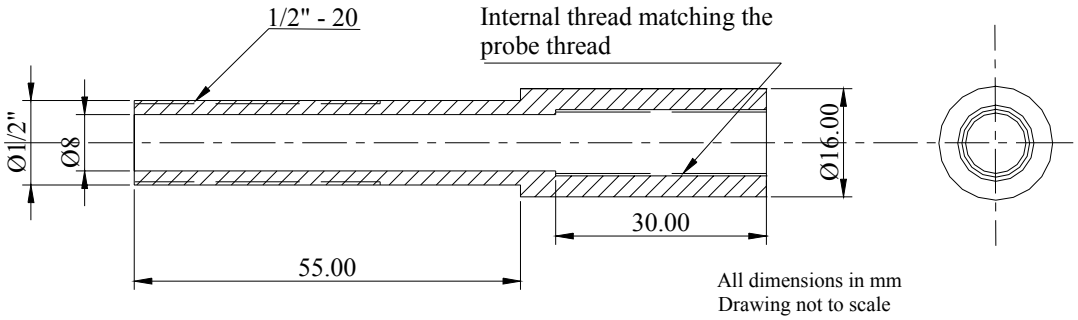

Fig 82. Proximity probe adaptor

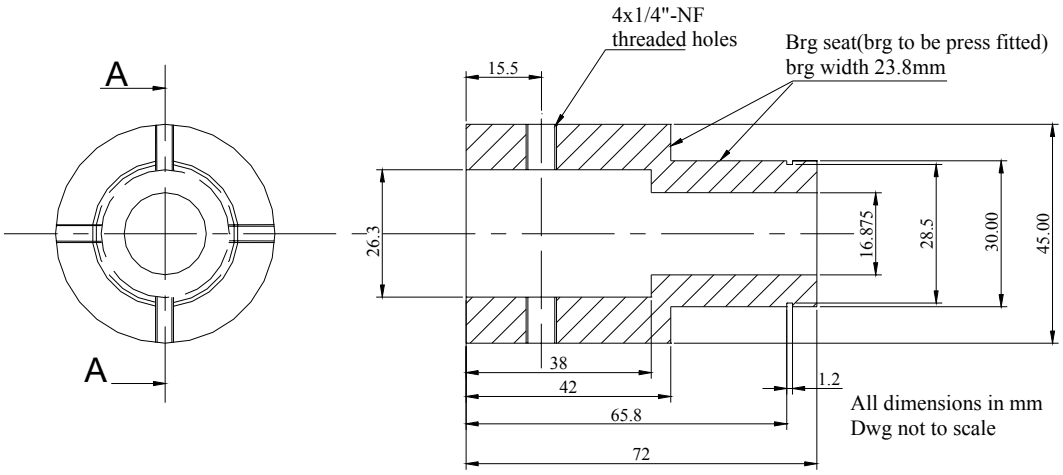

Fig 83. Whirl Cam

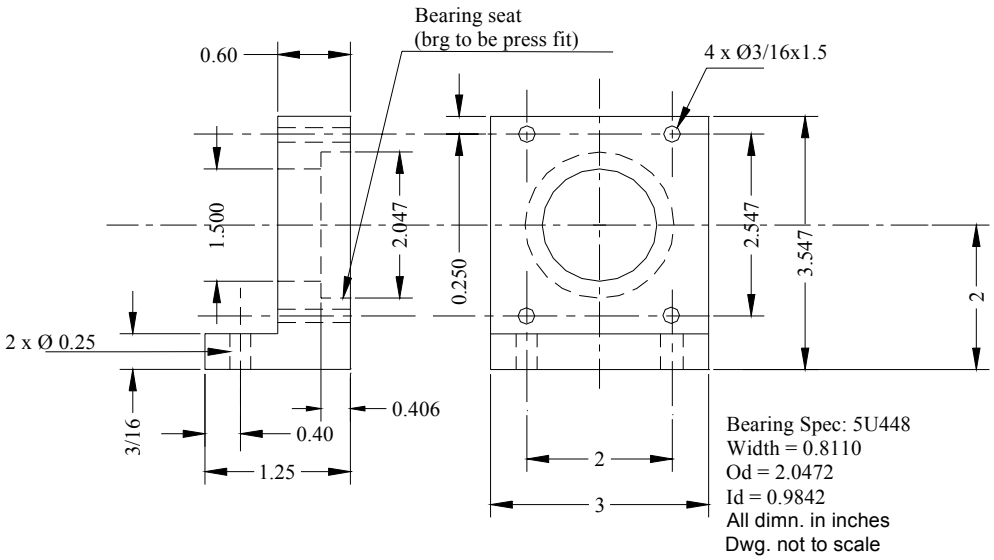

Fig 84. Pillow Block

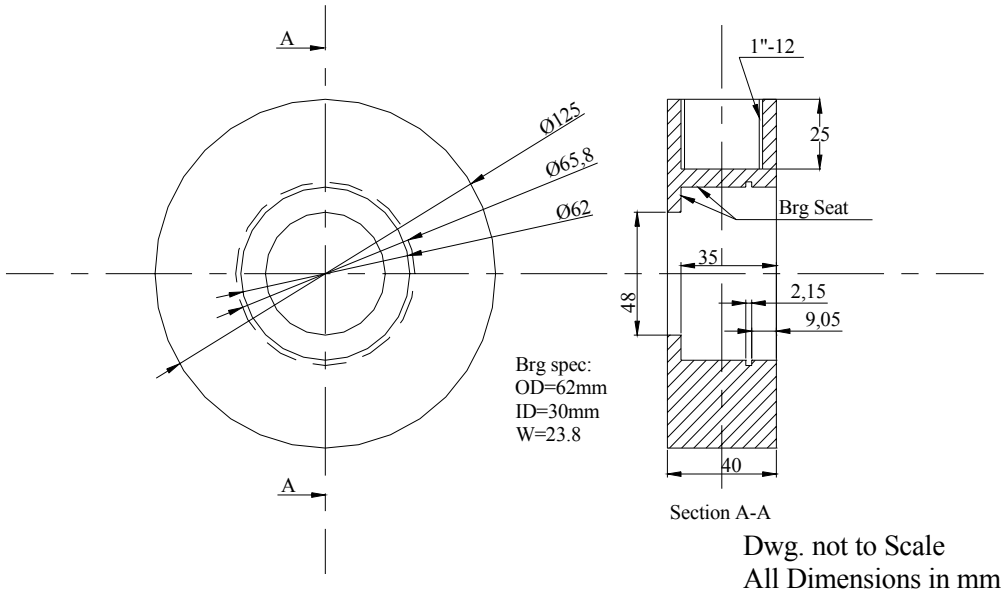

Fig 85. Cam Housing

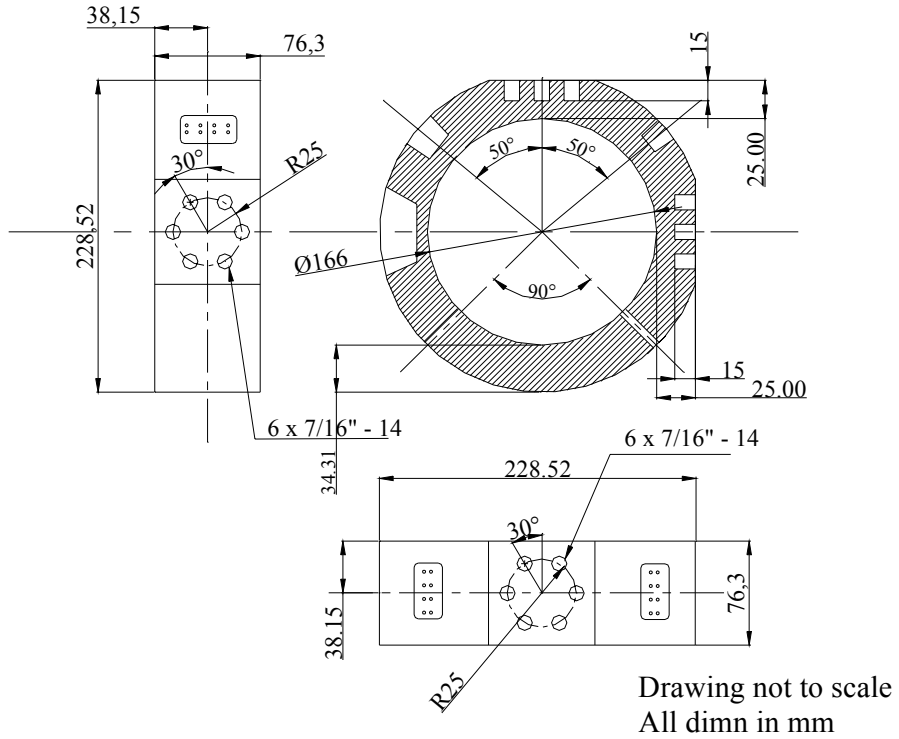

Fig 86. Modified Stator

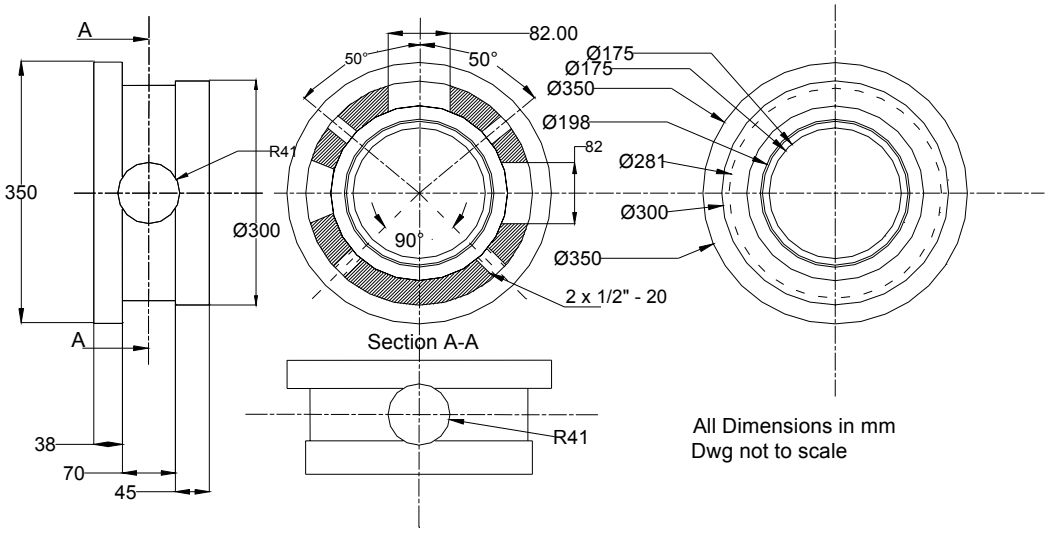

Fig 87. Modified Housing

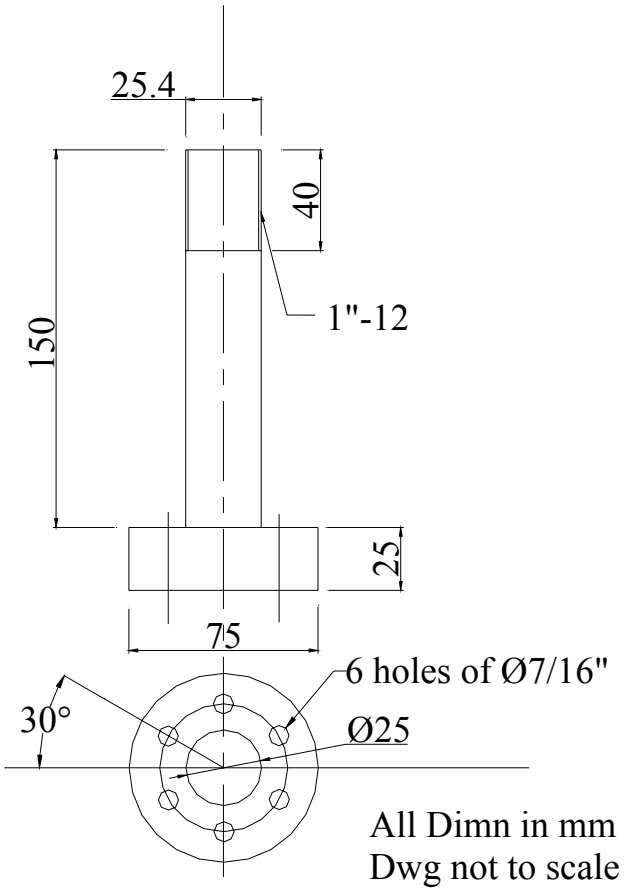

Fig 88. Plunger

Appendix C

TABLES AND PHOTOS OF THE SEAL TEST FACILITY

Whirl Ratio	1800	2700	3600
0.1	1.536	2.304	3.072
0.2	3.072	4.608	6.144
0.3	4.608	6.912	9.216
0.4	6.144	9.216	12.288
0.5	7.68	11.52	15.36
0.6	9.216	13.824	18.432
0.7	10.752	16.128	21.504
0.8	12.288	18.432	24.576
0.9	13.824	20.736	27.648
1	15.36	23.04	30.72

Fig 89. Number o f cycles of data acquired per whirl ratio

sl. no.	new z/l
1	-0.102222
2	-0.012936
3	0.076348
4	0.165635
5	0.254921
6	0.344207
7	0.433492
8	0.522778
9	0.612064
10	0.701349
11	0.790635
12	0.879921
13	0.969207
14	1.058492
15	1.147778
16	1.237007
17	1.326349

Fig 90. ScaniValve pressure tap location

Annular seal Plug positions				
Plug A Straight	0.126	0.252	0.6278	0.9838
Plug A Reverse	1.309	0.984	0.60578	0.2518
Plug B Straight	-0.015	0.313	1.0328	
Plug B Reverse	1.251	0.923	0.2028	
PlugC Reverse	0.094	0.444	0.7918	1.1418
Plug D Straight	0.037	0.384	0.7338	
Plug D Reverse	1.199	0.852	0.5018	

Fig 91. Axial locations on the Brass plugs for Kulite transducers.

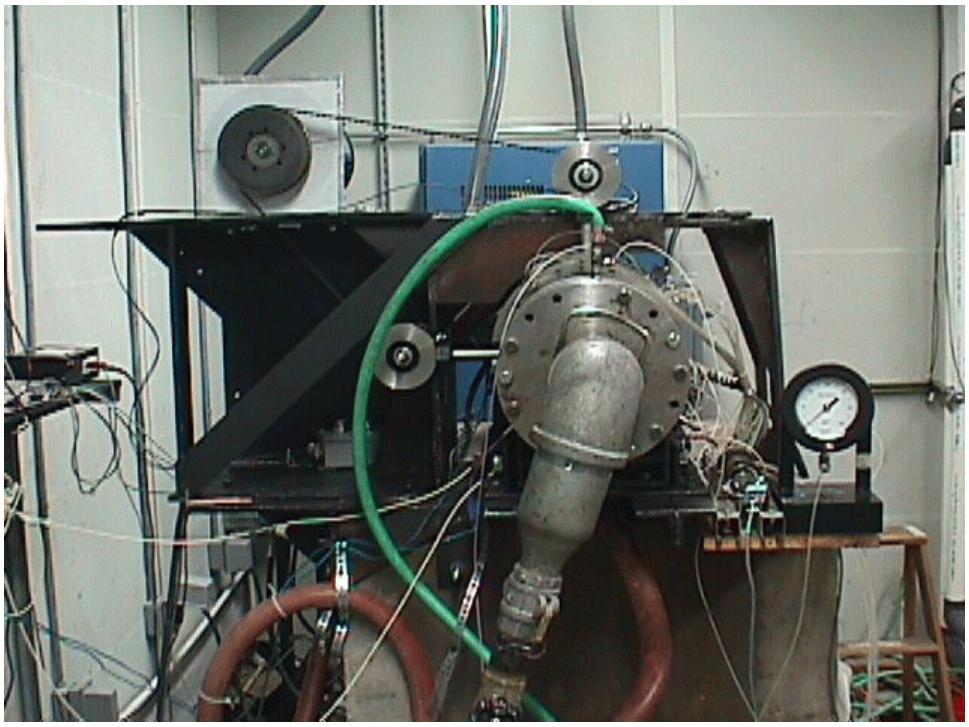

Fig 92. Front view of the seal test setup

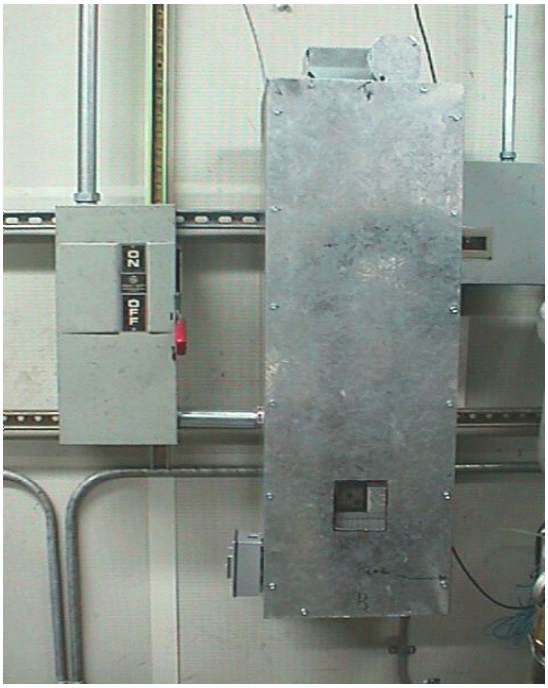

Fig 93.Whirl motor ac drive

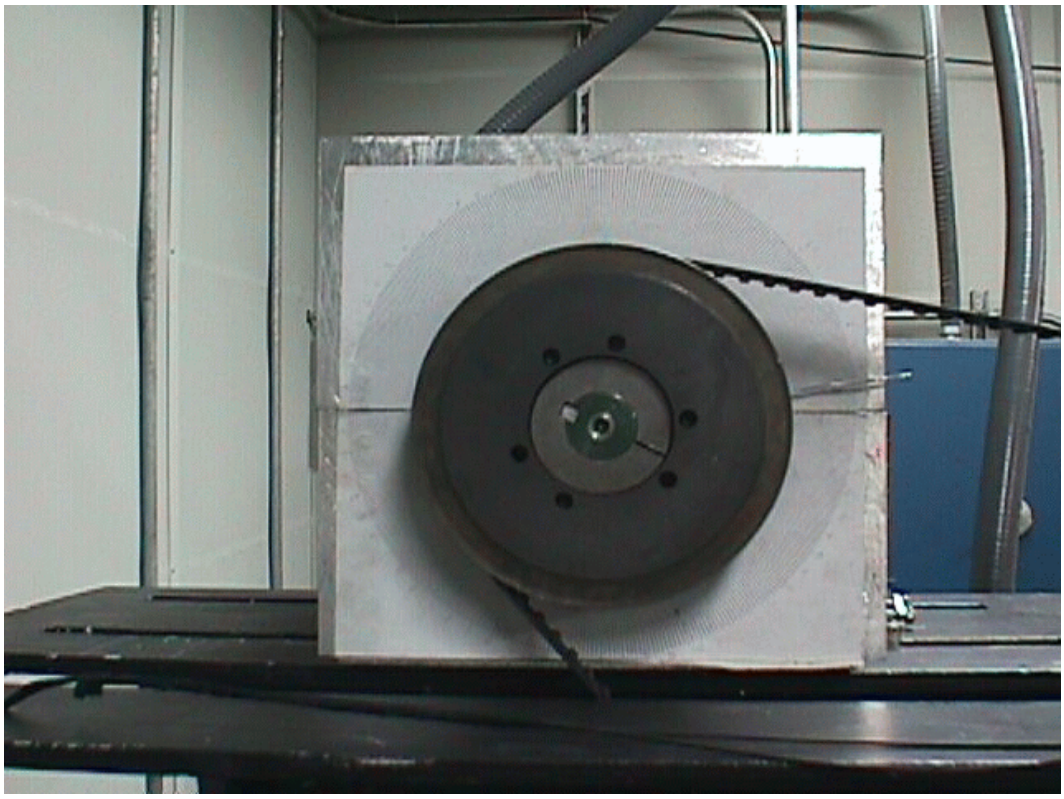

Fig 94. Circular scale for static testing

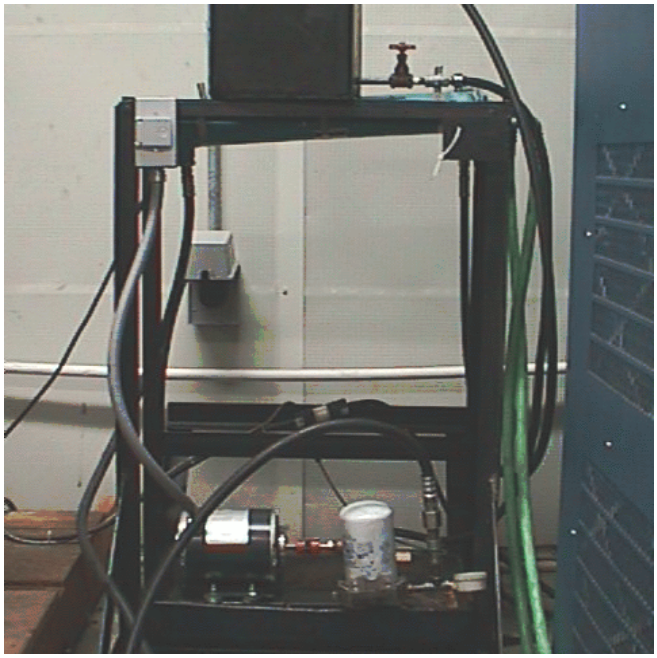

Fig 95. Main motor lubrication and cooling system

Fig 96. The main supply tank, heat exchanger and water filter

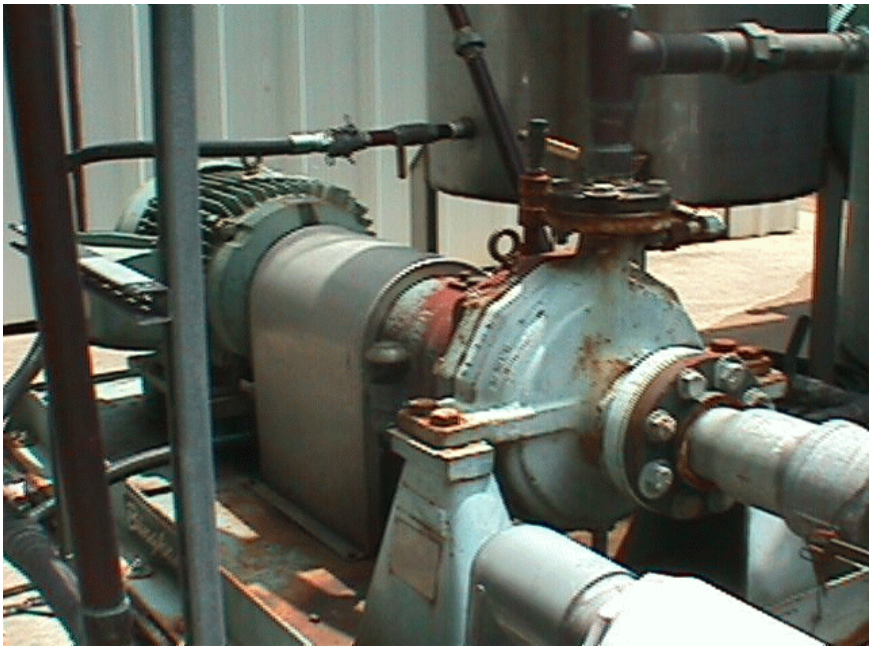

Fig 97. Water supply motor

Fig 98. Re-circulation pump of the heat exchanger

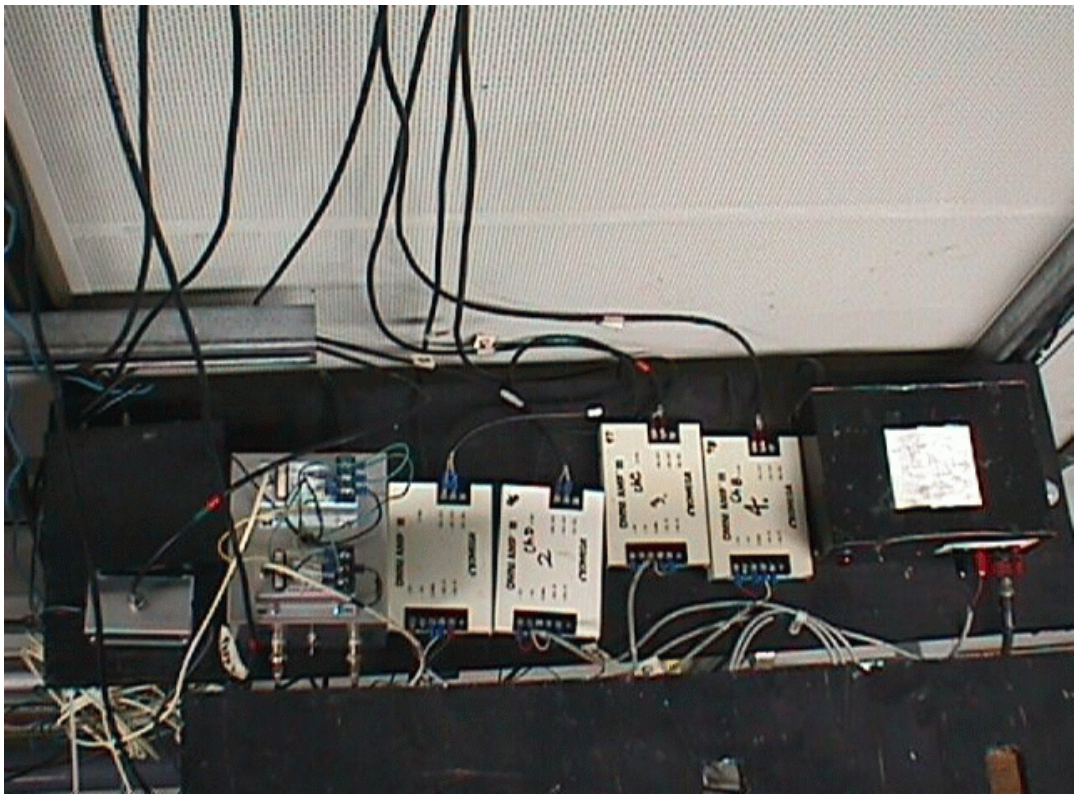

Fig 99. Instrumentation

Appendix D

C++ CODE

C++ Program to convert Binary Rapid system data to readable format

```
#include <float.h>
#include <math.h>
#include <stdio.h>
#include <process.h>
#include <io.h>
#include <iostream.h>
#include <direct.h>
#include <string.h>
#include <stdlib.h>
#include <dos.h>

char folder[200];
char directo1[50];
int datapoint[5000][4100],CHNS;
float row_avg_a[1025],row_avg_b[1025],row_avg_c[1025],row_avg_d[1025];
unsigned short TriggerChannel, NumberOfAverages, AveragedDataSaved;
long NumberOfDataSets, FirstSample, NumberOfSamples, Calibration[32];
double ConversionFactor;
char Units[5], Gain[32];


char *directory (char *directo)
{   char startdir[200];
        getcwd(startdir,200);
        printf("\n The starting directory is %s",startdir);
        if (chdir(directo))
        {
                perror("\n The path is not good \n");
```

```
                exit(1);
        }

        printf("\n The current directory is now %s\n",getcwd(startdir,200));
        printf("\n");
        return(directo);
}


void bintoascii ()
{
                FILE *binary;
                FILE *decimal;
                int i, j, k, c,point;
                char trash;
                char fileread[20];
                char filewrite[20];
                double TriggerValue,Psi2kPa;
                unsigned short FileType, DataFormat, NumberOfBits;
                unsigned short SamplingRate, TriggerMode;
                long Channels, start;
                printf("Enter the file name to read:");
                scanf("%s",&fileread);
                printf("Enter the file name to write :");
                scanf("%s",&filewrite);
                binary=fopen(fileread,"rb+");
                decimal=fopen(filewrite,"wt+");
                if (binary==NULL)
                {
                        printf("\n Error binary file\n");
```

```
        exit(0);
}
if (decimal==NULL)
{
        printf("\n Error decimal file\n");
        exit(0);
}
/*rewind to the beginning of the data in the binary file*/
rewind(binary);
fread(&FileType,2,1,binary);
fread(&NumberOfDataSets,4,1,binary);
fread(&DataFormat,2,1,binary);
fread(&NumberOfBits,2,1,binary);
fread(&FirstSample,4,1,binary);
fread(&NumberOfSamples,4,1,binary);
fread(&SamplingRate,2,1,binary);
fread(&TriggerMode,2,1,binary);
fread(&TriggerChannel,2,1,binary);
fread(&TriggerValue,8,1,binary);
fread(&NumberOfAverages,2,1,binary);
fread(&AveragedDataSaved,2,1,binary);
fread(&Channels,4,1,binary);
printf("\n FileType =%d ", FileType);
printf("\n Number of sample =%d ", NumberOfSamples);
printf("\n DataFormat =%d",DataFormat);
printf("\n NumberOfBits =%d ", NumberOfBits);
printf("\n SamplingRate =%d ", SamplingRate);
printf("\n FirstSample =%d",FirstSample);
printf("\n Number of data sets =%d",NumberOfDataSets);
printf("\n TriggerMode =%d ", TriggerMode);
```

```
printf("\n TriggerChannel =%d ", TriggerChannel);
printf("\n TriggerValue =%d",TriggerValue);
printf("\n NumberOfAverages =%d ", NumberOfAverages);
printf("\n AveragedDataSaved =%d ", AveragedDataSaved);
printf("\n Channels =%d",Channels);

if (Channels==1 || Channels==2 || Channels==4 || Channels==8)
 CHNS=1;
else if (Channels==7 || Channels==11 || Channels==13 || Channels==14)
 CHNS=3;
else if (Channels==15)
 CHNS=4;
else
 CHNS=2;

fread(&Gain[1],1,32,binary);
printf("\n Gain =%d ", Gain);
fread(&Calibration[1],4,32,binary);
fread(&ConversionFactor,8,1,binary);
fread(&Units[1],1,4,binary);
printf("\n Calibration =%d ", Calibration);
printf("\n ConversionFactor =%d ", ConversionFactor);
printf("\n Units =%d",Units);

for (i=1; i<45; i++)
 fread(&trash,1,1,binary);
Psi2kPa=6.895;
start=ftell(binary);

/* Loop over the data sets*/
```

```
for (j=1; j<(NumberOfDataSets+1); j++)
{

/* read and discard header information found at the start of each data set */
        for (k=1; k<65; k++)
                fread(&trash,1,1,binary);

        for (i=1; i<(CHNS+1); i++)
        {
                for (c=1; c<(NumberOfSamples+1); c++)
                {
                        point=fgetc(binary);
                datapoint[c][j+(NumberOfDataSets*(i-1))]=point;
                }

        }
}

fprintf (decimal,"\n File name: %s\n",fileread);
        for (i=1; i<(NumberOfSamples+1); i++)
        {
                for (c=1; c<((NumberOfDataSets*CHNS)+1); c++)
                        fprintf(decimal,"%d \t  ",datapoint[i][c]);
                        fprintf(decimal,"\n");
        }
printf("\n  I = %d\n",i);
printf("  J = %d\n",c);
printf("  K = %d\n",NumberOfSamples+1);

fprintf(decimal,"\n   ConversionFactor = %d \n  ",ConversionFactor);
```

```
                fprintf(decimal," Gain = %d \n  ",Gain);
                fprintf(decimal," Calibration = %d \n  ",Calibration);
                fprintf(decimal," Units = %d \n  ",Units);
               fclose(decimal);
               fclose(binary);
}

void readfile ()
{
 FILE *batchfile;
  char  batchname[20];
  printf (" \nConversion of data format  from Binary to ASCII\n");
  printf("\n name of the batchfile with extension is: ");
  scanf("%s",&batchname);
  batchfile=fopen(batchname,"rb+");

  if (batchfile==NULL)
        {
         printf("\n Batch File not found\n");
         exit(0);
        }
  else
        {
               while(!feof(batchfile))
               {
                      fscanf(batchfile,"%s \n",&folder);
                      printf("Name read from Batchfile: %s", folder);
                      sprintf(directo1,"C:\\%s\\reduce",folder);
                      printf("\n seek for: %s",directo1);
                      directory(directo1);
```

```
                }
        }

}

void data_averaging()
{
        int i,j,k;
        int count_1 = 1,count_2 = 1;
        char output[20];
        float time,time_step,percent_stator, percent_rotor;
        float sum_1,sum_2,sum_3,sum_4;
        float stator_freq, rotor_freq;
        FILE *write;
        printf("Enter name of the average file :  ");
        scanf("%s",&output);

        if((write=fopen(output,"wt+")) == NULL){
                printf("Error opening Averaging File\n");
        }

        time = 0.0;
        time_step = 0.0005;
        printf("Enter Rotor Frequency (in Hz) ");
        scanf("%f",&stator_freq);
        printf("Enter Stator Frequency (in Hz) ");
        scanf("%f",&rotor_freq);

        for(i=1;i<(NumberOfSamples+1);i++){
                        sum_1 = 0.0;
```

```
                    sum_2 = 0.0;
                    sum_3 = 0.0;
                    sum_4 = 0.0;

            for(k=1;k<CHNS+1;k++){

for(j=((NumberOfDataSets*(k-1))+1);j<(NumberOfDataSets*k);j++){
                        switch(k)
                        {
                                case 1:
                                        sum_1 = sum_1 + datapoint[i][j];
                                        break;
                                case 2:
                                        sum_2 = sum_2 + datapoint[i][j];
                                        break;
                                case 3:
                                        sum_3 = sum_3 + datapoint[i][j];
                                        break;
                                case 4:
                                        sum_4 = sum_4 + datapoint[i][j];
                                        break;
                        }
                    }
            }
            row_avg_a[i] = (sum_1 /(NumberOfDataSets-1));
            row_avg_b[i] = (sum_2 /(NumberOfDataSets-1));
            row_avg_c[i] = (sum_3 /(NumberOfDataSets-1));
            row_avg_d[i] = (sum_4 /(NumberOfDataSets-1));
        }
        fprintf(write,"    TIME      Rotor_Cycle   Stator_Cycle   Channel_A
```

```
Channel_B    Channel_C    Channel_D\n");

        for(i=1;i<(NumberOfSamples+1);i++){
                percent_stator = stator_freq*time;
                percent_rotor = rotor_freq*time;
                fprintf(write,"  %f     %f     %f     %f    %f    %f
%f\n",time,percent_stator,percent_rotor,row_avg_a[i],row_avg_b[i],row_avg_c[i],row_a
vg_d[i]);
                time = time + time_step;
        }

                fprintf(write,"\n  ConversionFactor= %d \n  ",ConversionFactor);
                fprintf(write,"Gain            = %d \n  ",Gain);
                fprintf(write,"Calibration     = %d \n  ",Calibration);
                fprintf(write,"Units           = %d \n  ",Units);
                fclose(write);
}

void main()

{
        int s;

   printf("\n Data Post Processing Software");
   printf("\n 1) Converting Binary to Ascii");
   printf("\n 2) Exit Program");
   printf("\n Make your choice:");
   scanf("%d",&s);
```

```
 switch(s)

 {
  case 1: printf("\n 1) Converting Binary to Ascii");
                          readfile();
                          bintoascii();
                          fflush(stdout);
                          break;
  case 2: printf("\n 2) Exit Program");
            exit(0);
  default: printf("\n Make a choice");
 }
        data_averaging();
        printf("\n Operation Completed \n");

}
```

VITA

Arun Suryanarayanan was born on June 23, 1976, in Madurai, Tamil Nadu, India. He attended primary and high school at Poorna Prajna Education Center, Bangalore, Karnataka, India. He attended Vijaya College, Basavangudi, between 1992-94 for his pre-university education. He completed his undergraduate education in mechanical engineering at Bangalore University. His permanent address is EV-002, Vignanapura Campus, Off New BEL Rd. Opp ISRO. H. O., Bangalore-560094, Karnataka India.